Predicting Steady-State Performance of Falling-Film Drain Water Heat Recovery Systems from Rating Data

by

Ramin Manouchehri

A thesis
presented to the University of Waterloo
in fulfillment of the
thesis requirement for the degree of
Master of Applied Science
in
Mechanical Engineering

Waterloo, Ontario, Canada, 2015

Author's Declaration

Several portions of this thesis consist of published material of which I was acknowledged as an author or co-author: see Statement of Contributions included in the thesis. This is a true copy of the thesis, including any required final revisions, as accepted by my examiners.

I understand that my thesis may be made electronically available to the public.

Statement of Contributions

A total of two journal papers have been published based on the results produced throughout this thesis. The co-authors for these papers were Prof. Mike Collins, Dr. Carsen Banister and Ivan Beentjes.

I hereby declare that I performed all the experiments, generated the results and devised the correlations in this thesis. The co-authors assisted with writing and organization of the papers.

Abstract

Drain Water Heat Recovery (DWHR) systems are counter-flow heat exchangers typically used to recover energy from warm water going down shower drains. Such systems are becoming commonplace in many residential buildings; however, the lack of reliable building simulation models has proven to be an obstacle when it comes to choosing the most suitable unit for a given application. The ultimate outcome of this thesis is a universal model that uses the existing rating data to predict the performance of DWHR systems operating under various conditions.

A test rig was constructed and programmed to measure the performance of DWHR systems in the Solar Thermal Research Laboratory (STRL). Highly accurate instruments were incorporated in the test rig to measure the flow rates, temperatures and pressures at multiple locations.

Through experiments, a model was created to predict the performance of DWHR systems operating under equal-flow conditions. A correction factor was developed to allow extrapolating the results of this model to flow rates higher than those available in the rating data.

The effects of varying inlet temperatures on the performance of DWHR systems were also found through experiments and a general correction factor was developed to compensate for these effects. A thermal resistor network was created based on the construction of DWHR systems in order to directly compare the theoretical expectations for the effects of temperature with the experimental data.

A universal correlation was also devised through experimentation which allows the use of rating data from equal-flow conditions to predict performance of systems operating under unequal-flow conditions.

The correlations developed throughout this thesis were compiled into a universal procedure, which was validated through experiments. In all cases, the experimental and predicted results were in good agreement, which lends credibility to the procedure developed in this work.

Dedications

This thesis is dedicated to my parents.

Acknowledgements

First and foremost, I would like to thank my supervisor, Professor Michael Collins, for providing me with the opportunity to work on this project, and for his time and effort. I learned many personal and technical skills through his guidance and this work would not have been as practical as it is, if not for him. It has been a pleasure working with him for the past couple of years.

I would also like to thank my colleagues and friends, Ivan Beentjes and Carsen Banister, who always took the time to help me, despite having their hands full with projects of their own. It has been a pleasure working alongside them. Their hard work and dedication inspired me to always do my best.

Thank you to Professor David Mather for providing me with the opportunity to present my research to students and engineers from the industry. These presentations and the feedback I received helped me address issues I had never thought of and to write a better thesis.

Thank you to Professor John Wright, who always provided me with his opinion and perspective on several aspects of my project, even though he is not my co-supervisor.

The assistance of RenewABILITY Energy Inc. is acknowledged. Their help in providing DWHR systems to our lab was instrumental in the completion of this work.

This work was financially supported by Natural Sciences and Engineering Research Council (NSERC) and Smart Net-zero Energy Buildings strategic Research Network (SNEBRN).

Finally, thank you to my parents for their encouragement and support throughout my time at the university.

Table of Contents

List of Figures

List of Tables

List of Abbreviations

CSA	Canadian Standards Association
DWHR	Drain Water Heat Recovery
FS	Full Scale
FW	Full Wetting; stands for a test procedure described in Chapter 3
HLR	High to Low; stands for a test procedure described in Chapter 3
ISO	International Organization for Standardization
LHR	Low to High; stands for a test procedure described in Chapter 3
LPM	Liters per Minute
PIV	Particle Image Velocimetry
RTD	Resistance Temperature Detector

Nomenclature

A	Heat transfer area (m^2)
C_c, C_h	Heat capacity rates corresponding to the cold and hot sides, respectively (W/ °C)
C_{flow}	Correction factor for flow rates above 14 LPM (Dimensionless)
$C_{\min}, C_{\max}$	Lesser and greater of C_c and C_h, respectively (W/ °C)
C_p	Specific heat (kJ/kg °C)
d	Tube diameter (m)
D	Mean coil diameter (m)
De	Dean number (Dimensionless)
F_C	The correction factor for converting $\varepsilon_{Reference}$ to $\varepsilon_{Corrected}$ (Dimensionless)
h_{coils}	Convective heat transfer coefficient for the coils, (kW/m^2 °C)
h_{film}	Convective heat transfer coefficient for the falling film, (kW/m^2 °C)
k	Thermal conductivity (W/m °C)
L	The length of the drain pipe in a DWHR system (m)
L_{Coil}	The length of the drain pipe that is wrapped with coils in a DWHR system (m)
$\dot{m}$	Mass flow rate (kg/s)
NTU	Number of transfer units (Dimensionless)
Nu	Nusselt number (Dimensionless)
Pr	Prandtl number (Dimensionless)
q	Heat transfer rate (kW)
q_c	Heat transfer rate based on the cold side of a DWHR system (kW)
$q_{\max}$	Maximum heat transfer rate (kW)
$R_{\#}$	Thermal resistance in resistor network (°C /W)
Re	Reynolds number (Dimensionless)
$T_{c,i}$	Temperature of mains-side, cold-water, inlet (°C)
$T_{c,o}$	Temperature of mains-side, cold-water, outlet (°C)
T_{drain}	Temperature of drain-side, average (°C)
$T_{h,i}$	Temperature of drain-side, hot-water, inlet (°C)
$T_{h,o}$	Temperature of drain-side, hot-water, outlet (°C)
T_{mains}	Temperature of mains-side, average (°C)
U	Overall heat transfer coefficient (kW/m^2 °C)
$\dot{V}$	Volumetric flow rate (liter/min)
$\dot{V}_c$	Volumetric flow rate based on the cold side of a DWHR system (liter/min)

Greek Symbols

ε	Effectiveness of the DWHR system (Dimensionless)
ε_c	Effectiveness calculated based on the cold side of a DWHR system (Dimensionless)
ε_r	Effectiveness at a given angle normalized by effectiveness at vertical (Dimensionless)
$\varepsilon_{Corrected}$	Corrected effectiveness of a DWHR system for given inlet temperatures (Dimensionless)
$\varepsilon_{Reference}$	Effectiveness of the DWHR system at the reference inlet temperatures (Dimensionless)
θ_T	Tilt angle with respect to the vertical, (°)
μ	Dynamic viscosity of water (Ns/m^2)
ρ	Density (kg/m^3)

Chapter 1 Introduction

1.1 Motivation

The world's population is on the rise and global energy consumption is increasing steadily. According to the International Energy Outlook 2013, the world's energy consumption in the year 2040 will be 50% higher than that of 2010, which translates to an additional 295 Quadrillion Btu's if current consumption rates continue [1]. The only way to alleviate such a large increase in energy consumption, is to conserve energy, and to reduce the amount of energy that is wasted on a regular basis.

Surveys have shown that in the year 2010, 16.4% of the total energy consumed in residences in the U.S. was for water heating purposes. That represents approximately 2025 PJ, which equates to approximately 17.7 GJ of energy consumed annually per household [2]. It was also estimated that Americans spent $33.8 billion on residential water heating in that year alone [3]. During the same year in Canada, water heating was responsible for 280 PJ or 19.5% of the total energy consumed in the residential sector. On average, this translated to 20.9 GJ of energy per household [4].

The energy consumption associated with water heating is immense, and there is significant potential to reclaim heat from grey water. A study conducted in Great Britain in the 1970s determined that a household grey water heat recovery system could save 10% of total household energy consumption, recovering the capital cost in only three years [5]. More recently, studies conducted at the Manitoba Advanced House in Winnipeg, Canada, estimated that 50% of a typical family's annual domestic hot water load could be recovered [6].

Drain Water Heat Recovery (DWHR) systems are becoming more common in new and energy efficient construction. In response to this, code and incentive programs are working to develop rating procedures for these systems. In Canada, for example, the "National Energy Code of Canada for Buildings 2011" was

updated in 2012 to incorporate DWHR systems [7]. The Government of Manitoba has also mandated installation of DWHR systems in new residential buildings starting April 2016 [8].

To standardize test methods and results for measuring performance of DWHR systems, the Canadian Standards Association (CSA) recently produced Standard B55.1-12 "Test method for measuring efficiency and pressure loss of drain water heat recovery units" [9]. The standard includes the requirements for the design and configuration of a testing apparatus which simulates the performance of a DWHR system in a typical installation.

This thesis focuses on investigating DWHR systems, and the factors that affect their performance. An attempt is made to create a reliable steady-state model to predict the energy savings associated with their use. An analysis of transient effects is outside the scope of the current work.

1.2 Basics of DWHR Systems

In general, DWHR systems are single pass, double walled, counter flow, vented, falling film heat exchangers similar to what is shown in Figure 1-1. They are comprised of a large diameter copper pipe, typically between 5.1 and 10.2cm (2 and 4 inches), set to match the size of the drain stack they would replace. Wrapped tightly around the large pipe, is a coil of small diameter copper tubes. The warm drain water flows into the top of the large diameter copper pipe, 'wetting' the inside by filming itself to the inner wall and exiting at the base, after transferring thermal energy to the copper. Cold mains water flows into the small tubes at the bottom of the heat exchanger and extracts heat from the falling film of warm water. There are different design variations for DWHR systems as shown in Figure 1-2.

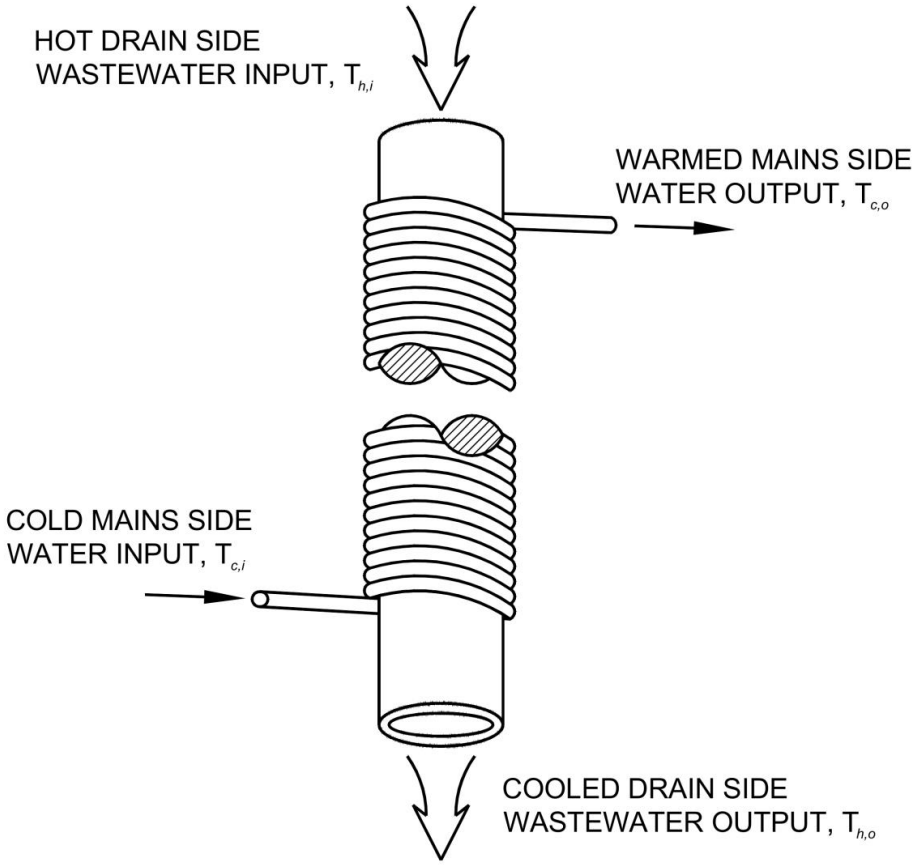

Figure 1-1 Diagram of a typical DWHR system.

Figure 1-2 Different designs for DWHR systems.

The falling film is imperative for proper operation of DWHR systems. The performance of such systems relies on water falling as an annular film, and wetting the inner surface of the drain pipe. This phenomenon results in high heat transfer rates on the drain-side of the system, maximizes the amount of surface area for heat transfer to take place, and minimizes the thickness of water through which heat must be conducted and convected to the walls. DWHR systems are designed to be installed vertically, which allows water to fall as a relatively uniform thin film [10,11,12]. A photograph of the falling film inside a vertically installed DWHR system is shown in Figure 1-3.

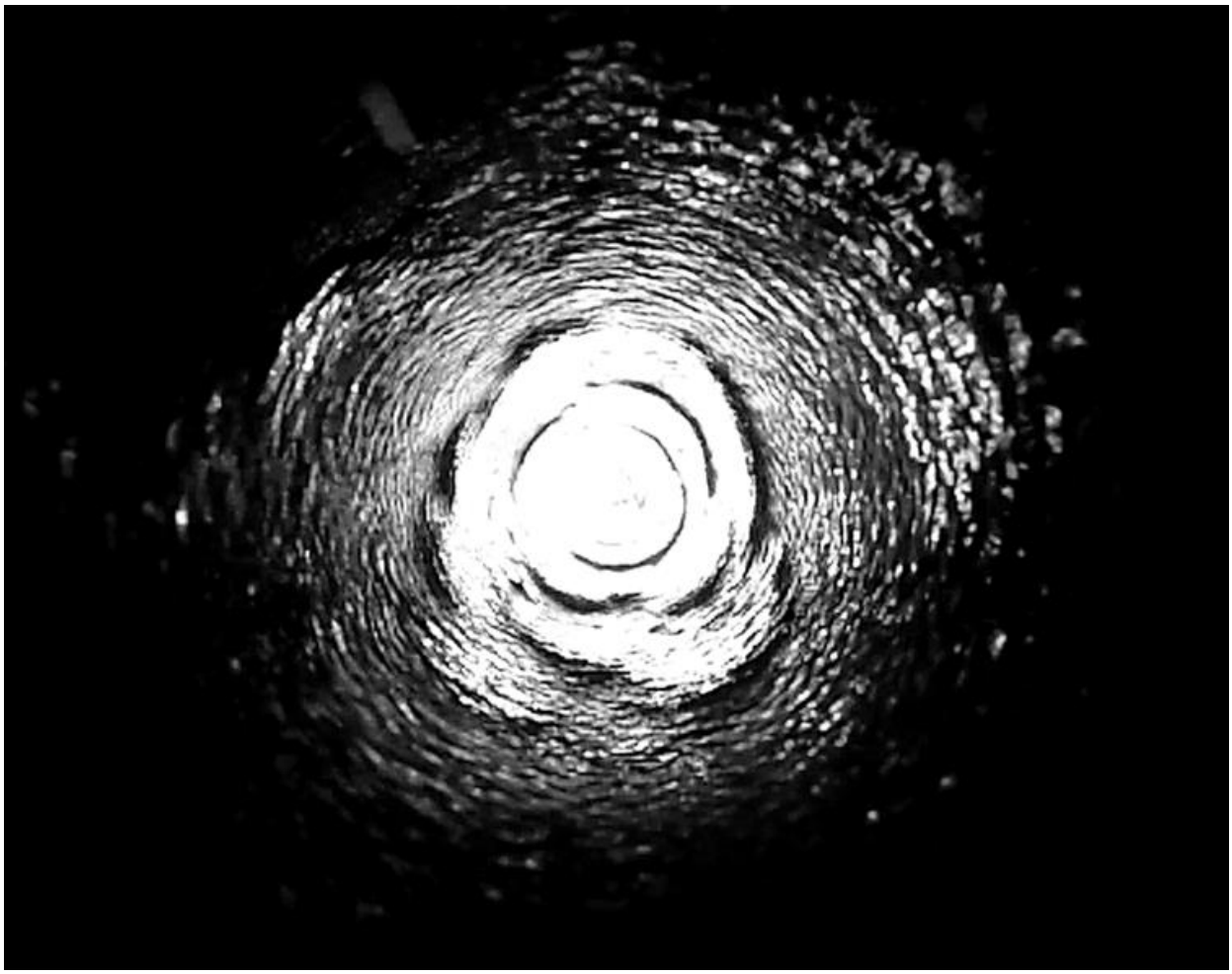

Figure 1-3 Falling film of water inside the drain pipe in a DWHR system.

1.3 Review of Relevant Literature

The following section attempts to summarize the most relevant journal and conference papers as well as reports pertaining to DWHR systems. It is worth mentioning that at the time this thesis was written, there was a lack of relevant information available in the literature about DWHR systems. Each study is analysed in detail to highlight the findings, as well as possible flaws and limitations.

1.3.1 Study #1

Title: Characteristic Effectiveness Curves for Falling-Film Drain Water Heat Recovery Systems [13]

This study, conducted at the University of Waterloo, aimed to develop the characteristic effectiveness vs. flow rate curves for multiple DWHR systems. The performance of the systems was also investigated experimentally under counter-flow and parallel-flow configurations. The theoretical characteristic curve provided by the authors is shown in Figure 1-4. This study is the only one available in the literature that attempted to measure the performance of DWHR systems using high accuracy instruments.

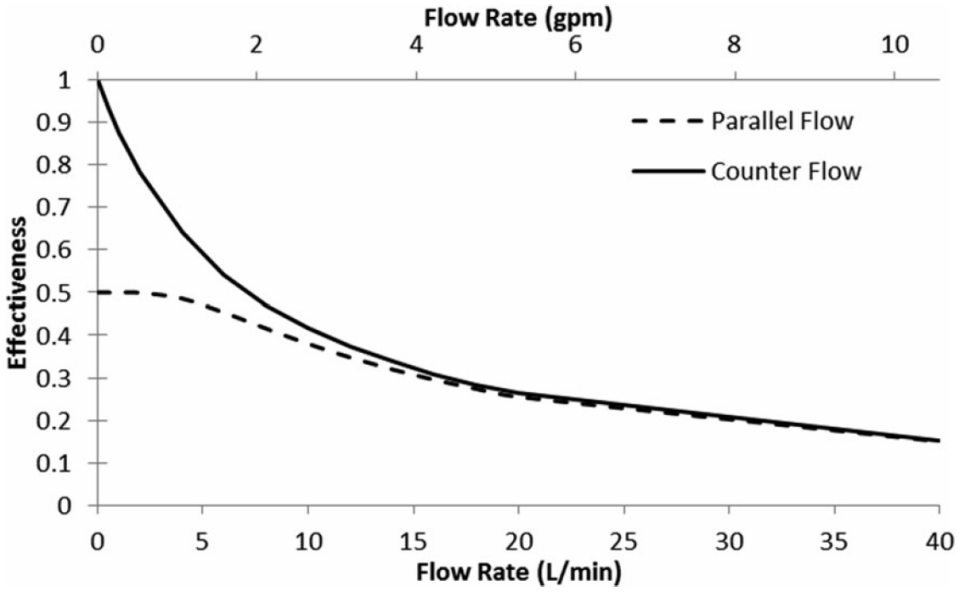

Figure 1-4 Theoretical characteristic curve for effectiveness vs. flowrate [13].

The test results produced curves similar to the theoretical curve shown in Figure 1-4 with the exception of an unexpected inflection point at the lower flow rates. The authors theorized that this phenomenon was likely due to the laminar to turbulent flow transition for the flow within the coils. Further investigations were recommended to better understand the behavior of falling films in DWHR systems.

1.3.2 Study #2

Title: Performance Evaluation of Drain Water Heat Recovery Technology at the Canadian Centre for Housing Technology [14]

Three DWHR systems with different designs as shown in Figure 1-5 were tested in this study by the Canadian Centre for Housing Technology. The units were installed in a basement and the plumbing system was instrumented to measure appropriate temperatures and flow rates through the units. Each system was tested under two different configurations; the first configuration directed all the preheated water exiting the DWHR system into the hot water tank, while the second configuration divided the preheated water between the hot water tank and the cold water supply at the shower fixture. The objectives of the study were to measure the daily gas savings for each of the pipes under different configurations, to measure their effectiveness, and to determine if non-simultaneous draws have any impact on the energy savings.

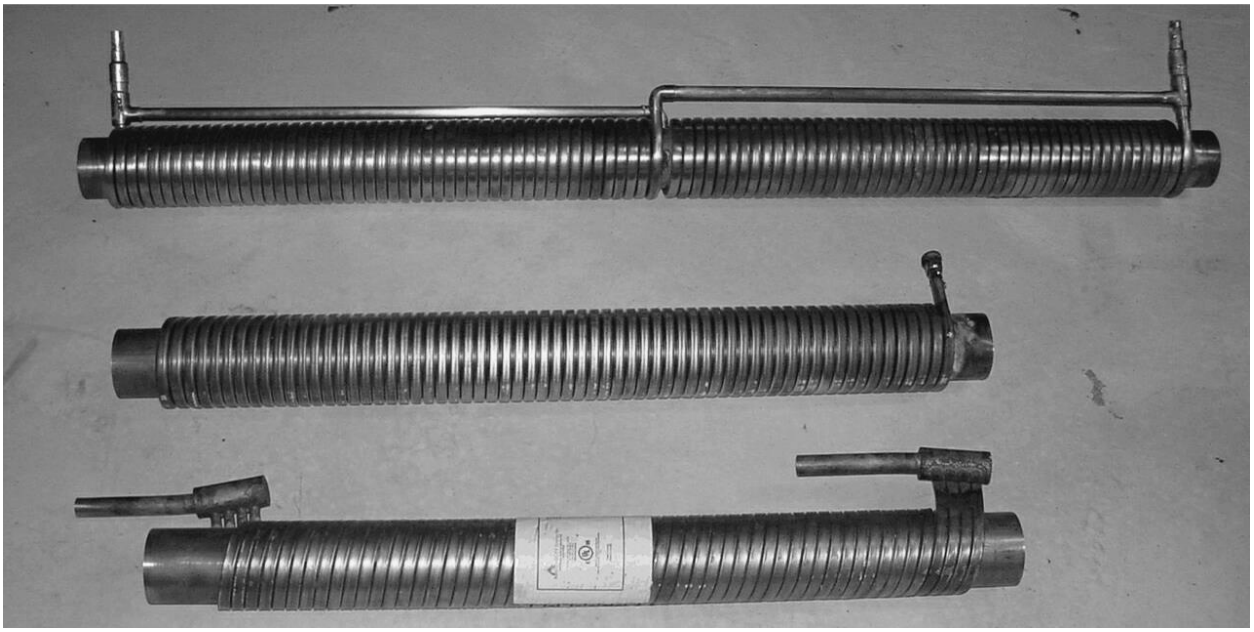

Figure 1-5 Three different DWHR designs that were tested as part of this study [14].

The results showed that DWHR systems reduced gas consumption for water heating by 9 to 27%. It was also clear that the effectiveness values measured for the systems tested under the first configuration were generally higher. Furthermore, the results did not indicate any significant savings associated with non-simultaneous draws through each system due to the small thermal mass of the systems. The authors recognized that their results were not completely satisfactory since the temperatures through the systems were not controlled, and the instruments lacked high precision. Nevertheless, the results were indicative of the performance of DWHR systems in a typical household.

1.3.3 Study #3

Title: Impact of Grey Water Heat Recovery on the Electrical Demand of Domestic Hot Water Heaters [15]

This study, conducted by École Polytechnique de Montréal, aimed to determine the impact of DWHR systems on peak electrical demand in residential dwellings with electric water heaters. The effectiveness of a 7.6cm diameter, 127cm long DWHR system was fed into a TRNSYS model to simulate the system on

an annual basis in Montreal, Canada. The effect of mains water temperature on the annual savings was also investigated. A daily domestic hot water consumption of 240 Liters was picked to represent an average family. The schematic of this TRNSYS model is presented in Figure 1-6.

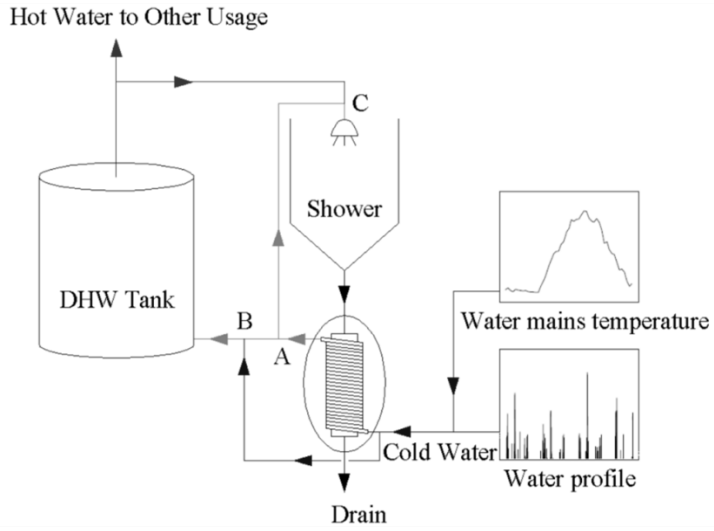

Figure 1-6 Schematic of the TRNSYS model used [15].

The results showed that this particular DWHR system could potentially reduce the annual energy consumption for domestic water heating purposes by 798 kilowatt hours, and reduce the peak electrical load by up to 21.5%. As for the mains inlet water temperature, it was found that the energy savings associated with an inlet temperature of 1.8°C are 2.4 times higher than the savings associated with an inlet water temperature of 20.6°C.

The authors did not explain how the performance of the DWHR system was simulated under flow rates different than the 9.5 LPM at which it was rated. This is a significant limitation for the study since the performance of DWHR systems is a function of flow rate of water. The effectiveness of the system cannot be assumed to stay constant and the results produced in this study may not be a good representation of a realistic installation. The effectiveness of a DWHR system is also dependent on the

inlet water temperatures, and again, it cannot be assumed to stay constant for different inlet temperatures as was implied in this study. The combination of the above two factors could have a substantial impact on the simulated results.

1.3.4 Study #4

Title: Financial Analysis of the Implementation of a Drain Water Heat Recovery Unit in Residential Housing [16]

This study, conducted by Słyś et al., aimed to numerically analyse the benefits of DWHR systems installed in three different plumbing configurations shown in Figure 1-7. The effectiveness of a 7.6cm diameter, 153cm long DWHR system was modelled for the different configurations. It was assumed that the mains temperature and the shower temperatures were constant and no heat losses occurred in the plumbing system. The numerical results of this study showed that the first configuration was the most beneficial option for installation of DWHR systems.

The main issue with this study was the assumption of constant temperatures in the simulations. The inlet temperatures have a clear impact on the effectiveness of DWHR systems, and since this model was based on a constant effectiveness assumption, the produced results may not be accurate. More importantly, two of the three configurations simulated in this study required effectiveness data measured under unequal flow rates, which were provided by the manufacturer in this case. It is worth noting that no reliable experimental models existed for determining performance of DWHR systems under unequal flow rates at the time of publication, and the data used in this study were not available anywhere in the literature. Hence, the results of this study should be considered unreliable until more experimental results become available to validate the authors' claims.

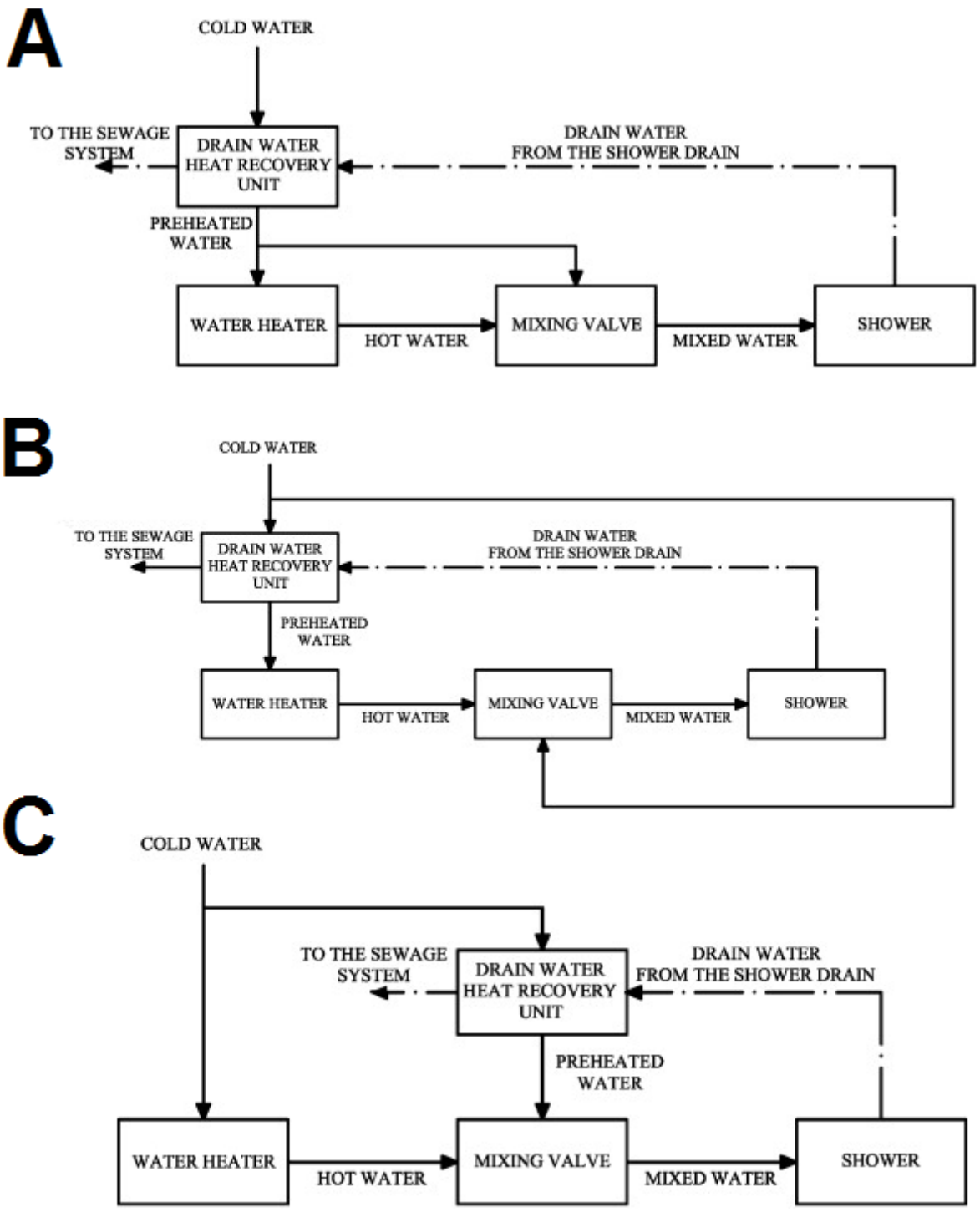

Figure 1-7 Schematics of configurations 1, 2 and 3, labeled as A, B and C respectively [16].

1.3.5 Study #5

Title: Heat Recovery from Wastewater using a Gravity-Film Heat Exchanger [17]

This study, conducted by the Oak Ridge National Laboratory, aimed to experimentally determine the feasibility of using a DWHR system by installing it in a single family home in Knoxville, Tennessee. The plumbing system was instrumented to measure the temperatures (T's) and flow rates (M's) at locations shown in Figure 1-8. This particular setup allowed the authors to investigate the impact of equal vs. unequal flow rates through the DWHR system on the energy savings. The results showed that the DWHR system was able to reduce the energy consumed for water heating by 50% under equal flow condition and between 30 to 45% under unequal flow conditions.

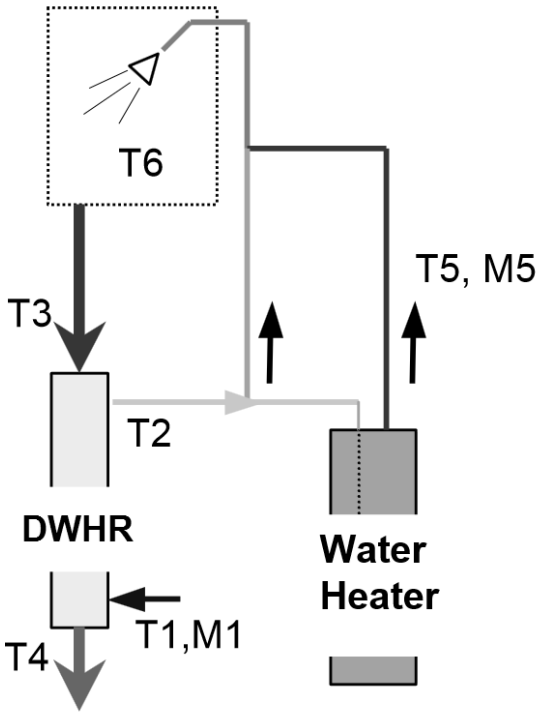

Figure 1-8 Schematic of locations where flow rates and temperatures were measured [17].

The study provided no information about the length and diameter of the particular DWHR system used. Other missing information include the duration of shower events, flowrates, instruments' uncertainties and plumbing system's thermal losses. It is also important to note that the data used in this study was produced in only one single household.

1.3.6 Study #6

Title: Energy Performance of a Drainwater Heat Recovery System [18]

This study, conducted by Schuitema et al., aimed to experimentally measure the potential savings associated with a DWHR system by installing it in a high performance residential dwelling in Netherlands. The DWHR system used in the study was 2 meters long with unspecified diameter and model. The plumbing system was instrumented to measure the temperatures (T's) at locations shown in Figure 1-9. The shower events had a flow rate of 5.5 liters per minute for 20 minutes, twice per day.

The results showed that on a weekly basis, the DWHR system reduced the energy required for domestic water heating by 29.6% under equal flow condition, and by 26.1% under unequal flow condition. It was also found that the DWHR system took up to 3 minutes to 'heat up' every time the shower was used. The water heater used in the dwelling was a gas-fired boiler which was noticed to behave unstably due to the fact that the inlet water was being preheated by the DWHR system. The instabilities caused the boiler's outlet temperature and flow rate to be unsteady, resulting in lower boiler efficiency.

No information was provided in the paper regarding the thermal losses in the plumbing system, the flow rates under unequal flow condition and the mains inlet water temperatures. One major source of error in the results produced in this study could be attributed to the fact that the temperatures were measured using thermocouples attached to the outside of the pipes. The mean flow temperature inside the pipes could be very different than what the thermocouples show on the outside of the pipes, creating a potential bias in all temperature measurements.

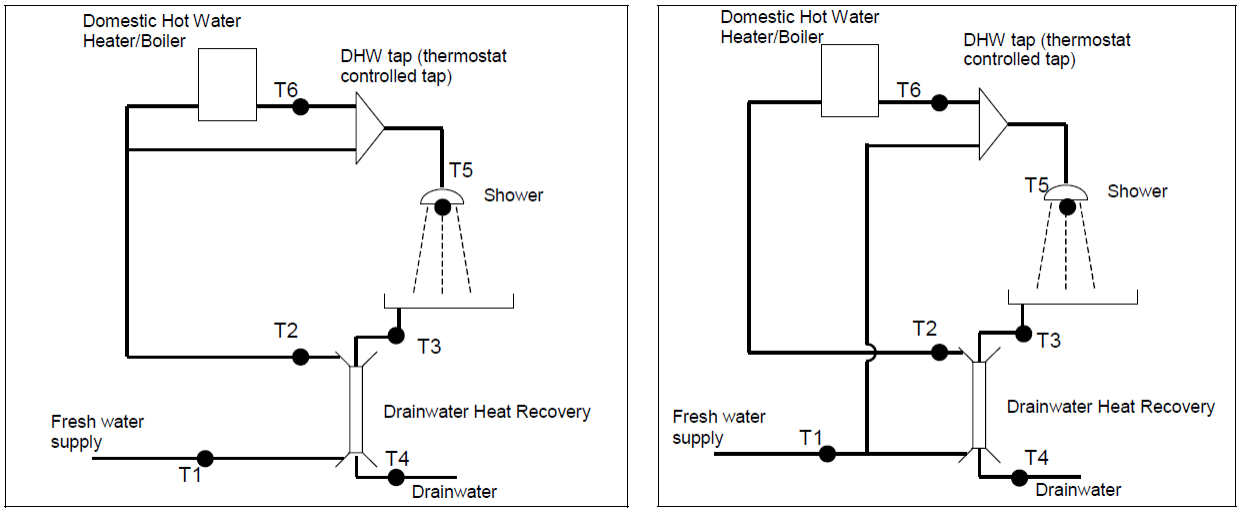

Figure 1-9 Plumbing schematics with the thermocouple locations marked for the equal flow (left) and unequal flow (right) configurations [18].

1.3.7 Author's Verdict

Most of the articles discussed previously focused on proving the feasibility of using DWHR systems to reduce energy consumption by monitoring performance in actual installations. None of these studies attempted to create correlations or models that would apply to systems other than what was used in their respective paper. This stems from the lack of theoretical and experimental models for DWHR systems. Only the study by Collins et al. [13] attempted to provide some fundamental understanding of how DWHR systems actually worked. This thesis aims to fill this gap in the literature by providing information about the performance of DWHR systems under various conditions.

It is imperative to clarify that this thesis is mainly focused on developing correlations based on experimental results and observations. Although theoretical correlations are useful to designers, experimental correlations are more practical for building simulation purposes. Theoretical modelling is briefly covered to introduce relevant concepts and notations. Detailed theoretical modelling is outside the scope of this thesis, and is among the topics for future theses on DWHR systems.

1.4 Topics Covered in This Thesis

The topics covered in this thesis are as follows:

- The apparatus built for testing DWHR systems.
- The performance of DWHR systems under equal flow conditions.
- The performance of DWHR systems under varying inlet water temperatures.
- The performance of DWHR systems under unequal flow conditions.
- The procedure to combine the developed correlations for predicting the heat transfer rates at any condition.

All analysis was conducted for steady-state conditions. Consideration of the transient behavior of DWHR systems was outside the scope of the current work. The models developed as a part of this thesis rely on existing performance data available to the manufacturers from CSA ratings. These models use the existing data to predict the heat transfer rate depending on flow rates and temperatures.

Chapter 2 Test Apparatus

2.1 Theory

DWHR systems are rated using the ε-*NTU* method [19]. By this method, the effectiveness, ε, is defined as the ratio of heat transfer, q, to the maximum heat transfer, q_{max} , which can occur in the heat exchanger. This effectiveness is expressed as:

$$\varepsilon = \frac{q}{q_{\max}} = \frac{C_c\left(T_{c,o} - T_{c,i}\right)}{C_{\min}\left(T_{h,i} - T_{c,i}\right)} = \frac{\left(\dot{m}C_p\right)_c\left(T_{c,o} - T_{c,i}\right)}{\left(\dot{m}C_p\right)_{\min}\left(T_{h,i} - T_{c,i}\right)} = \frac{C_h\left(T_{h,i} - T_{h,o}\right)}{C_{\min}\left(T_{h,i} - T_{c,i}\right)} = \frac{\left(\dot{m}C_p\right)_h\left(T_{h,o} - T_{h,i}\right)}{\left(\dot{m}C_p\right)_{\min}\left(T_{h,i} - T_{c,i}\right)} \quad (2.1)$$

In the above equation, C represents the heat capacity rate, $\dot{m}$ represents the mass flow rate, C_p represents the specific heat and T represents the temperature. The subscripts c and h refer to the cold mains-side and hot drain-side respectively. The subscripts i and 0 refer to the inlet and outlet. Lastly, the subscript *min* refers to the lesser of C_c and C_h .

This equation is used to quantify the effectiveness of a DWHR system under equal flow conditions, when the hot water flows through the drain-side at the same time as cold water is drawn though the mains-side. By assuming that C_p does not change significantly across the DWHR system, it can be said that:

$$\left(\dot{m}C_p\right)_h = \left(\dot{m}C_p\right)_c = \left(\dot{m}C_p\right)_{min} = \dot{m}C_p \quad (2.2)$$

Hence, a DWHR system's effectiveness can be determined using:

$$\varepsilon = \frac{\left(T_{c,o} - T_{c,i}\right)}{\left(T_{h,i} - T_{c,i}\right)} = \frac{\left(T_{h,i} - T_{h,o}\right)}{\left(T_{h,i} - T_{c,i}\right)} \quad (2.3)$$

Equation 2.3 reduces the complexity of determining a given system's effectiveness to a simple ratio of the inlet and outlet water temperatures.

Since the purpose of DWHR systems is to preheat the cold water, the effectiveness is always calculated based on the mains-side temperatures as shown in equation 2.4.

$$\varepsilon = \frac{\left(T_{c,o} - T_{c,i}\right)}{\left(T_{h,i} - T_{c,i}\right)} \tag{2.4}$$

Equation 2.4 is mandated for rating DWHR systems according to CSA standard B55.1-12 [9]. Except for tests done under unequal flow rates, Equation 2.4 is used for all effectiveness calculations throughout this thesis for consistency with the standards.

2.2 Test Apparatus

In order conduct research on DWHR systems based on the theory described above, a test apparatus had to be designed and constructed. The backbone of the system was construted by co-op student Ivan Beentjes who deserves credit for building and programming the entire test rig with the exception of its modes of operation under unequal flow rates.

2.2.1 Design Criteria

The test platform had to have the following features:

1) Delivery of water at a prescribed temperature, representative of those found in real world applications. The cold water between the range of 5-20°C, the hot between 20-50°C.

2) Stable delivery of volumetric flow rate on both sides of the DWHR system from 2-25 L/min.

3) Automated data acquisition.

4) Engineering uncertainty to less than 1% of effectiveness, full scale, at conditions meeting CSA requirements.

5) Meets CSA requirements in all ways [9]. This includes location of instrumentation, ambient temperature, installation characteristics, test stability etc.

It was decided to build a closed, pump driven system. This ensured that the system had stable flow and the appropriate temperatures for the inlet water were not climate dependent. Figure 2-1 through Figure 2-4 depict the schematic design of the system under different modes of operation, where the greyed out portions are the sections of the system that are not involved in a given operation. A photograph of the system is presented in Figure 2-5. Specific aspects of the design will be described in the sections which follow.

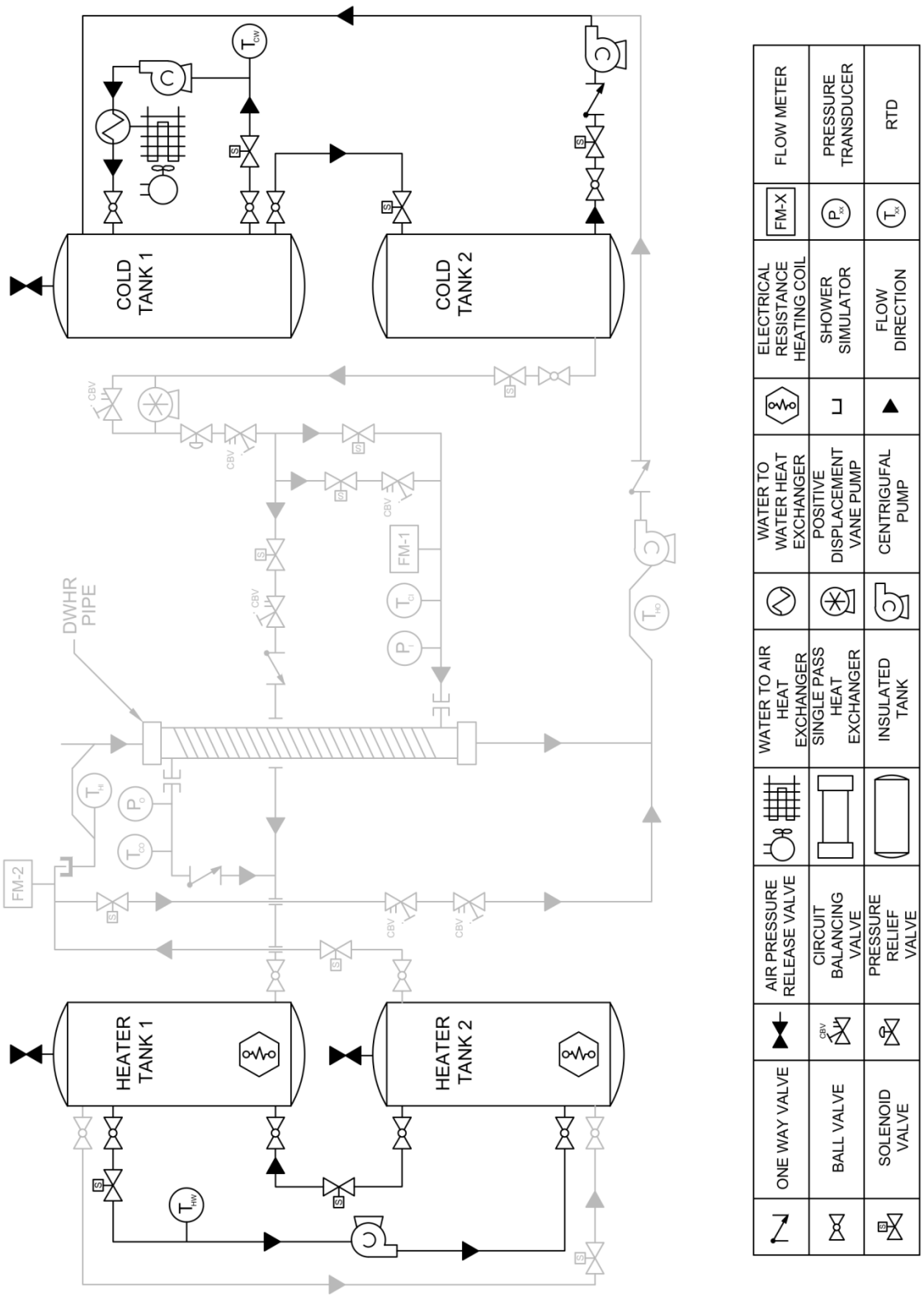

Figure 2-1 Main diagram of the plumbing configuration for DWHR apparatus operating under 'conditioning mode'. The greyed out portions are the sections of the system that are not included in a given operation.

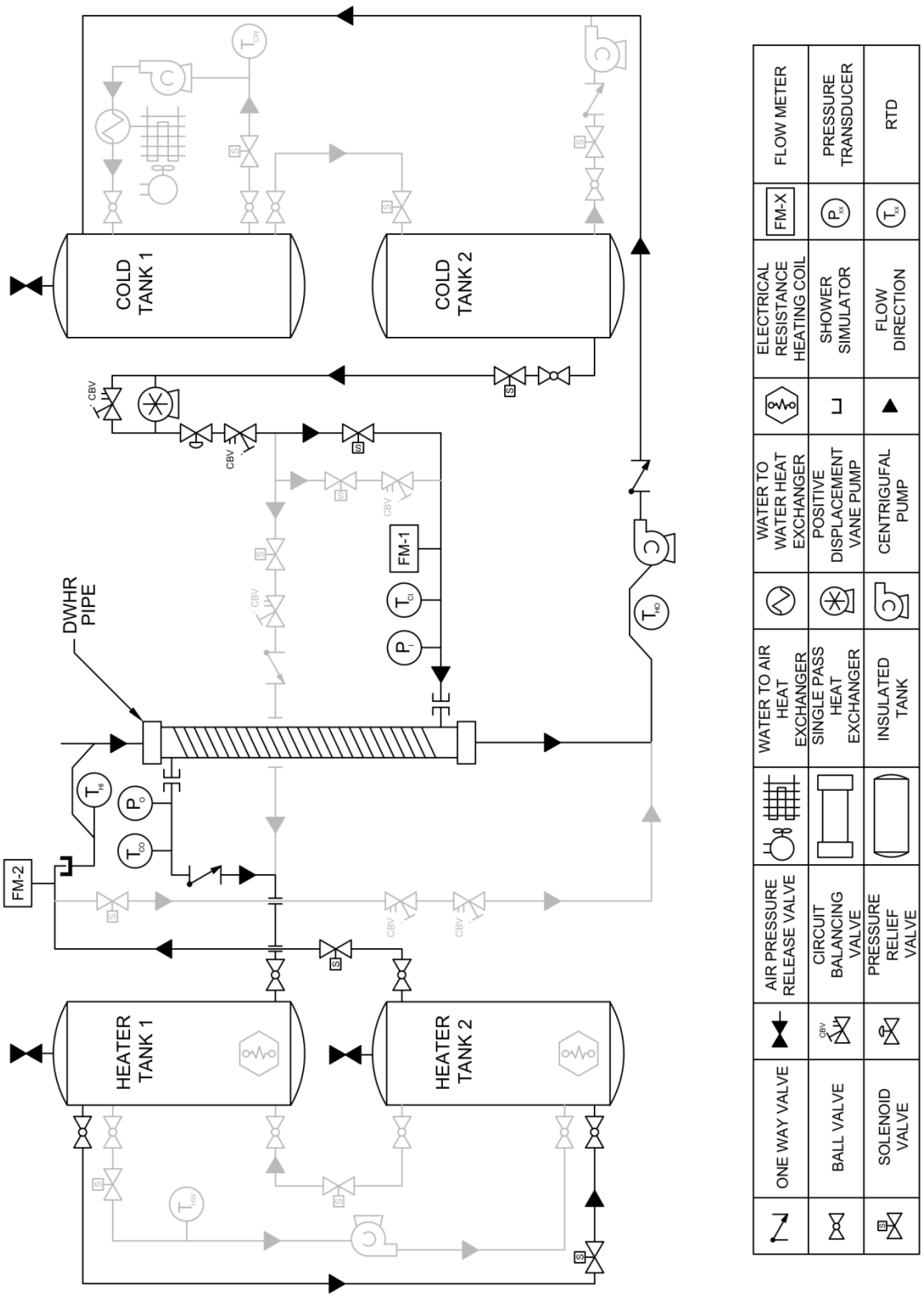

Figure 2-2 Main diagram of the plumbing configuration for DWHR apparatus operating under 'equal flow mode'. The greyed out portions are the sections of the system that are not included in a given operation.

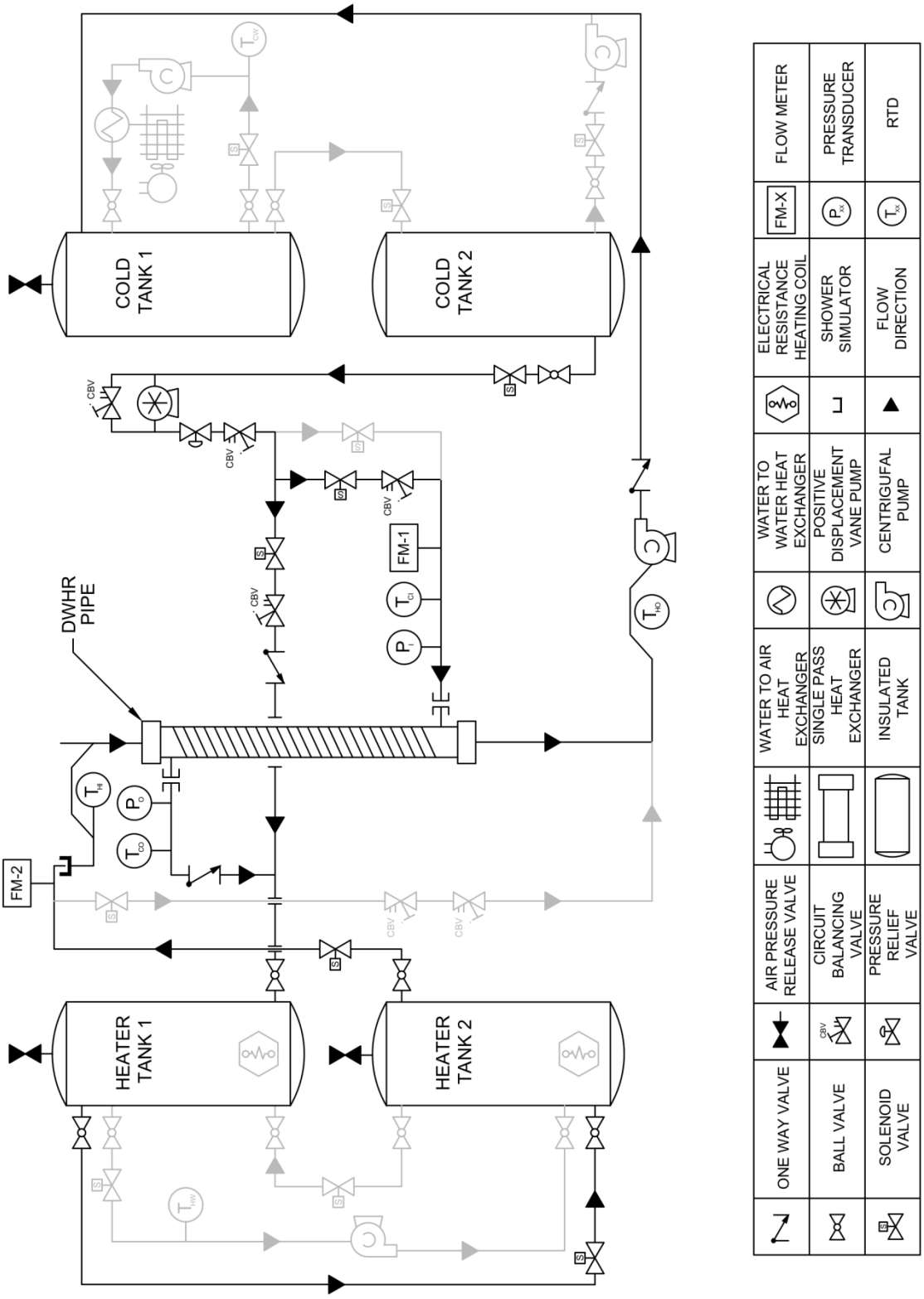

Figure 2-3 Main diagram of the plumbing configuration for DWHR apparatus operating under 'variable cold flow rate mode'. The greyed out portions are the sections of the system that are not included in a given operation.

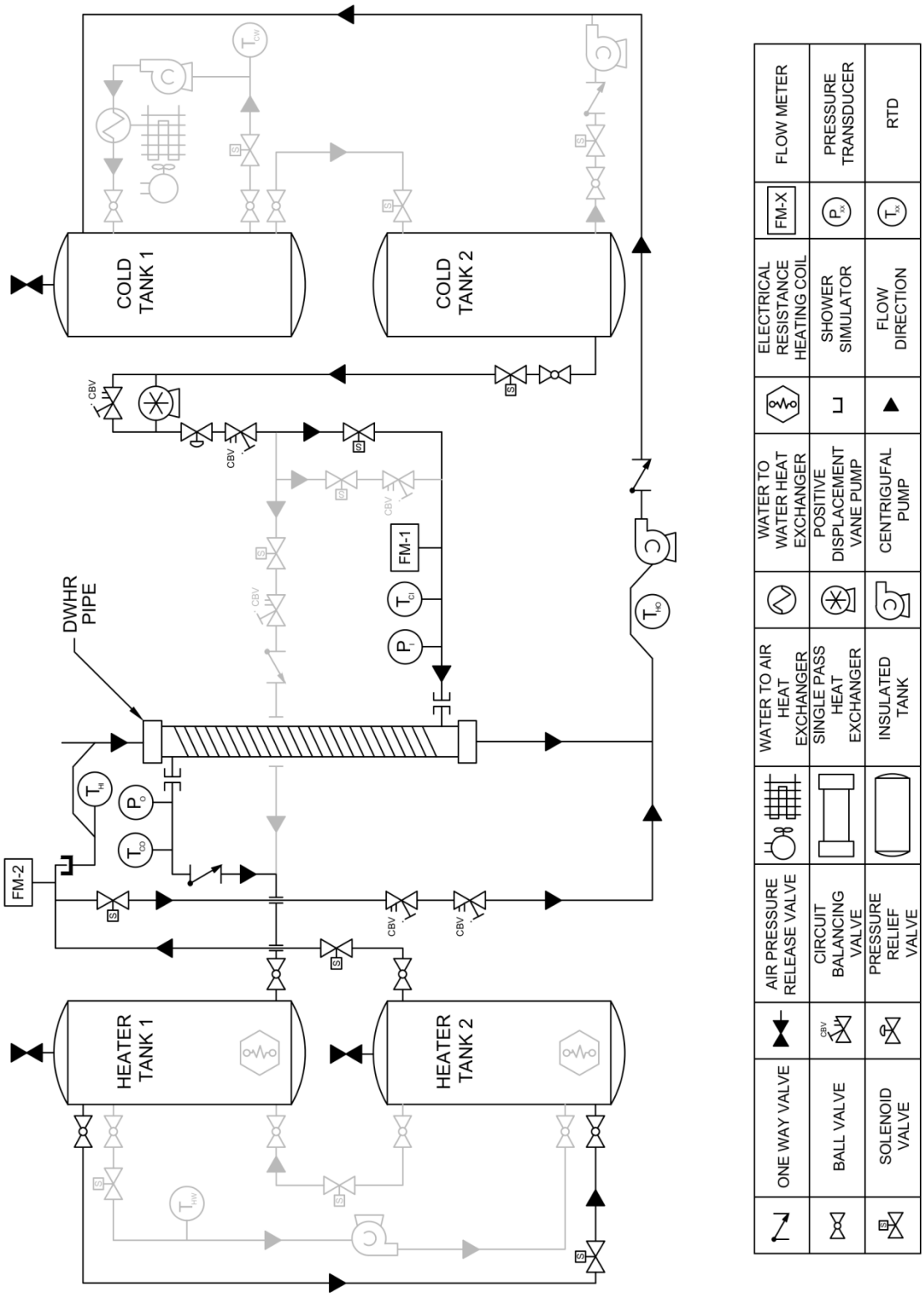

Figure 2-4 Main diagram of the plumbing configuration for DWHR apparatus operating under 'variable hot flow rate mode'. The greyed out portions are the sections of the system that are not included in a given operation.

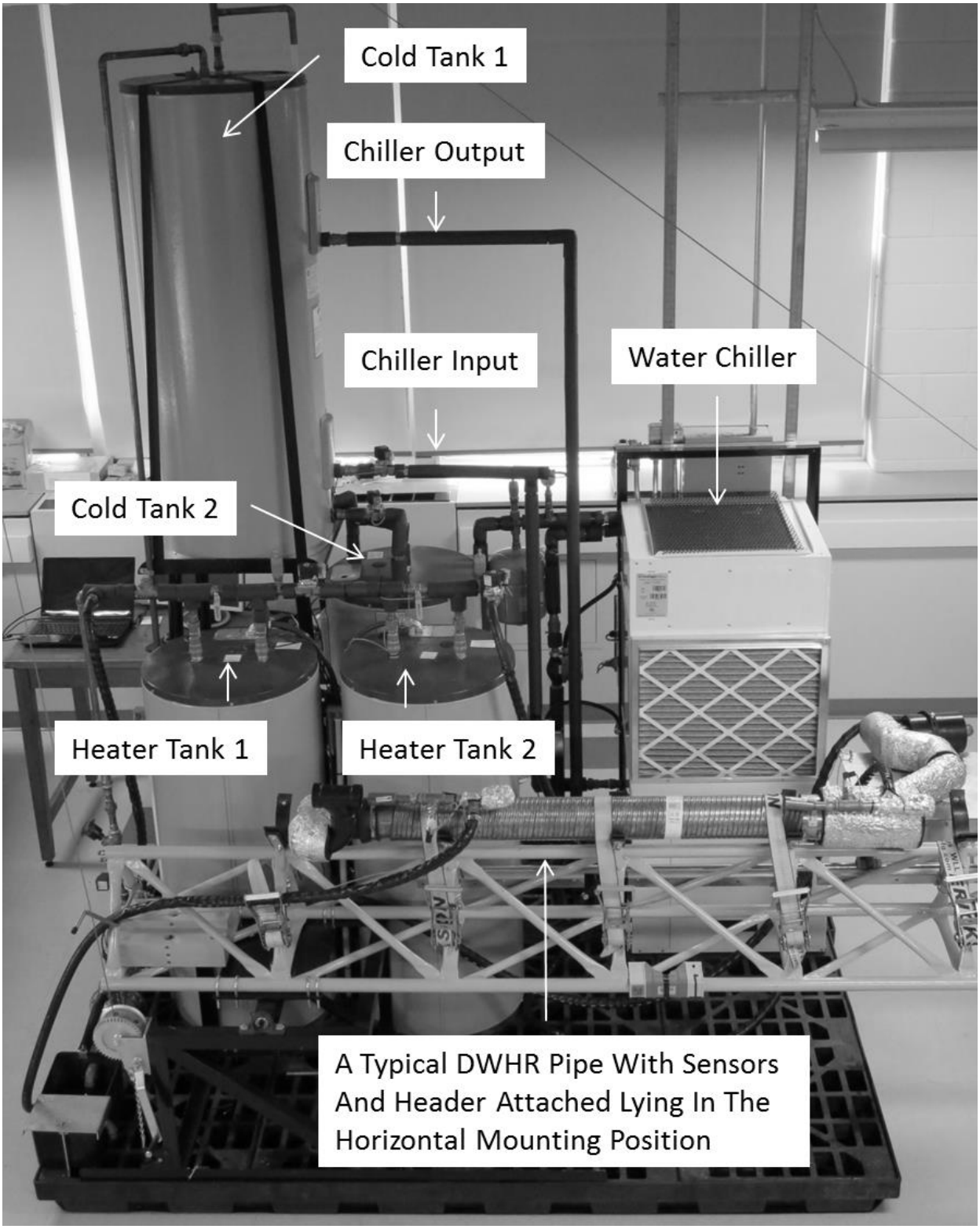

Figure 2-5 The DWHR apparatus with the main pivoting arm and DWHR pipe in the horizontal mounting position.

2.2.2 Description of the Apparatus

This description of components uses the schematic from Figure 2-1 to sequentially move through the components.

To perform a test, the water entering either side of the DWHR system must be chilled and heated to predetermined temperatures. Cold water for the test is chilled by a 10.5 kW (36000 Btu/h) water-to-water heat exchanger, and then the extracted heat is expelled by a 10 kW (34000 Btu/h) water-to-air heat exchanger. The chilled water circulates through Cold Water Tank 1, a 284-liter insulated tank, gradually dropping the temperature to the pre-set cold-side temperature. The chilling system can drop the water to its freezing point. Freshly chilled water is pumped into the very top of Cold Water Tank 1, through a modified 90° angled pipe, and then extracted from the bottom of the tank (see Figure 2-6). This configuration utilizes the tendency of the cold water to sink to maximize the overall stirring effect. Much attention was given to achieving a stable temperature throughout the tank, due to the effect of temperature measurements on ε. Once the desired temperature is reached, the chilling system shuts off, and a volume of water sufficient in amount to run a test is released into the second 184-liter cold-water tank, giving the cold water a further mixing (see Cold Water Tank 2 in Figure 2-1).

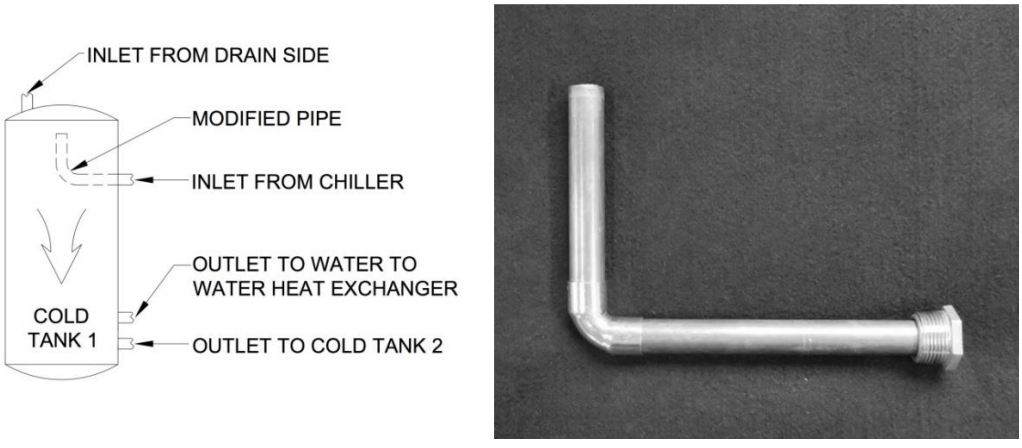

Figure 2-6 Diagram of the water flow in Cold Tank 1, and the modified pipe used to direct the cold water from the chiller to the very top of the tank.

On the hot side, the water is heated in two hot-water tanks by 4.5 kW electrical resistance elements at the bottom of each tank. To equalize the temperature between the two tanks, a circulator pump draws hot water from the top of one heater tank and inputs it into the bottom of the second tank. An 'open' line equalizes the pressure difference between the two tanks using the same principle. This mixing action is amplified by the warmer water rising to the top of the tank in conjunction with the currents of hot water rising from the heating elements (see Figure 2-7).

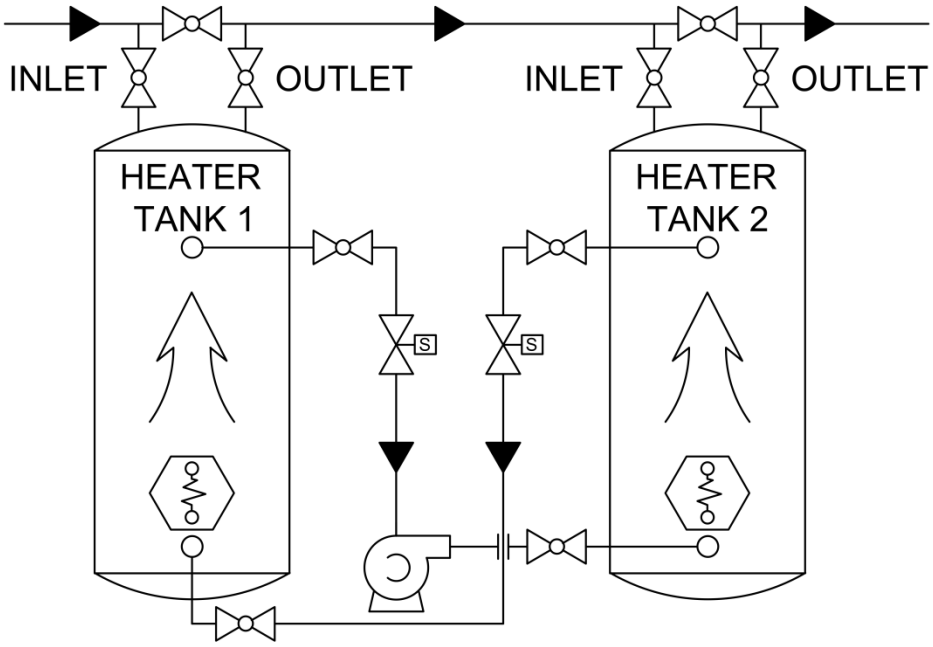

Figure 2-7 Diagram of the water flow in Heater Tanks 1 and 2.

To achieve equal flow, a single vane pump drives the water through the entire system. This positive displacement pump stabilizes the water flow despite the range of lengths of DWHR systems. The conditioned cold water, after being drawn by the vane pump, from Cold Tank 2, passes through the mains-side of the DWHR system. After exiting the top of the DWHR system, the water enters the bottom of Heater Tank 1, and leaves from the top. The same configuration applies to Heater Tank 2. Upon exiting Heater Tank 2, it drops down through the DWHR system's drain-side. This configuration prevents significant mixing of the conditioned hot water, and the water entering the hot water tanks

from the DWHR system, and allows for a constant temperature supply of hot water to the drain-side of the DWHR system. The water is finally collected below the DWHR system and sent to Cold Tank 1 for conditioning, completing the circuit of the system.

The CSA standard requires testing at multiple flow rates; however, since the positive displacement pump cannot be regulated to change its output, a bypass was built into the system. The given bypass simply feeds some of the pump's output flow back into its input. Minor adjustment of a circuit balancing valve is needed during each test to achieve desired flow rates. Metering of the hot and cold water flows is done by two turbine flow meters with an accuracy of ±1% of reading [20].

For tests conducted under unequal flow conditions, the same positive displacement pump is used to achieve different flow rates on both sides without the assistance of any additional pumps. This is done using different bypasses to allow different volumes of water to flow through the drain-side and the mains-side, as was shown in the schematics in Figure 2-3 and Figure 2-4. These flow rates are adjusted using circuit balancing valves.

The system's cold mains side temperature and pressure sensors are mounted right at the inlet connection to a given DWHR system (see Figure 2-8). Water temperatures are measured throughout the system by an ISO 19025 calibrated/certified RTD whose accuracy is ± 0.03 to 0.08℃ [21]. A conservative worst case accuracy of $\pm$ 0.1℃ is used when measuring temperature. Water pressure is measured at the cold mains water input and output on a DWHR system. They are measured by ISO 19025 calibrated/certified pressure transducers which have an accuracy of 0.25% full scale [22].

Table 2-1 The DWHR apparatus' parameters and sensors

Parameter	Operating Range	Accuracy
RTD Probes	0-100 °C	± 0.1 °C
Temperature of Cold-side	0-20 °C	± 0.1 °C
Temperature of Hot-side	20-50 °C	± 0.1 °C
Cold Water Flow Meter	2.8-28 L/min	± 1% Reading
Hot Water Flow Meter	2.8-28 L/min	± 1% Reading
Pressure Transducer	0-100 psig	± 0.25% FS

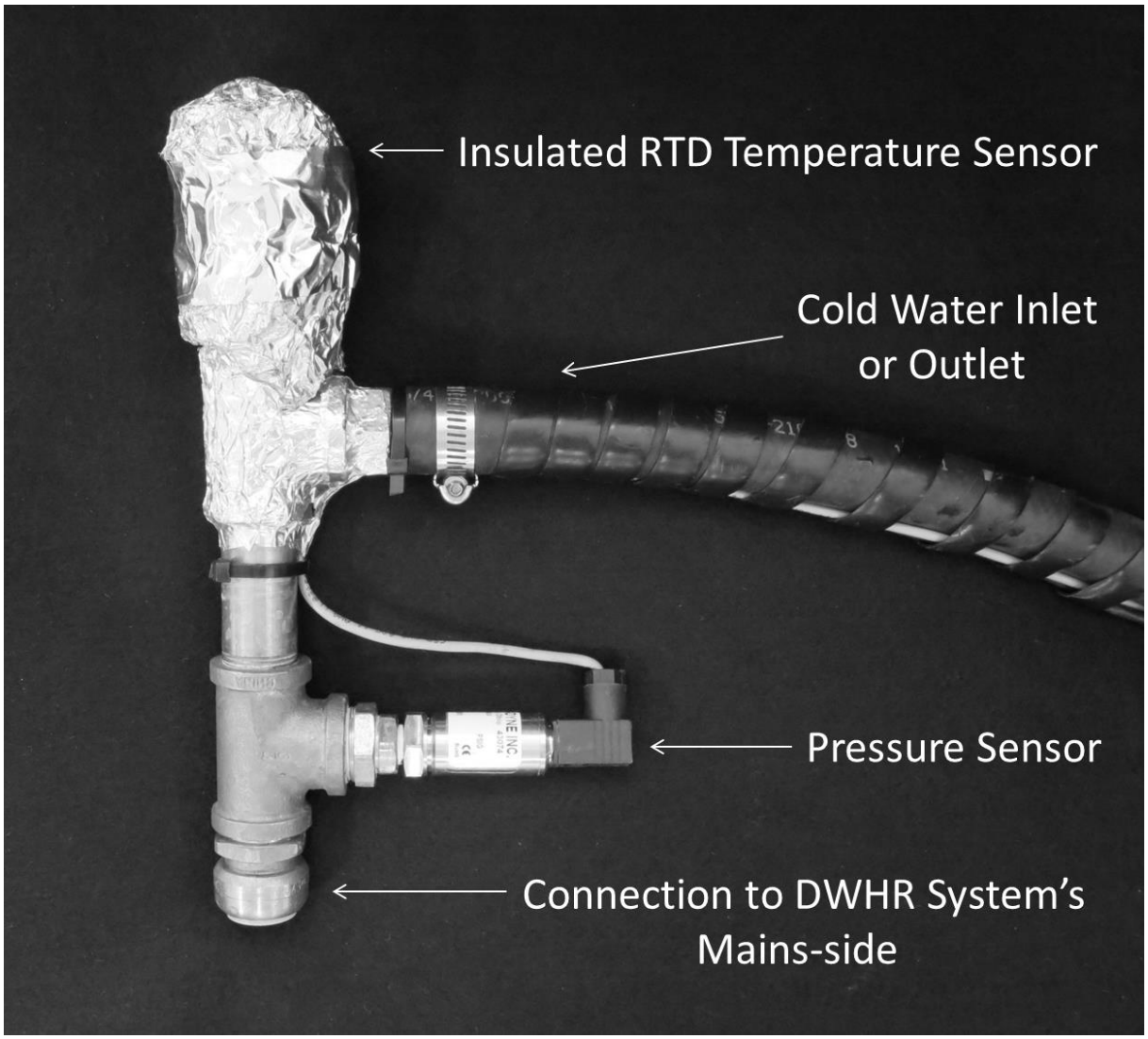

Figure 2-8 One of the two identical sensor bearing units mounted on a DWHR system's mains-side input and output.

The ABS pipe that connects to the DWHR system's hot water drain-side input is called the *header*. An open to atmosphere water line (simulating a drain) channels the hot water from the heater tanks into an insulated trap where the temperature is measured. The water exits the trap into a Tee connected to the DWHR system. This header was built to the specifications given by the CSA standard which stipulates "*The vertical straight distance from the bottom of the …DWV Tee… to the DWHR shall be 750±50mm.*" [9]. Three headers were built with diameters of 5.1, 7.6, and 10.2cm to allow testing of all DWHR systems available. All headers were insulated similar to what is shown in Figure 2-9 to minimize thermal losses.

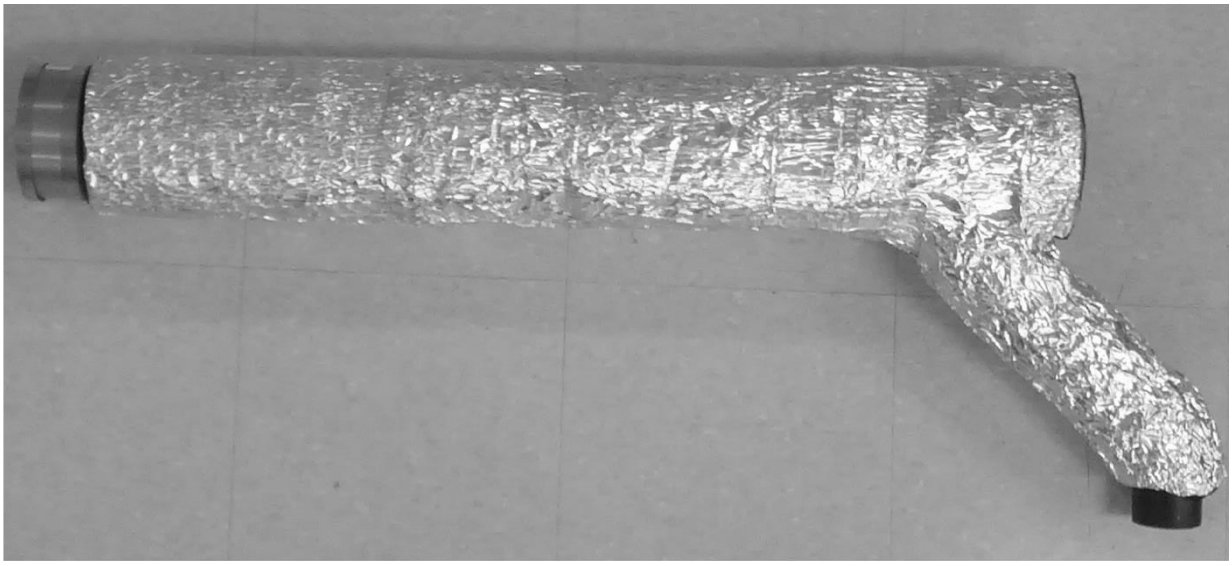

Figure 2-9 The 10.2cm diameter ABS header covered in insulation to minimize thermal losses.

Hot water exiting the DWHR pipe is collected and its temperature measured in another insulated trap. Finally, the water enters a catch basin from which it is returned to the main cold-water tank.

Realizing water spills would occur during operation of the DWHR apparatus, a series of chemical catchment platforms were connected together to form a single base capable of holding 551 liters. The DWHR apparatus rests on top of this foundation as shown in Figure 2-10.

Figure 2-10 Containment platforms installed beneath the test apparatus to prevent water spillage onto the floors.

Operation by a single technician, even with systems of 366cm in length weighing up to 40 kg was achieved by constructing a pivoting arm on which a DWHR system could be placed while lying in the horizontal mounting position (see Figure 2-5). Once a DWHR system was secured in place, the arm could then be winched into the vertical testing position. Other amenities such an adjustable board on which the sensors and DWHR system header are attached were affixed to the arm. To reduce the risk of accidents, counter weights, safety locks and a safety factor of ten, for cables and bolts, were incorporated into the arm's manufacture.

Customized software controls the entire system and records the data. A variety of safeguards including automatic pressure, temperature, time and pump cut-offs were incorporated to protect the test apparatus. The user selects a test from a drop down menu and then watches the test running to determine when sufficient data on the system's performance, after reaching steady state, has been collected. Over this period of time, the flow rates and temperatures for the cold and hot water are recorded. The inlet and outlet pressures for the cold water are also measured to determine the total pressure drop across the DWHR system.

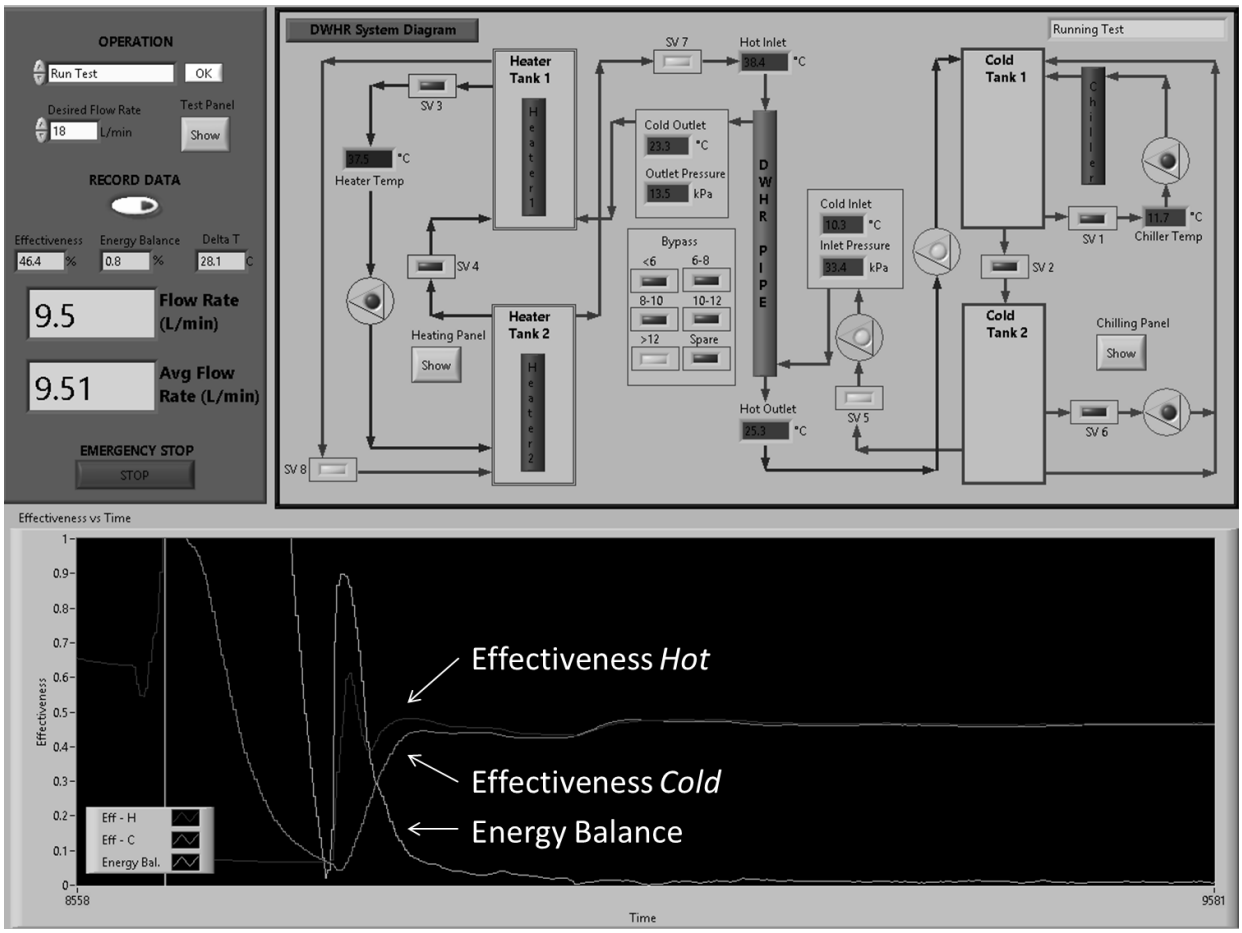

Figure 2-11 The LabView interface used by the operator to run a test at a chosen flow rate. This screen shot is the plot of a 9.5 L/min test on a 10.2cm diameter DWHR system.

In Figure 2-11, the 'effectiveness *hot'* represents the effectiveness, ε, calculated using the hot water side of the DWHR system. The 'effectiveness *cold'* represents the effectiveness based on the cold water side. The 'Energy balance' is the expression for the difference between the two effectiveness values, with zero being the ideal. The displayed effectiveness' show an initial period of adjustment while a given test comes to steady state. The last third of the graph displays what is considered steady state. Once this steady state has been reached, the operator can start recording the data by pressing the button called "Record Data" on the user interface. By doing so, the temperatures, pressures and flow rates for the duration of the test will be recorded in an Excel file for data processing.

Chapter 3 Performance of DWHR Systems under Equal Flow Conditions

3.1 Introduction

DWHR systems are typically installed in basements, with the drain water flowing downward inside the drain stack, and the mains water moving upward from the basement to the fixtures upstairs. Therefore, it is logical to install these systems under counter-flow arrangement. It is also widely known that a heat exchanger operating under counter-flow arrangement would outperform the same heat exchanger operating under parallel-flow arrangement for all values of C_{min}/C_{max} [19]. A typical installation for DWHR systems is displayed in Figure 3-1 [23].

Figure 3-1 A DWHR system connected to a tankless water heater in a basement [23].

A study by Collins et al. [13] investigated the performance of DWHR systems under parallel-flow and counter-flow arrangements. The results of the study showed that DWHR systems tested under counter-flow arrangement outperform the same systems tested under parallel-flow arrangement. The general characteristic effectiveness curves as a function of flow rate for different flow arrangements were previously provided in Figure 1-4 [13].

Manufacturers require DWHR systems to be installed under a counter-flow arrangement [10,11,12]. As a result of the factors stated thus far, this thesis only focuses on this arrangement.

As was mentioned previously, DWHR systems are rated according to the CSA standard B55.1-12 [9]. This standard requires the effectiveness of DWHR systems to be measured at equal flow rates of 5.5, 7.0, 9.0, 10.0, 12.0 and 14.0 liters per minute (LPM). This range covers the typical flow rates associated with showerheads in a residential building.

Designers have shown interest in using DWHR systems for applications other than houses; however, the lack of information about the performance of such systems at flow rates other than the ones listed by the CSA has made it difficult to justify utilization of DWHR systems. The characteristic effectiveness curve for a DWHR system can be divided into three regions based on flow rates; the low flow range, the CSA range and the high flow range (Figure 3-2).

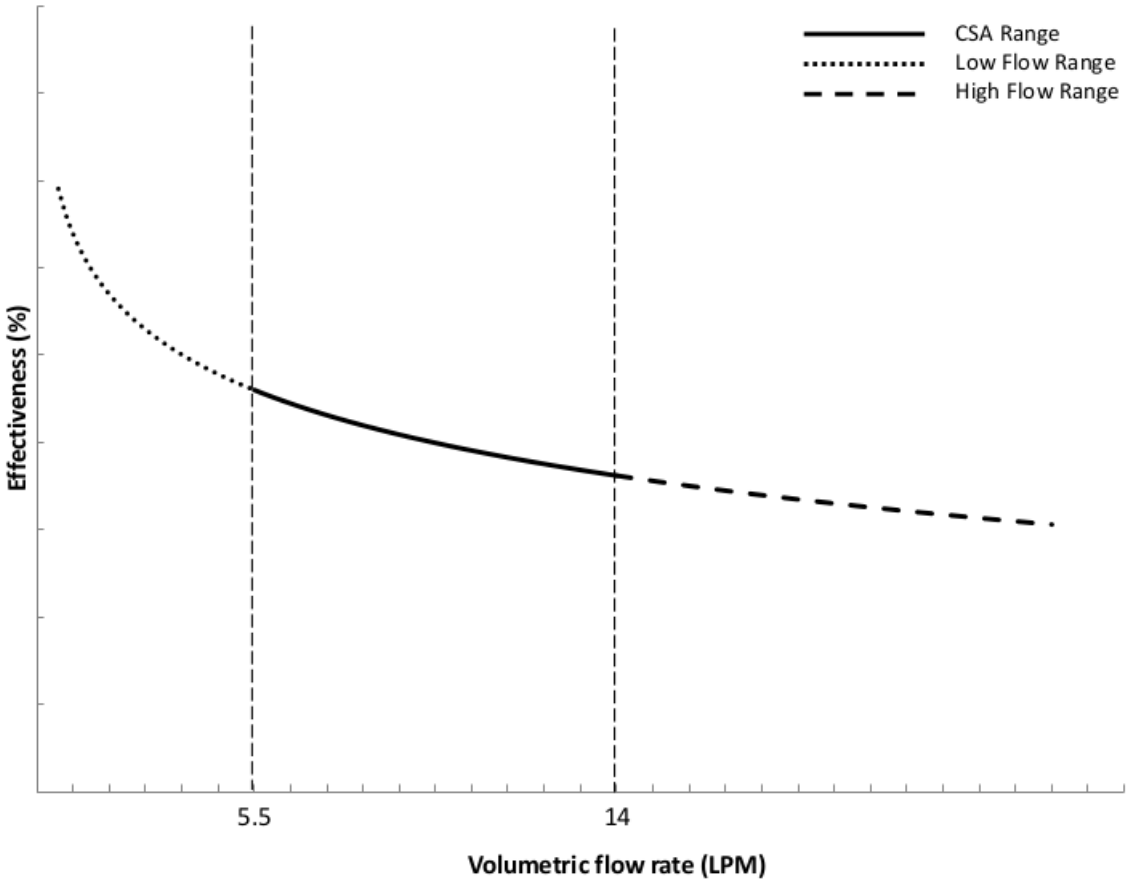

Figure 3-2 Characteristic effectiveness curve divided into different regions based on flow rate.

This Chapter investigates the performance of systems in the specified ranges and attempts to come up with a method to extrapolate the CSA data to predict the performance of DWHR systems at various flow rates. First, the phenomena that occur at different flow regions are studied in Section 3.2 and general conclusions are made about the low flow rate region. Next, the flow rates within the CSA range and higher are studied in Section 3.3. Each section has its own set of experiments.

3.2 Flow Behaviors and Hysteresis[1]

A DWHR system can be classified as a concentric tube heat exchanger. Given this, and the fact that DWHR systems are rated under equal flow rate conditions, it can be shown that the effectiveness of a DWHR system could be expressed as a function of NTU [19]:

$$\varepsilon = \frac{NTU}{1+NTU} \tag{3.1}$$

where NTU represents the number of transfer units and is defined as:

$$NTU = \frac{UA}{\dot{m}C_p} \tag{3.2}$$

Here, U represents the overall heat transfer coefficient and A is the heat transfer area [19]. Combining, Equation 3.1 becomes:

$$\varepsilon = \frac{\frac{UA}{\dot{m}C_p}}{1+\frac{UA}{\dot{m}C_p}} = \frac{UA}{\dot{m}C_p+UA} = \frac{UA}{\rho C_p \dot{V}+UA} \tag{3.3}$$

where $\dot{V}$ is the volumetric flow rate.

In fundamental texts, the *NTU*s for a given heat exchanger is assumed to be constant. This, however, is usually not the case. In reality, the *UA* product for DWHR systems has been seen to vary significantly with flow rate [13], and in the case of DWHRs, with the wetted area of the drain-side film. At high drain-side flow rates, the entire interior surface of the drain-pipe will be covered by a falling film, while at low flow rates, the falling film may never form. When the area covered by the falling film of water is less than the overall inner surface area of the pipe, will be referred to as *partial wetting*. *Full wetting* occurs when the entire inner surface area of the pipe is covered by a film of falling hot water. It is further

[1] The contents of this section have been published and are available under the following reference: Ivan Beentjes, Ramin Manouchehri, and Michael R. Collins, "An investigation of drain-side wetting on the performance of falling film drain water heat recovery systems," Energy and Buildings, vol. 82, no. October, pp. 660-667, October 2014.

noted that even when fully wetted, the falling film may not be uniformly distributed. The *UA* product will vary significantly with wetting, and this should be apparent in the characteristic performance curve for the DWHR system.

The theoretical characteristic behavior is shown in Figure 3-3. At high flow rates, the quantity of water is sufficient to cover the entire inner surface of the drain pipe, keeping the wetted area constant. This range of high flow rates will be referred to as the *stable full wetting* region. Conversely, very low flow rates only allow a small trickle of water to stream down the pipe. Since the flow rate is so low, the area covered by the steam of water remains constant. This range of low flow rates is referred to as the *stable partial wetting* region. Between these two regions of *stable full wetting* and *stable partial wetting*, there will be a *transition region*. In this region, the flow rate of water is not high enough to cover the entire surface area of the pipe, nor is the flow rate low enough to be limited to a single stream of water traversing down the pipe. The wetted area would differ from test to test, even at the same flow rate, depending on the path the water takes. Then, within the transition region, tests would generate a range of different effectiveness values, depending on the area covered in water.

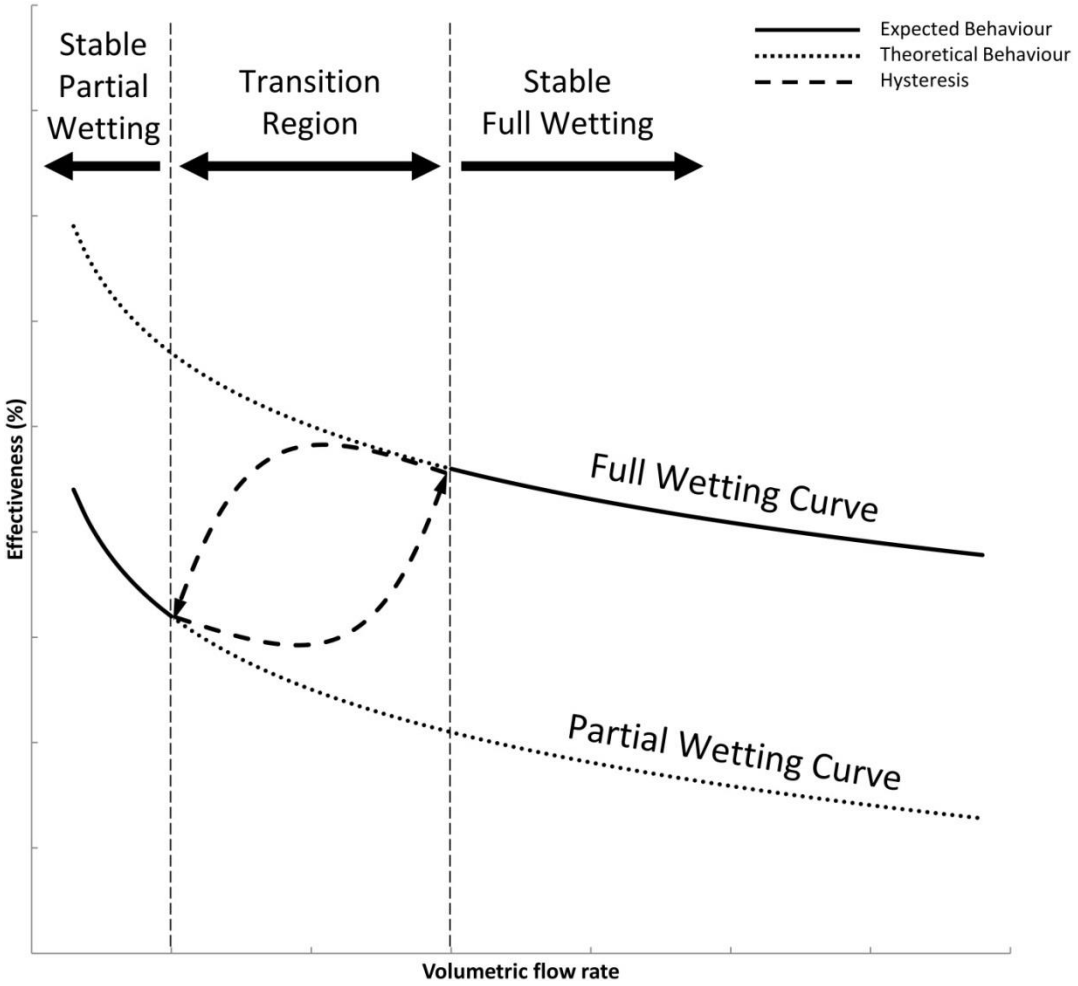

Figure 3-3 The anticipated effect of the three regions: stable partial wetting, stable full wetting, and the transition region on the effectiveness of a DWHR system. These regions would change depending on the diameter of the DWHR system.

A transition region between *stable partial wetting* and *stable full wetting* implies hysteresis. Conditions occurring shortly before a test reaches a steady wetted area might have a direct bearing on the test. For example, an area covered by water at the current flow rate could depend on the area that was covered with water shortly before. Presumably, due to the hydrophobic nature of copper, the wetted area would be greater if the test was begun at a high flow rate and then reduced to a desired flow rate. Conversely, if the test was started at a very low flow rate and then increased to the same desired flow rate the wetted area would be smaller.

3.2.1 Method

To generate experimental data, three 122cm long DWHR systems of the same design were selected. Their diameters were the standard 5.1, 7.6 and 10.2cm (2, 3, and 4 in). The tests were performed at flow rates ranging from 2 to 25 LPM. Three test procedures were used:

1) HLR (High-to-Low) was to start the experiment at a relatively high flow rate of 20 LPM, and then reduce it to the lower flow rate of the test. The intent was to establish a fully wetted drain-side film, and then observe when irregularities occurred.
2) LHR (Low-to-High) was to start at a flow rate of about 2 LPM, and then increase it to the required higher flow rate. The intent here was to encourage partial wetting of the drain-side film, and then observe when full wetting occurred.
3) FW (Maximum) involved the use of an *insert* at the drain-side that encouraged full wetting of the drain-side film. Here, maximum drain-side performance was being established.

An attempt will be made to take photographs of the falling-film flow inside the drain pipe for the wetting conditions depicted in Figure 3-3.

3.2.2 Results

A camera was installed at the outlet of the 7.6 cm diameter DWHR system to observe the flow within the drain pipe. Full wetting region, partial wetting region and the transition region were each photographed.

A photograph of the full wetting region is presented in Figure 3-4. The inside diameter of the drain pipe was fully covered by the falling film, which implies that the heat transfer area was likely at maximum, as was intended by the designers.

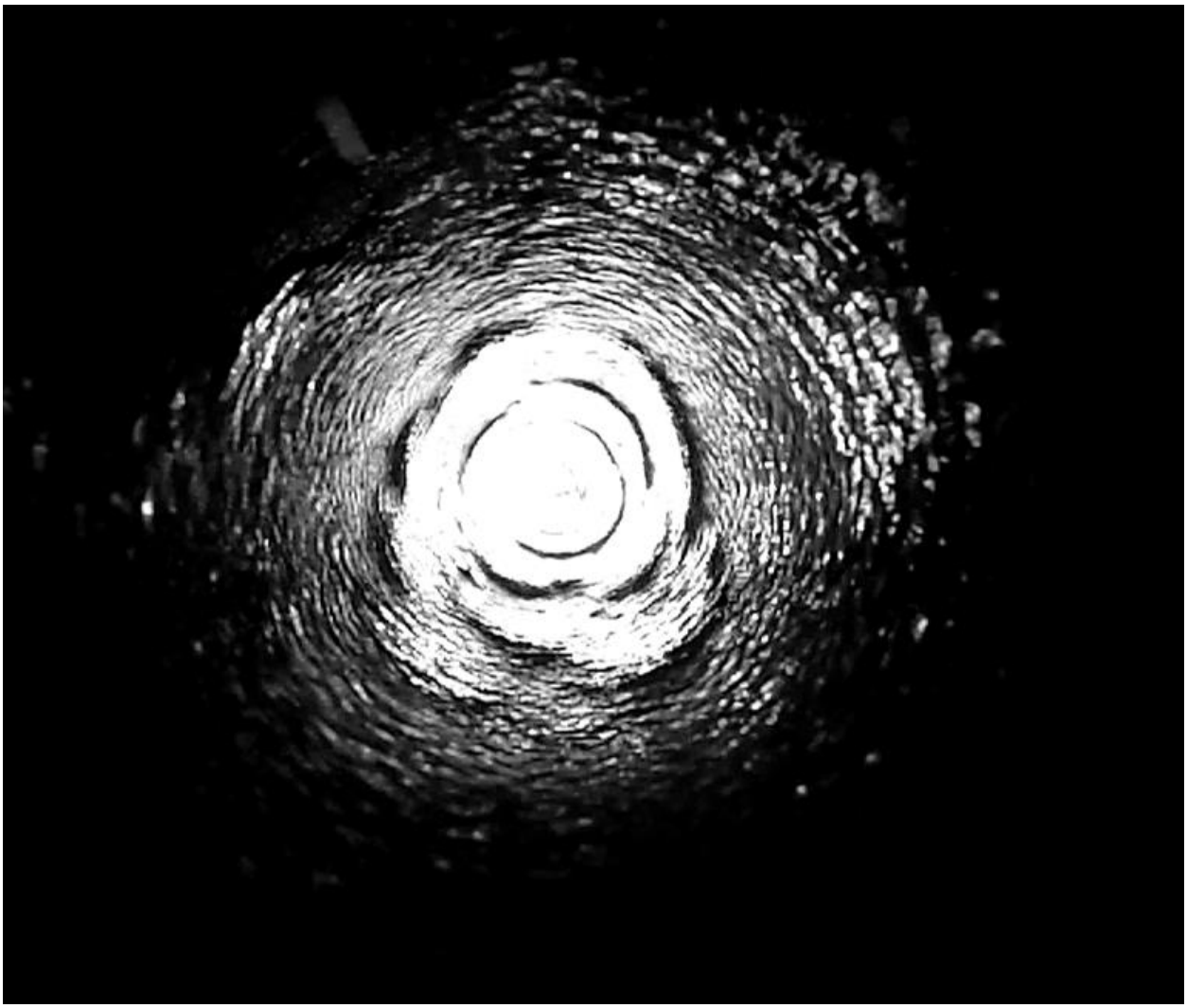

Figure 3-4 Full wetting of the drain pipe observed inside a 7.6cm diameter DWHR system at a flow rate of 9 LPM.

A photograph of the system at a low flow rate of 2.0 LPM is presented in Figure 3-5. Only one small stream of water was visible in drain pipe which significantly reduced the heat transfer area. This is the reason why DWHR systems perform poorly at very low flow rates. The stream of water did not grow in size for the duration of the test, which resulted in a relatively constant effectiveness reading.

Figure 3-5 Stable partial wetting of the drain pipe observed inside a 7.6cm diameter DWHR system at a flow rate of 2 LPM.

A photograph of the transition region is shown in Figure 3-6. In this region, the flow rate of water was neither sufficient to cover the entire drain pipe, nor low enough to form one stable stream. Instead, multiple unstable streams of water were observed. These streams would join or detach at random, constantly changing the heat transfer area inside the drain pipe. This wetted area differed from test to test, even at the same flow rate, depending on the path the water took. As a result, the effectiveness readings from the system were unsteady.

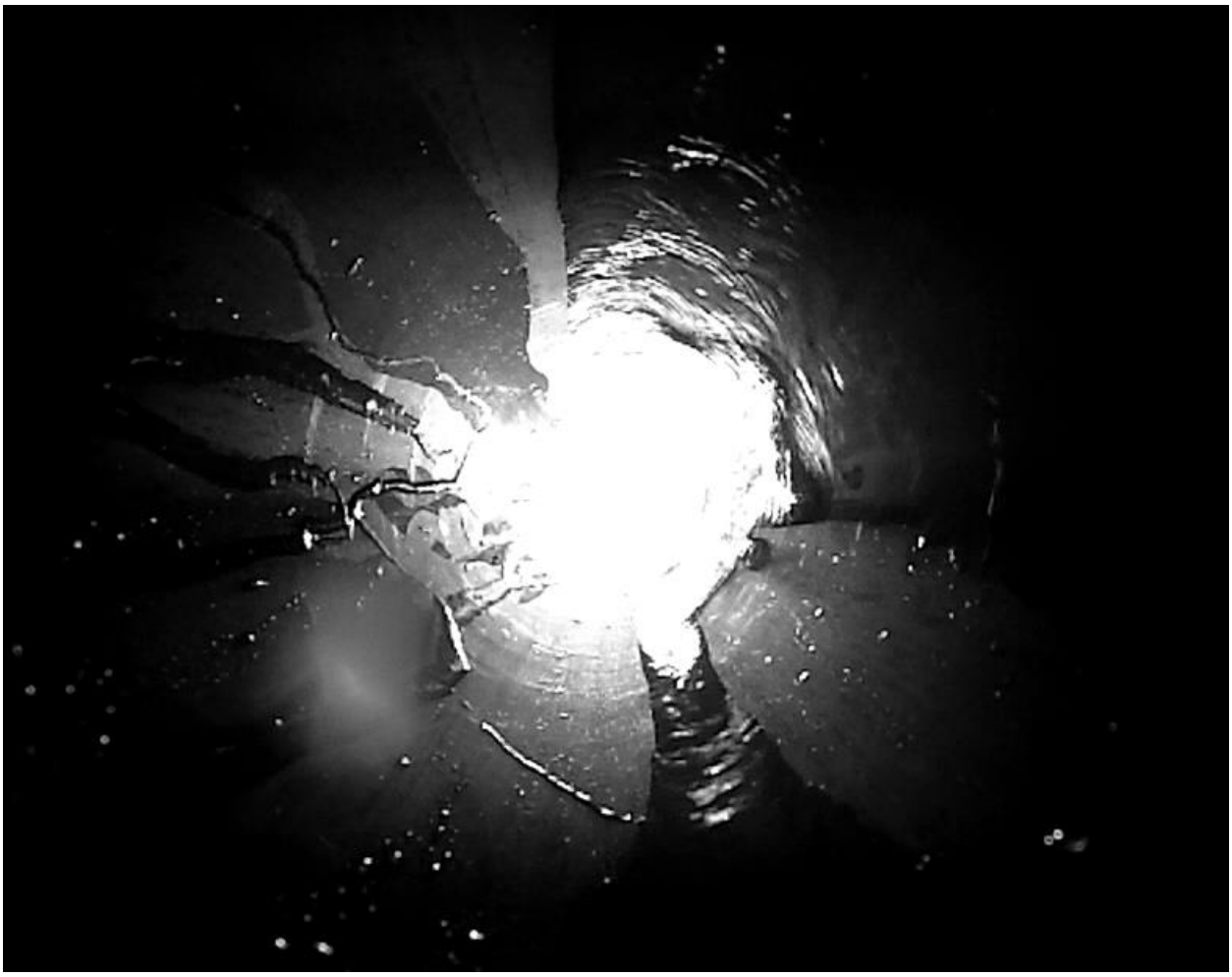

Figure 3-6 Wetting of the drain pipe at the transition region of the drain pipe observed inside a 7.6cm diameter DWHR system at a flow rate of 4 LPM.

It was observed that the transition region was a function of the pipe diameter. This was logical since larger diameter pipes would have a larger surface area, requiring a higher volumetric flow rate in order to develop a stable falling film. The results of the tests are shown in Figure 3-7, Figure 3-8 and Figure 3-9. Error bars for the volumetric flow rate are the RMS of the maximum possible error of ±0.25 L/min. The error bars for the effectiveness are based on the data uncertainty of ±0.6% which was determined using the constant odds method by Moffat described in Appendix B [24]. However, these effectiveness error bars are not readily noticeable on the graphs due to their close proximity to the data points.

For the 5.1cm diameter system, the differences between the three test procedures were not very distinct for flow rates above 5 LPM (Figure 3-7). This is likely due to the smaller interior surface area of DWHR system, mitigating the anticipated effects. Also, the smaller size of the ABS header caused the water to spread more evenly. However, it can still be noticed that the transition from LHR generated slightly reduced effectiveness results. The LHR and HLR methods produced lower effectiveness results for flow rates below 5 LPM, but the transition region hysteresis was not clearly observed for the reasons mentioned previously.

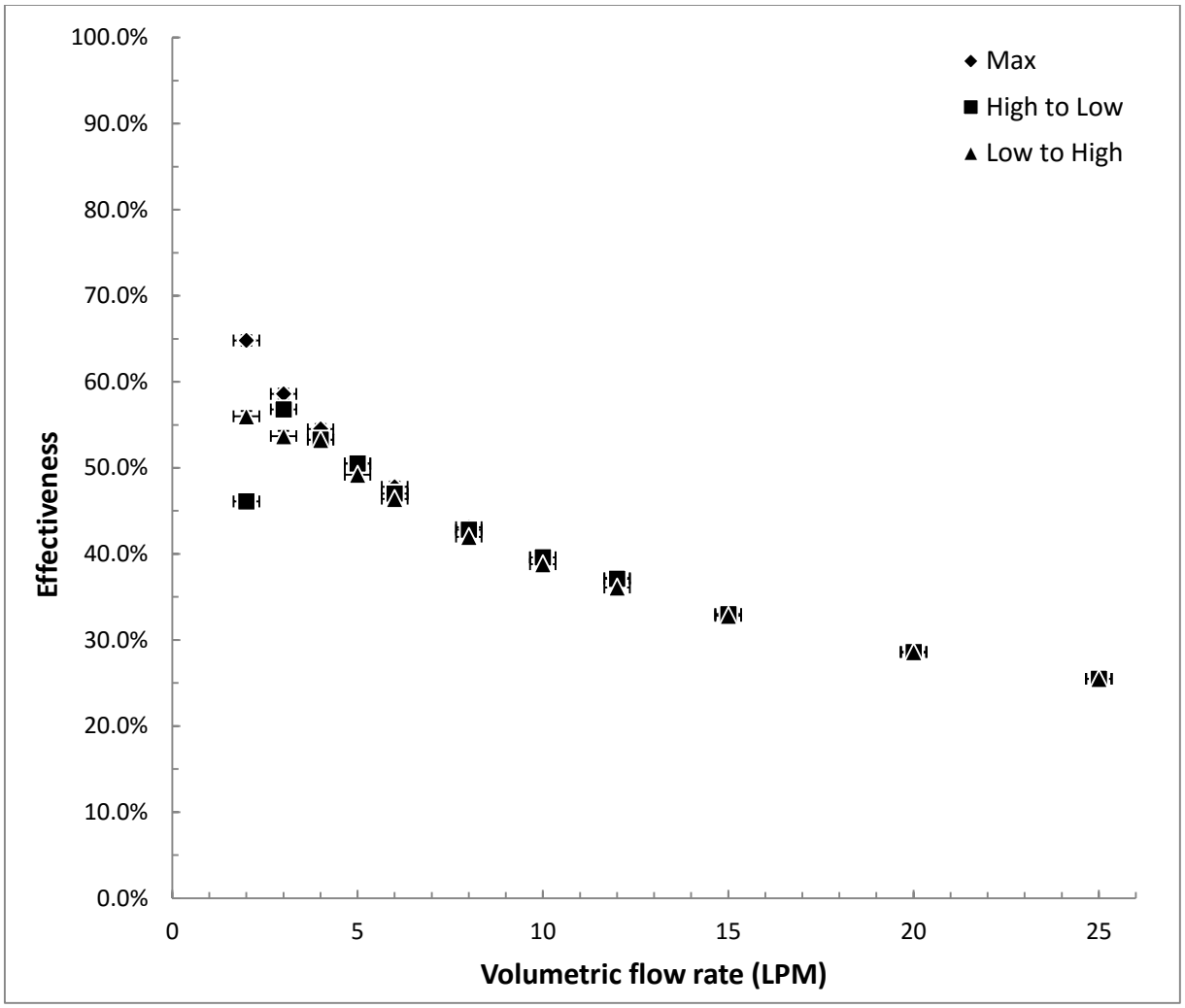

Figure 3-7 Effectiveness vs. Volumetric flow rate for a 122cm long, 5.1cm diameter DWHR system.

For the 7.6cm diameter system, the data was consistent for the FW procedure (Figure 3-8). At flow rates greater than 6 LPM, the data were consistent and repeatable. The effectiveness at FW was higher than the LHR or HLR procedures, but neither the LHR nor HLR method appeared to consistently outperform the other. At flow rates lower than 6 LPM, the effectiveness of the DWHR system fell within a range of values. The results generated by the LHR and HLR methods at these low flow rates closely followed the hypothesized transition region hysteresis, see Figure 3-3.

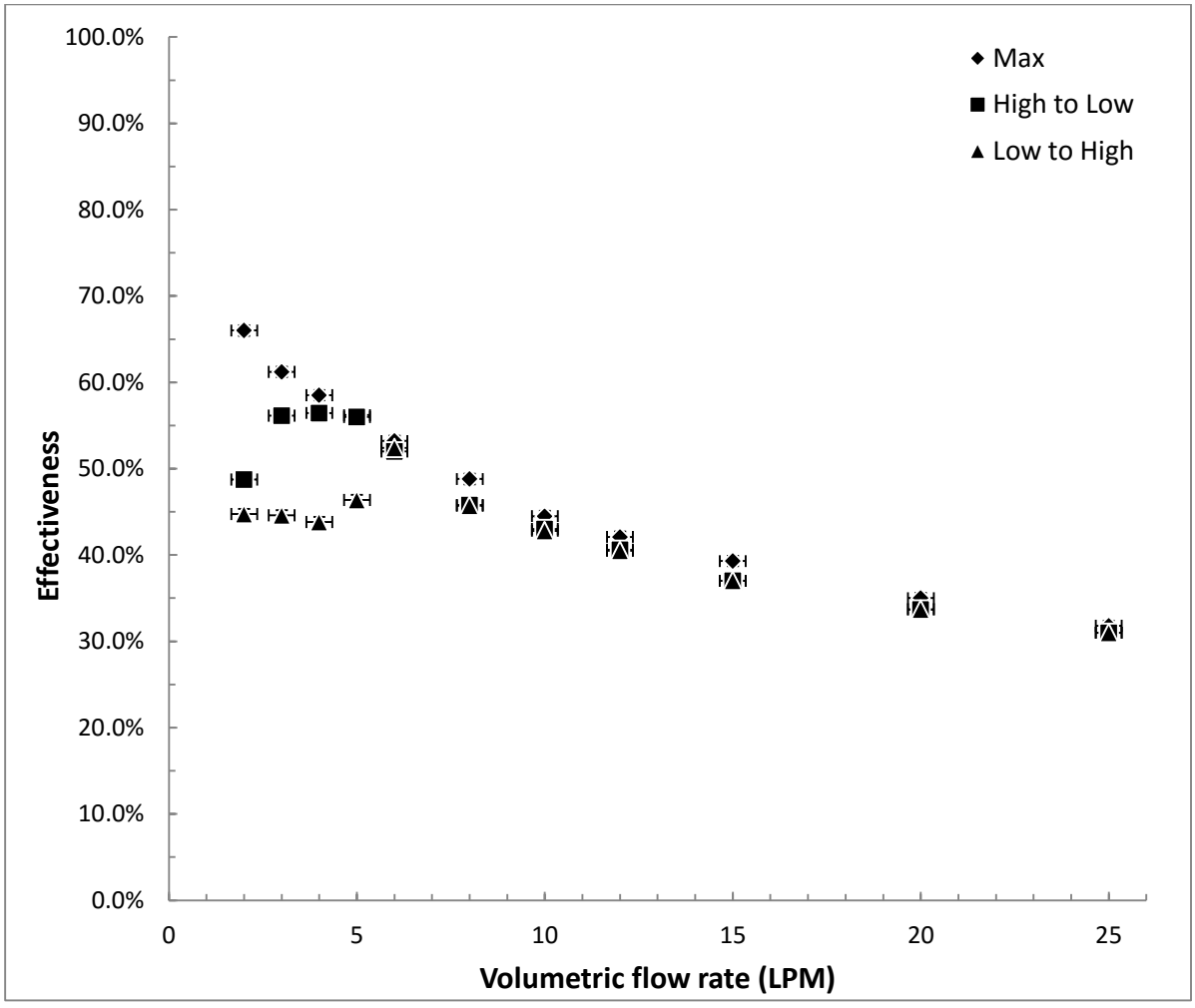

Figure 3-8 Effectiveness vs. Volumetric flow rate for a 122cm long, 7.6cm diameter DWHR system.

At low flow rates, the 10.2cm diameter DWHR system also generated effectiveness data within a range of values, though in a tighter range (Figure 3-9). The transition from random to repeatable data occurred between 6 and 8 LPM. At flow rates greater than 8 LPM the effectiveness at FW was clearly higher than the LHR or HLR procedures, but neither the LHR nor HLR method appeared to consistently outperform the other. At flow rates below 8 LPM, the HLR method consistently produced higher effectiveness values than the LHR method, but transition region hysteresis was not observed. This was most likely due to the larger interior surface area of DWHR pipe promoting uneven wetting; thereby mitigating the anticipated hysteresis.

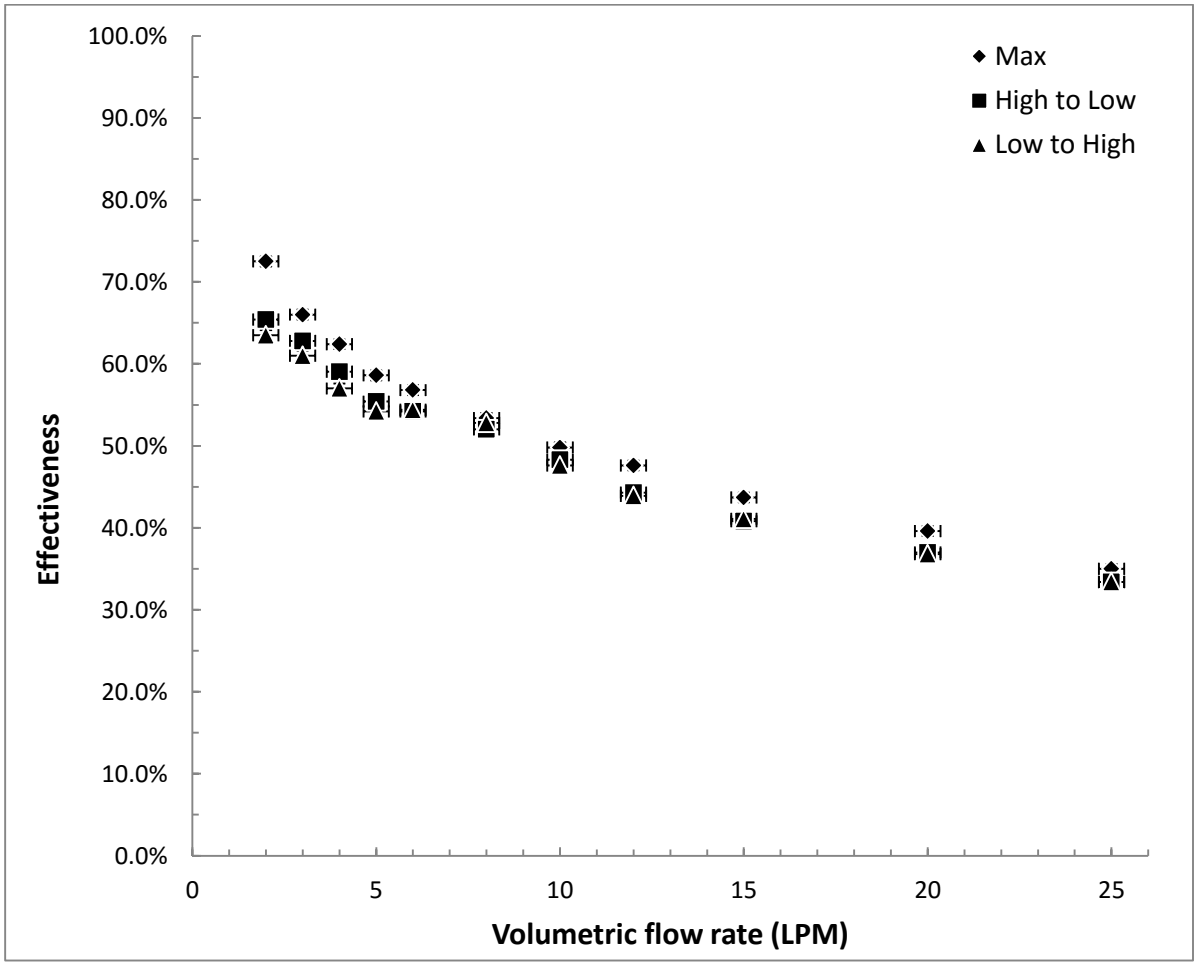

Figure 3-9 Effectiveness vs. Volumetric flow rate for a 122cm long, 10.2cm diameter DWHR system.

Splashing inside the DWHR system occurred at flow rates greater than 6 LPM. This allowed some droplets of water to traverse the length of the pipe and not contact the sides. Additionally, at high flow rates, with full wetting occurring, the water film did not appear to spread uniformly around the pipe's interior wall. This resulted in visibly 'thicker' areas of falling water. At low flow rates the flow *insert* directed the water into a swirling pattern wetting otherwise dry areas. At high flow rates, with full wetting, the flow insert reduced splashing and induced 'even' wetting. Use of the flow insert increased a DWHR system's effectiveness. However, at high flow rates it was not determined if the change in effectiveness was due, in greater part, to excessive splashing or the uneven thickness of the falling water.

All the data indicated that as the flow rate is increased, the effectiveness of the system is decreased. This was due to the reduced period of time cold water spent in the heat exchanger. This same factor and the increased interior surface area were the reasons the larger diameter systems display higher effectiveness values. Each individual test showed consistent effectiveness values; however, at low flow rates the tests returned data within a range of effectiveness values depending on the wetting pattern of the falling film for a given test.

The range of effectiveness values are regarded as validation of the *transition region*, see Figure 3-3. Therefore, rated values from the CSA tests with flow rates ranging from 5.5 to 14 LPM cannot be extrapolated to flow rates below 5.5 LPM for any DWHR systems. However, it is worth noting that at such low flow rates, the magnitude of heat recovery is bound to be small; hence, the magnitude of extrapolation errors would likely be too small to be a concern. This is left to the designers' discretions'.

The materials presented after this statement were not a part of the journal paper and are solely written by the author.

3.3 CSA and High Flow Range

The most convenient approach to developing a generalized model is to fit a curve to the experimental data and determine how well suited it is for extrapolating the effectiveness curve beyond the CSA range. While extrapolation is rarely the best approach, it is acknowledged that the CSA data is likely all that will be available, and that DWHRs often operate outside the tested range. Equation 3.3 showed the theoretical expression for the effectiveness of a DWHR system as a function of volumetric flow rate, operating at equal flow rates under counter-flow arrangement. Using the form of Equation 3.3, Equation 3.4 was devised to express the curve of best fit for the experimental data.

$$\varepsilon = \frac{1}{G\dot{V}+H} \tag{3.4}$$

where G and H are constants found through regression.

The first step was to look at the data gathered in section 3.2 using the full wetting method (maximum), which involved insertion of an external object inside the pipe to make the falling film more uniform. A curve of best fit in the form of Equation 3.4 was fitted to the effectiveness values measured at flow rates of 5, 6, 8, 10, 12 and 15 LPM. Table 3-1 contains the measured results and the values predicted by the curve fit.

Table 3-1 The measured effectiveness of three DWHR systems alongside their effectiveness calculated using a curve fit of data from the full wetting method. The highlighted cells contain the extrapolated points.

Flowrate (LPM)	⌀ 5.1cm DWHR system		⌀ 7.6cm DWHR system		⌀ 10.2cm DWHR system	
	Measured Effectiveness	Calculated Effectiveness	Measured Effectiveness	Calculated Effectiveness	Measured Effectiveness	Calculated Effectiveness
5	50.5%	50.2%	56.2%	55.3%	58.6%	58.7%
6	47.8%	47.7%	53.2%	53.0%	56.8%	56.8%
8	43.1%	43.4%	48.8%	49.0%	53.4%	53.2%
10	39.6%	39.9%	44.5%	45.5%	49.8%	50.1%
12	37.2%	36.8%	42.1%	42.5%	47.6%	47.4%
15	33.0%	33.1%	39.3%	38.7%	43.7%	43.8%
20	28.6%	28.2%	35.0%	33.6%	39.6%	38.8%
25	25.5%	24.6%	31.8%	29.7%	35.0%	34.9%

Extrapolating the curve fit for the 5.1cm diameter DHWR system resulted in fairly accurate numbers. The error between the measured and extrapolated numbers became larger with increasing flow rate and pipe diameter.

The extrapolation error associated with increasing flow rate was due to the inaccuracies in the curve fit and did not reveal any new information about the systems. However, the fact that the errors became larger with increasing diameter was a possible indication of a non-uniform falling film. As the diameter became larger, the contact area between the falling film and the drain pipe became larger, which resulted in a higher probability of having a non-uniform film thickness. The full wetting method only insured that the inside diameter was fully wet; the uniformity of the falling film could not be fully controlled during the tests.

The high to low (HLR) method is the method used by the CSA standards and is a much better representation of what would happen in a household's drain stack. It was of interest to see if the patterns noticed in the full wetting curve fit would match the results from the HLR method as well. A curve of best fit in the form of Equation 3.4 was fitted to the values measured at flow rates of 5, 6, 8, 10, 12 and 15 LPM. Table 3-2 contains the measured results and the values predicted by the curve fit.

Table 3-2 The measured effectiveness of three DWHR systems alongside their effectiveness calculated using a curve fit of data from the HLR method. The highlighted cells contain the extrapolated points.

Flowrate (LPM)	⌀ 5.1cm DWHR system		⌀ 7.6cm DWHR system		⌀ 10.2cm DWHR system	
	Measured Effectiveness	Calculated Effectiveness	Measured Effectiveness	Calculated Effectiveness	Measured Effectiveness	Calculated Effectiveness
5	50.5%	49.8%	56.0%	54.2%	55.4%	56.5%
6	47.0%	47.4%	52.0%	51.7%	54.2%	54.5%
8	42.8%	43.2%	45.8%	47.4%	52.0%	50.8%
10	39.6%	39.7%	43.0%	43.7%	48.3%	47.6%
12	37.1%	36.8%	40.6%	40.5%	44.3%	44.7%
15	33.0%	33.1%	37.0%	36.5%	40.8%	41.1%
20	28.6%	28.3%	33.7%	31.4%	37.0%	36.1%
25	25.5%	24.7%	31.0%	27.5%	33.4%	32.2%

Similar to what was discussed for the full wetting case, extrapolating the curve fit for the 5.1cm diameter DHWR system resulted in fairly accurate numbers. The error between the measured and extrapolated numbers became larger with increasing flow rate and pipe diameter. This supported the hypothesis about the non-uniform falling film thickness at large pipe diameters.

Accurate measurements for the falling film thickness require Particle Image Velocimetry (PIV) which can be used measure the velocity profile at different planes. However, using PIV on DWHR systems is outside the scope of the current work.

Instead, it was decided to perform HLR testing in the CSA range for six systems with different lengths and diameters. The reason why different length pipes were chosen was to determine if the correlation errors would be affected by length. If the hypothesis about non-uniform thickness is correct, it would mean that longer pipes would have lower correlation errors since the pipe friction would even-out the falling film. This was to be revealed through experimentation.

3.3.1 Method

To generate experimental data, DWHR systems with different lengths and diameters were selected as listed in Table 3-3. The systems were tested at flow rates of 5.5, 7.0, 9.0, 10.0, 12.0, 14.0, 16.0, 19.0, 22.0 and 25.0 LPM. The inlet temperatures for the drain-side and mains-side for all tests were kept at 38±1°C and 10±1°C, respectively. All systems tested in this section had the same design.

Table 3-3 Diameters and lengths of DWHR systems studied.

Pipe #	Diameter (cm)	Length (cm)
1	5.1	122
2	7.6	92
3	7.6	122
4	7.6	153
5	10.2	122
6	10.2	153

3.3.2 Results

The experimental results are summarized in Table 3-4, where the highlighted cells represent the values measured outside the CSA range. The data corresponding to the CSA range was plotted for each system and presented in Figure 3-10 through Figure 3-15. The curve of best fit for each plot was also displayed with its corresponding regression coefficients. Note that for the 10.2cm diameter systems, the effectiveness value at 5.5 LPM was not repeatable and hence, it was excluded from the analysis.

Table 3-4 Measured effectiveness values for six different DWHR systems at different flow rates, where the highlighted cells contain data points for flow rates above the CSA range.

Flowrate (LPM)	Measured effectiveness values for each system					
	⌀ 5.1cm, 122cm long DWHR system	⌀ 7.6cm, 92cm long DWHR system	⌀ 7.6cm, 122cm long DWHR system	⌀ 7.6cm, 153cm long DWHR system	⌀ 10.2cm, 122cm long DWHR system	⌀ 10.2cm, 153cm long DWHR system
5.5	48.9%	48.4%	55.9%	61.8%	N/A	N/A
7	44.6%	43.5%	51.0%	57.1%	54.9%	60.5%
9	40.5%	38.8%	46.4%	52.6%	51.6%	57.4%
10	39.1%	37.2%	44.5%	50.8%	49.3%	55.1%
12	36.3%	34.5%	41.4%	47.9%	46.0%	51.5%
14	34.0%	32.4%	38.9%	45.6%	43.7%	49.4%
16	31.9%	30.6%	37.1%	43.6%	41.7%	47.3%
19	29.3%	28.5%	35.1%	41.1%	39.1%	44.6%
22	27.5%	26.9%	33.2%	39.3%	37.0%	42.3%
25	25.6%	25.3%	31.4%	37.6%	34.8%	40.1%

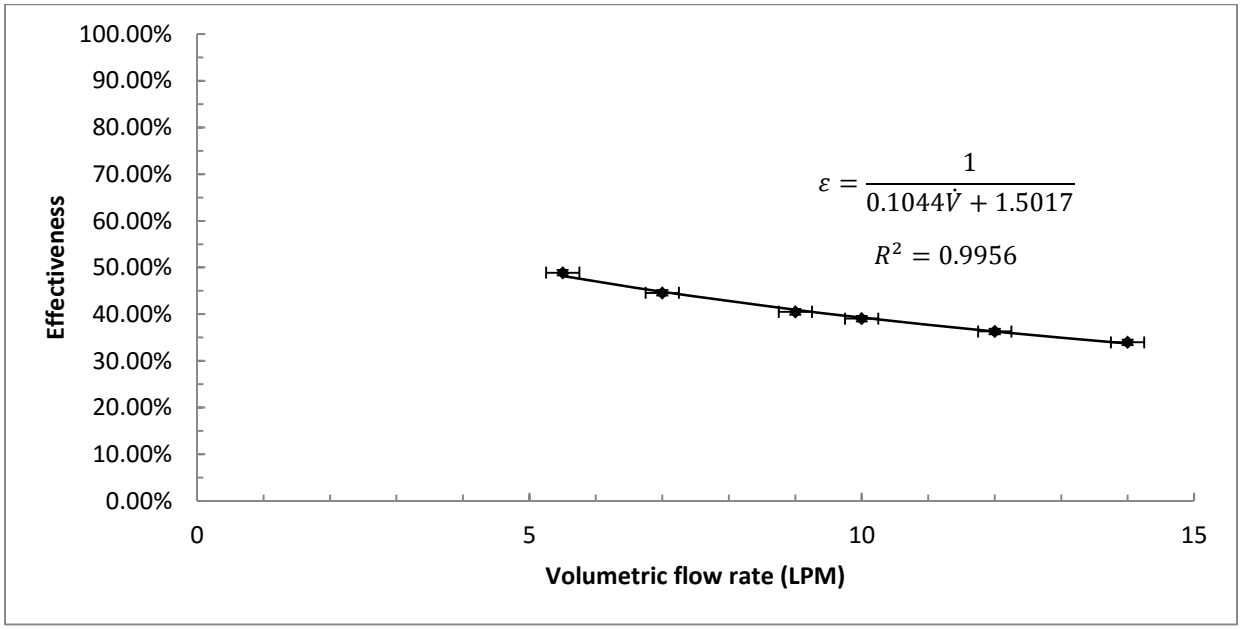

Figure 3-10 The characteristic curve for effectiveness vs volumetric flow rate within the CSA range for the 5.1cm diameter, 122cm long DWHR system.

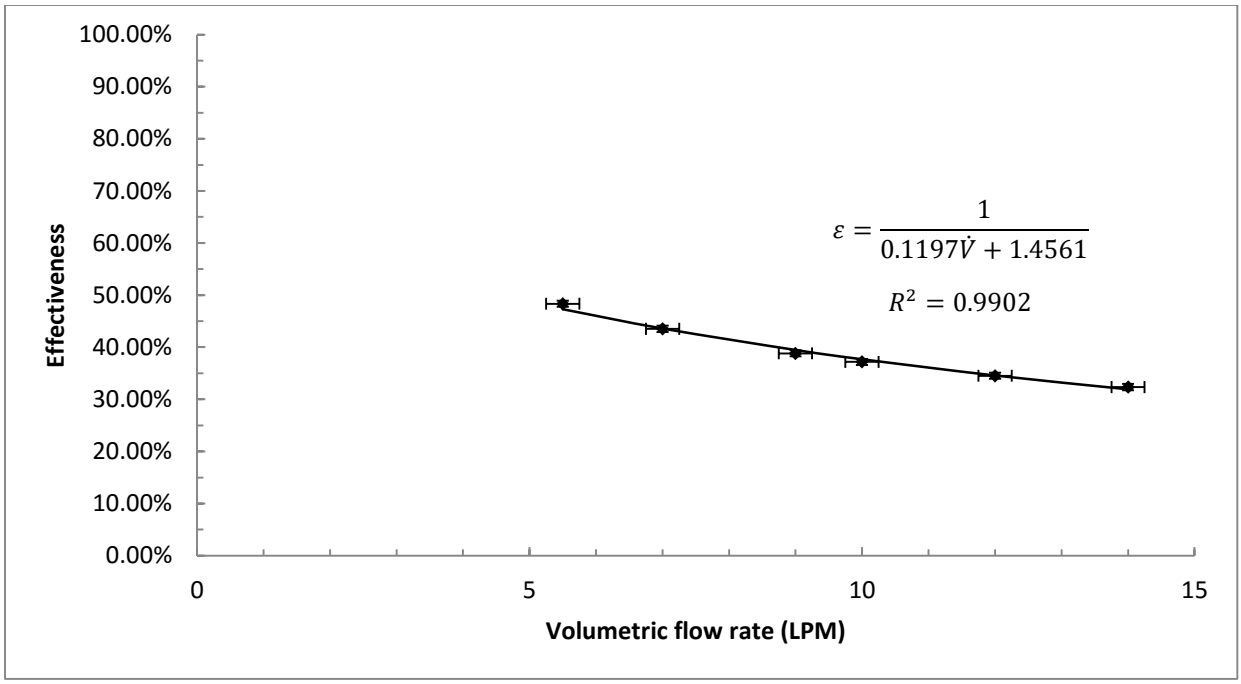

Figure 3-11 The characteristic curve for effectiveness vs volumetric flow rate within the CSA range for the 7.6cm diameter, 92cm long DWHR system.

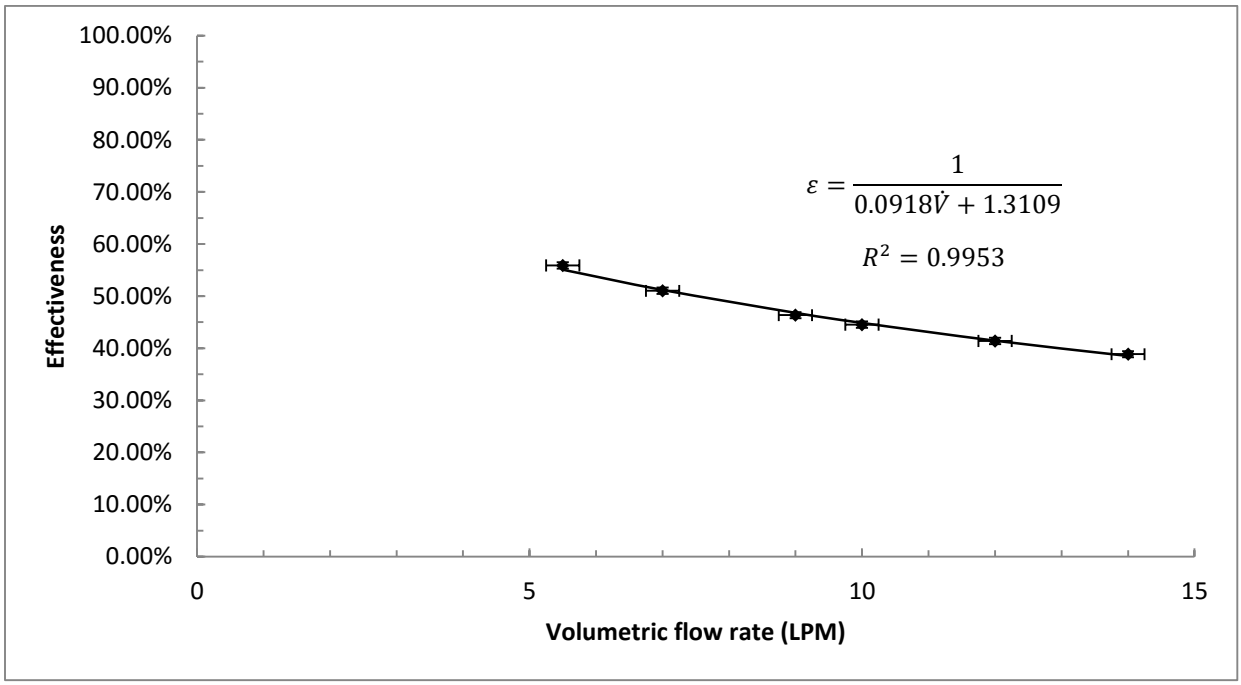

Figure 3-12 The characteristic curve for effectiveness vs volumetric flow rate within the CSA range for the 7.6cm diameter, 122cm long DWHR system.

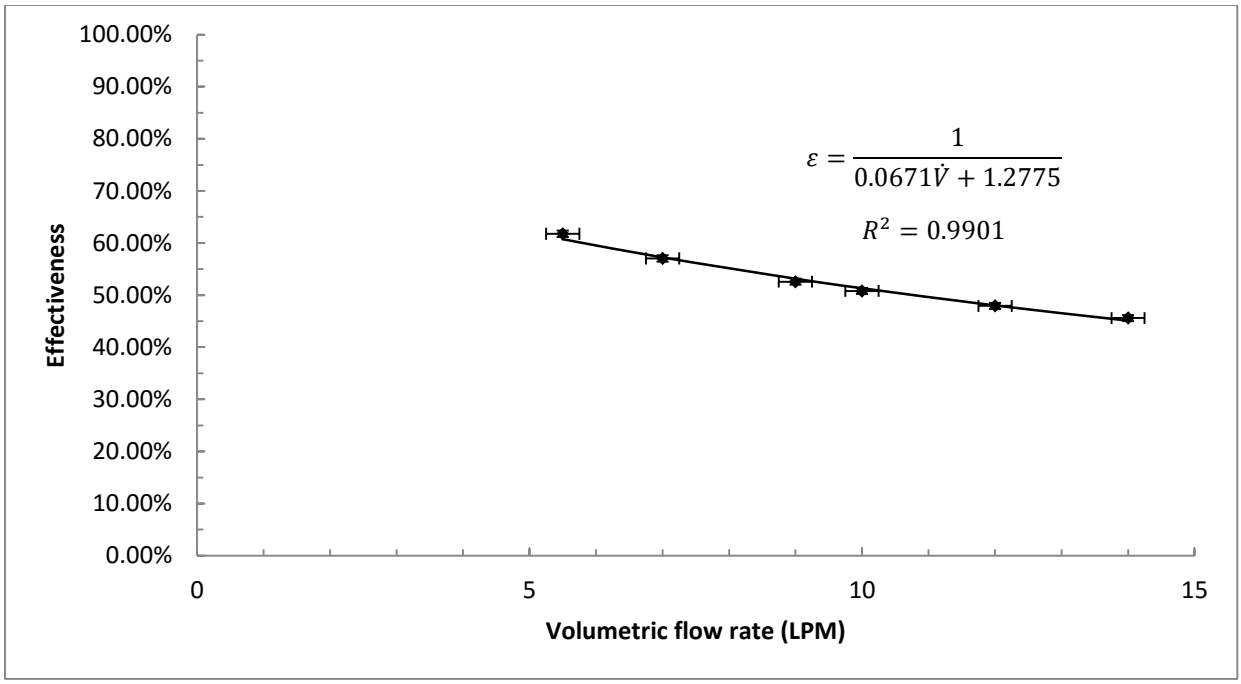

Figure 3-13 The characteristic curve for effectiveness vs volumetric flow rate within the CSA range for the 7.6cm diameter, 153cm long DWHR system.

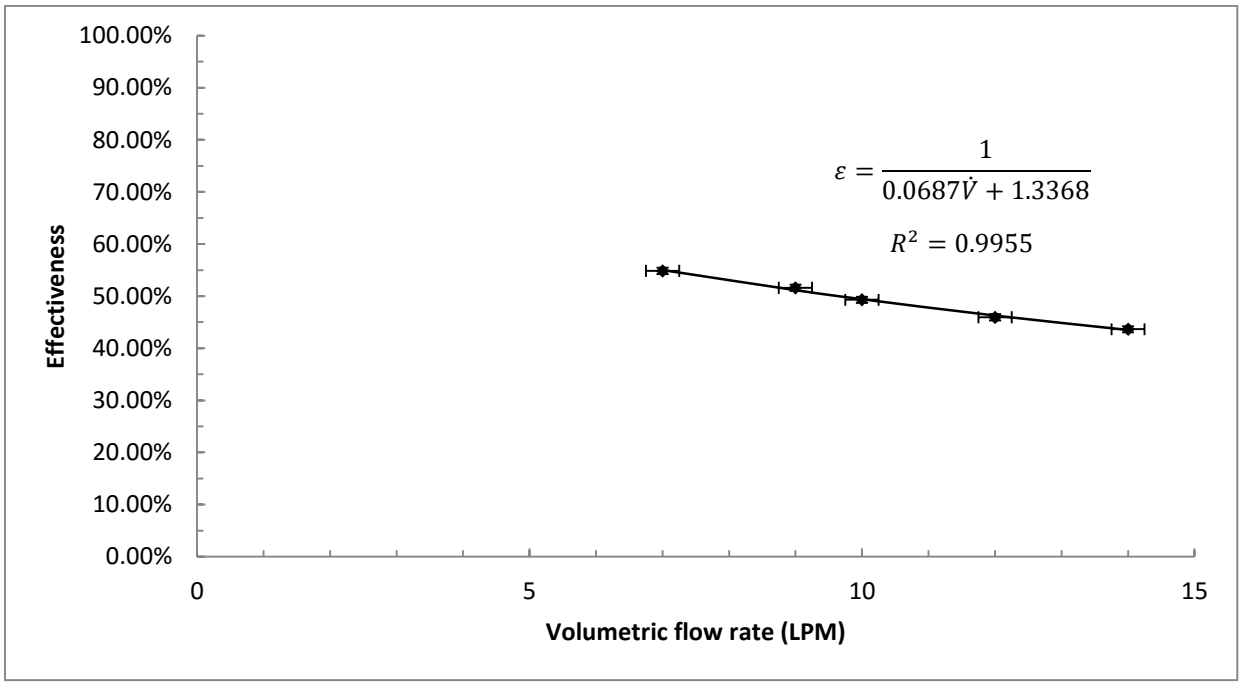

Figure 3-14 The characteristic curve for effectiveness vs volumetric flow rate within the CSA range for the 10.2cm diameter, 122cm long DWHR system.

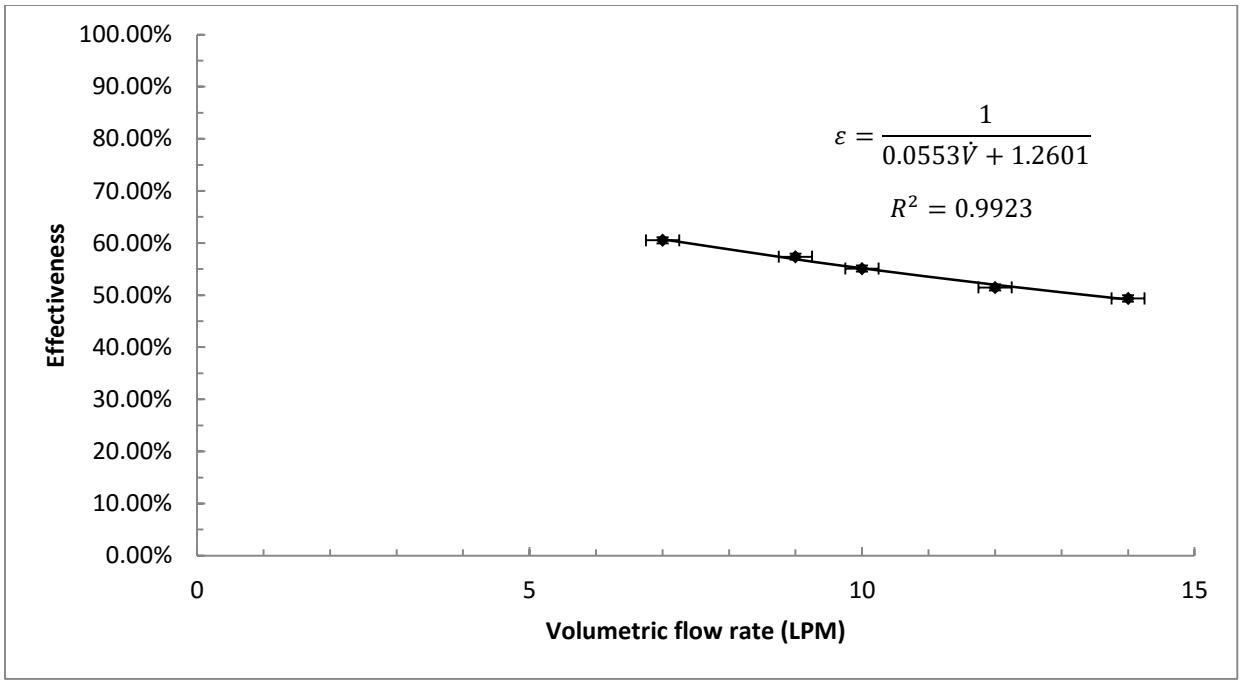

Figure 3-15 The characteristic curve for effectiveness vs volumetric flow rate within the CSA range for the 10.2cm diameter, 153cm long DWHR system.

The correlations shown in Figure 3-10 through Figure 3-15 were used to extrapolate the effectiveness of each system beyond the CSA range and were compared to the measured values from Table 3-4. The results are shown in Table 3-5 through Table 3-10. The highlighted cells in each table show values corresponding to flow rates outside the CSA range.

Table 3-5 The measured effectiveness of the 5.1cm diameter, 122cm long DWHR system alongside its effectiveness calculated using a curve fit and the percent error between the two values.

Flowrate (LPM)	Measured Effectiveness	Calculated Effectiveness	Percent Error
5.5	48.90%	48.17%	1.51%
7	44.60%	44.79%	0.43%
9	40.50%	40.96%	1.13%
10	39.10%	39.28%	0.46%
12	36.30%	36.30%	0.01%
14	34.00%	33.75%	0.75%
16	31.90%	31.52%	1.19%
19	29.30%	28.69%	2.12%
22	27.50%	26.33%	4.46%
25	25.60%	24.32%	5.26%

Table 3-6 The measured effectiveness of the 7.6cm diameter, 92cm long DWHR system alongside its effectiveness calculated using a curve fit and the percent error between the two values.

Flowrate (LPM)	Measured Effectiveness	Calculated Effectiveness	Percent Error
5.5	48.40%	47.29%	2.34%
7	43.50%	43.59%	0.21%
9	38.80%	39.47%	1.70%
10	37.20%	37.69%	1.30%
12	34.50%	34.57%	0.21%
14	32.40%	31.93%	1.47%
16	30.60%	29.66%	3.16%
19	28.50%	26.81%	6.32%
22	26.90%	24.45%	10.01%
25	25.30%	22.48%	12.55%

Table 3-7 The measured effectiveness of the 7.6cm diameter, 122cm long DWHR system alongside its effectiveness calculated using a curve fit and the percent error between the two values.

Flowrate (LPM)	Measured Effectiveness	Calculated Effectiveness	Percent Error
5.5	55.90%	55.07%	1.50%
7	51.00%	51.19%	0.37%
9	46.40%	46.79%	0.84%
10	44.50%	44.87%	0.81%
12	41.40%	41.45%	0.12%
14	38.90%	38.52%	0.99%
16	37.10%	35.98%	3.13%
19	35.10%	32.73%	7.23%
22	33.20%	30.03%	10.57%
25	31.40%	27.73%	13.23%

Table 3-8 The measured effectiveness of the 7.6cm diameter, 153cm long DWHR system alongside its effectiveness calculated using a curve fit and the percent error between the two values.

Flowrate (LPM)	Measured Effectiveness	Calculated Effectiveness	Percent Error
5.5	61.80%	60.73%	1.76%
7	57.10%	57.23%	0.23%
9	52.60%	53.15%	1.04%
10	50.80%	51.32%	1.02%
12	47.90%	48.01%	0.24%
14	45.60%	45.11%	1.09%
16	43.60%	42.53%	2.51%
19	41.10%	39.18%	4.90%
22	39.30%	36.31%	8.22%
25	37.60%	33.84%	11.11%

Table 3-9 The measured effectiveness of the 10.2cm diameter, 122cm long DWHR system alongside its effectiveness calculated using a curve fit and the percent error between the two values.

Flowrate (LPM)	Measured Effectiveness	Calculated Effectiveness	Percent Error
7	54.90%	55.01%	0.21%
9	51.60%	51.15%	0.88%
10	49.30%	49.41%	0.23%
12	46.00%	46.27%	0.58%
14	43.70%	43.50%	0.45%
16	41.70%	41.05%	1.58%
19	39.10%	37.85%	3.31%
22	37.00%	35.11%	5.38%
25	34.80%	32.74%	6.29%

Table 3-10 The measured effectiveness of the 10.2cm diameter, 153cm long DWHR system alongside its effectiveness calculated using a curve fit and the percent error between the two values.

Flowrate (LPM)	Measured Effectiveness	Calculated Effectiveness	Percent Error
7	60.50%	60.71%	0.34%
9	57.40%	56.89%	0.90%
10	55.10%	55.15%	0.10%
12	51.50%	51.98%	0.93%
14	49.40%	49.16%	0.49%
16	47.30%	46.62%	1.45%
19	44.60%	43.28%	3.06%
22	42.30%	40.38%	4.76%
25	40.10%	37.84%	5.97%

The percent errors between the measured and calculated values within the CSA range were less than 2% for systems at all flow rates and diameters. This supported the fact that a curve of best fit in the form of Equation 3.4 was appropriate for representing the characteristic effectiveness vs. flow rate curve for any DWHR system in the CSA range.

The percent error between the measured and calculated results was used to find trends for flow rates above 14 LPM. The 5.1cm diameter system had the smallest percent error at all flow rates. For systems

with the same diameter, it was observed that the percent error decreased linearly as the pipe length increased. The percent error also increased with increasing flow rate through the system. These factors suggested that the non-uniformity in the falling film in the CSA range was exactly the reason why the curve fit could not be extrapolated without any correction factors.

Based on the observed trends described thus far, it was attempted to make a general correction factor to improve the extrapolated results based on a given DWHR system's length, diameter and flow rate. It was decided to develop separate correction factors for different diameter systems since it could not be assumed that the falling film would behave exactly the same in different geometries. Therefore, the correction had to have a form similar to Equation 3.5.

$$Flow\ Correction\ Factor = C_{Flow} \sim \frac{\dot{V}}{L} \tag{3.5}$$

where $\dot{V}$ is the volumetric flow rate in LPM and L is the length of the DWHR system in meters. A qualitative approach was not enough, and It was of interest to use the experimental results to assign numbers to the correction factor. Hence, Equation 3.6 was devised for C_{Flow}:

$$C_{Flow} = \frac{A\dot{V}+B}{L} + 1 \tag{3.6}$$

where A and B are constants corresponding to different diameters as shown in Table 3-11:

Table 3-11 Correlation constants determined for each diameter based on the experimental results.

Correlation Constants	⌀ 5.1cm systems	⌀ 7.6cm systems	⌀ 10.2cm systems
A (m/LPM)	5.80E-03	1.27E-02	7.10E-03
B (m)	-7.96E-02	-1.67E-01	-9.14E-02

The corrected effectiveness is expressed in Equation 3.7.

$$\varepsilon_{corrected} = \varepsilon_{predicted} \times C_{Flow} = \varepsilon_{predicted} \times \left(\frac{A\dot{V}+B}{L} + 1\right) \tag{3.7}$$

where $\varepsilon_{predicted}$ is the extrapolated effectiveness values calculated in Table 3-5 through Table 3-10 using the curves of best fit. Table 3-12 through Table 3-17 contain the effectiveness values before and after they were corrected using Equation 3.7, to provide a means for the readers to compare the values.

Table 3-12 The measured effectiveness of the 5.1cm diameter, 122cm long DWHR system alongside its effectiveness calculated using a curve of best fit and the effectiveness after the correction is applied.

Flowrate (LPM)	Measured Effectiveness	Calculated Effectiveness Without Correction	Calculated Effectiveness With Correction
16	31.90%	31.52%	31.87%
19	29.30%	28.69%	29.41%
22	27.50%	26.33%	27.36%
25	25.60%	24.32%	25.63%

Table 3-13 The measured effectiveness of the 7.6cm diameter, 92cm long DWHR system alongside its effectiveness calculated using a curve of best fit and the effectiveness after the correction is applied.

Flowrate (LPM)	Measured Effectiveness	Calculated Effectiveness Without Correction	Calculated Effectiveness With Correction
16	30.60%	29.66%	30.83%
19	28.50%	26.81%	28.98%
22	26.90%	24.45%	27.45%
25	25.30%	22.48%	26.16%

Table 3-14 The measured effectiveness of the 7.6cm diameter, 122cm long DWHR system alongside its effectiveness calculated using a curve of best fit and the effectiveness after the correction is applied.

Flowrate (LPM)	Measured Effectiveness	Calculated Effectiveness Without Correction	Calculated Effectiveness With Correction
16	37.10%	35.98%	37.04%
19	35.10%	32.73%	34.73%
22	33.20%	30.03%	32.80%
25	31.40%	27.73%	31.16%

Table 3-15 The measured effectiveness of the 7.6cm diameter, 153cm long DWHR system alongside its effectiveness calculated using a curve of best fit and the effectiveness after the correction is applied.

Flowrate (LPM)	Measured Effectiveness	Calculated Effectiveness Without Correction	Calculated Effectiveness With Correction
16	43.60%	42.53%	43.54%
19	41.10%	39.18%	41.09%
22	39.30%	36.31%	38.99%
25	37.60%	33.84%	37.18%

Table 3-16 The measured effectiveness of the 10.2cm diameter, 122cm long DWHR system alongside its effectiveness calculated using a curve of best fit and the effectiveness after the correction is applied.

Flowrate (LPM)	Measured Effectiveness	Calculated Effectiveness Without Correction	Calculated Effectiveness With Correction
16	41.70%	41.05%	41.80%
19	39.10%	37.85%	39.20%
22	37.00%	35.11%	36.97%
25	34.80%	32.74%	35.05%

Table 3-17 The measured effectiveness of the 10.2cm diameter, 153cm long DWHR system alongside its effectiveness calculated using a curve of best fit and the effectiveness after the correction is applied.

Flowrate (LPM)	Measured Effectiveness	Calculated Effectiveness Without Correction	Calculated Effectiveness With Correction
16	47.30%	46.62%	47.30%
19	44.60%	43.28%	44.50%
22	42.30%	40.38%	42.08%
25	40.10%	37.84%	39.97%

The maximum difference between the corrected values and the measured values in the tables above was 0.86% full scale (FS).

To provide an alternative method to illustrate the effect of the correction, the CSA curve for the 7.6cm diameter, 122cm long system was plotted with and without the correction, alongside the measured values in Figure 3-16. This was to show that without any correction, extrapolating the CSA curve would underestimate the effectiveness of DWHR systems at flow rates above 14 LPM and the error would get

larger with flow rate. Lastly, this underestimation would occur for all DWHR systems, regardless of diameter, which could be confirmed by looking at the signs for constants A and B in Table 3-11.

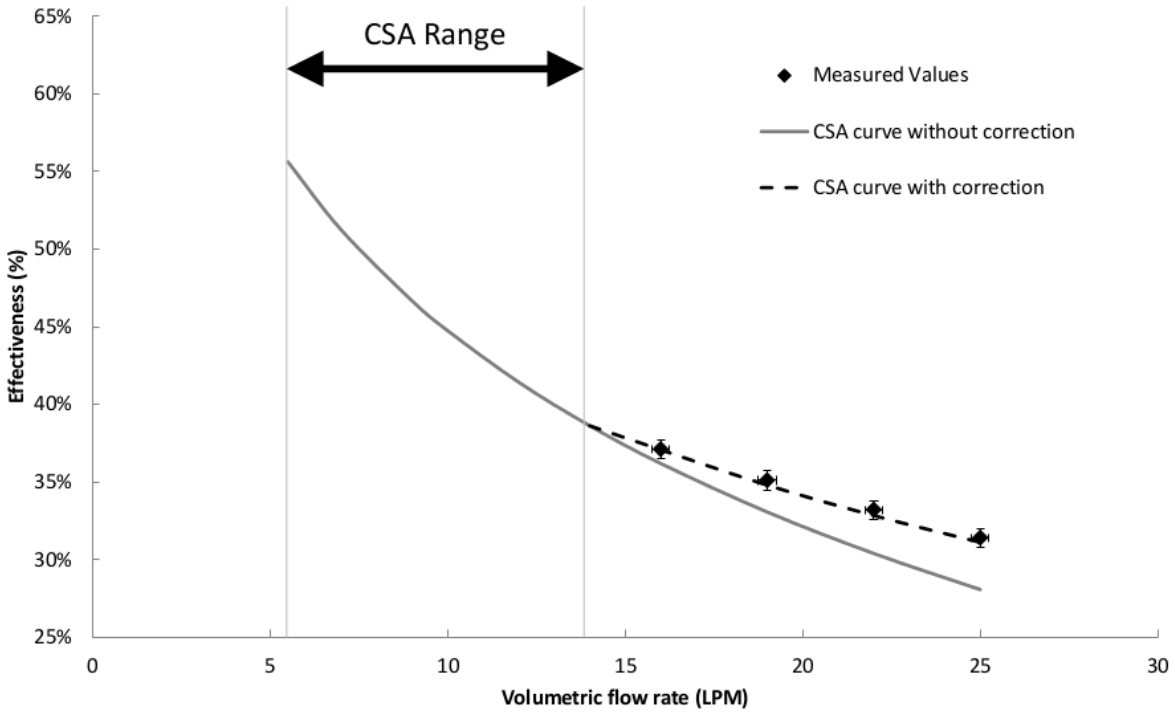

Figure 3-16 Visual representation of the correlation developed to correct the CSA curves for flow rates above 14 LPM.

Generally, the difference between the designs of falling-film DWHR systems is due to the design of coils wrapped around the drain pipe; however, the drain pipe itself is the common factor among all designs. Since the drain pipe is the location where the falling film forms and the variations in the results were determined to be due to the non-uniformity in the falling film, it can be concluded that the correlation developed in this chapter can be used for any DWHR system.

Note that the test apparatus could not produce results for flow rates above 25 LPM. As a result, this correction factor may or may not produce acceptable values for flow rates above 25 LPM. However, this flow rate is enough for operating 4 low-flow showerheads (5.5 LPM each) simultaneously, which is not

very likely to occur in a residential dwelling. C_{Flow} was deemed adequate for building simulation purposes.

3.3.3 Estimating the Pressure Drop through the Coils

This section will attempt to establish a general rule of thumb for predicting the dynamic pressure drop through DWHR systems. Pressure measurements were taken during the tests performed in the previous section and the results are shown in Figure 3-17. Regression analysis showed that all pressure curves are best fitted with 2nd degree polynomials, with regression coefficients very close to 1. Accurate predictions for pressure measurements are of very little practical use, and as such, a generalized approach is provided here.

If it is desired to estimate the dynamic pressure drop within the CSA range, a 2nd degree polynomial should be fitted to the existing CSA data, which can predict the pressure drop very well. If it is desired to estimate the dynamic pressure drop beyond the CSA range, one could use the same polynomial as the one above, and apply a safety factor of 1.1. This approach typically overestimates the actual pressure drop, but as already mentioned, accurate predictions are of little practical use. This should allow homeowners and designers to determine if the water pressure at a particular house is sufficient for a particular DWHR system to operate intended.

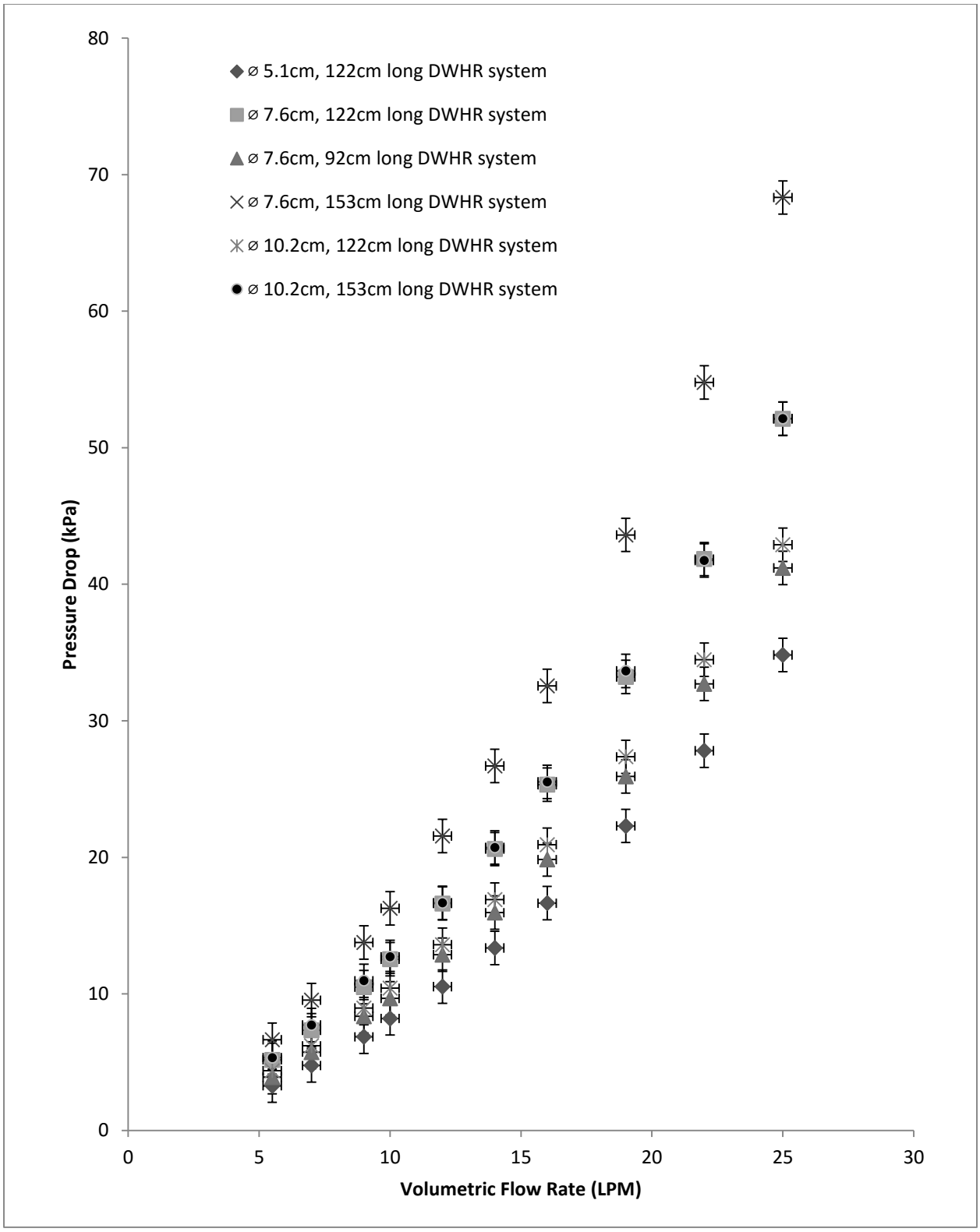

Figure 3-17 The pressure drop as a function of the volumetric flow rate for all DWHR systems tested.

3.4 Equal Flow Model

It is helpful to summarize the results discussed so far in this chapter to create a simple procedure for predicting the performance of DWHR systems based on the data available from CSA tests.

For flow rates lower than the CSA range (i.e. below 5.5 LPM), the CSA data cannot be extrapolated to accurately predict the effectiveness of a DWHR system. This is due to non-uniform film thickness, break-down of the falling film and the hysteresis that occur at low flow rates. It is important to point out that such low flow rates result in small magnitudes for the heat transfer rate. Therefore, even if the curve from the CSA range is extrapolated to the low flow rate region, the magnitudes of errors may be too small to be a concern. This is left to the designers' discretions'.

For flow rates within the CSA range, the existing CSA data can be used to create the characteristic effectiveness curve for the DWHR system of interest. This study suggests that a curve of best fit in the form of Equation 3.4 is the most suitable for representing this data set. For DWHR systems with diameters of 10.2cm, the effectiveness at 5.5 LPM must be excluded when developing the characteristic curves. This curve can readily be used to predict the effectiveness at flow rates between 5.5 and 14 LPM.

For flow rates higher than the CSA range, the first step is to develop the characteristic curve described in the previous paragraph. The next step is to use it to predict a first estimate for the effectiveness using this characteristic curve at the desired flow rate. The last step is to correct it using Equation 3.7, which is a function of the system's diameter, length and flow rate. Note that this method was only tested for flow rates up to 25 LPM and the author does not guarantee its accuracy for flow rates beyond 25 LPM.

For estimating pressure drop at any flow rate, first step is to use the CSA data to construct a curve of pressure drop as a function of flow rate. The next step is to fit a 2^{nd} degree polynomial to this curve and use this polynomial to predict a first estimate for the pressure drop at any given flow rate. If the flow rate of interest is above 14 LPM, a safety factor of 1.1 should be applied to the predicted value.

Chapter 4 Performance under Varying Temperatures

4.1 Introduction

DHWR systems are rated under very specific conditions, with the intent of allowing direct comparison of different products. In Europe, standard NEN 5128:2004+A1:2009 is used to rate DWHR systems at inlet temperatures of 40°C and 10°C on the drain-side and the mains side, respectively [25]. In North America, CSA standard B55.1-12 governs the rating procedure for measuring performance of DWHR systems. This standard requires the mains-side inlet to be maintained between 7-17°C and a temperature difference of 28 ± 1°C between the water entering the mains-side inlet and the drain-side inlet [9]. All standards require the units to be tested under equal flow conditions. The outcome of the tests is a standardized rating enabling comparison of devices on a common basis. Due to the standardized nature of the tests, the rated values cannot be expected to accurately represent a product's performance under real operating conditions.

For end-use installations, DWHR systems operate under conditions very different than those specified by any test standard. The mains inlet temperature may be affected by trends in ground temperature, which varies seasonally and is based on climate. The drain-side inlet conditions vary based on household equipment and the occupants' behavior. Throughout the tests done to produce the results for the previous chapters, it was observed that increased water temperature resulted in increased effectiveness, even when the flow rate $(\dot{V})$ and the difference between drain-side and mains-side inlet water temperatures (ΔT) were kept constant. No studies were found to explain the theory behind this phenomenon for DWHR systems.

This chapter investigates the impact of inlet water temperatures on the performance of DWHR systems. The conditions prescribed by the CSA standard are used as a basis for the experiments. A method is presented to correct the rated effectiveness values for non-standard operation temperatures.

4.2 Theory

Analytical models are needed to predict the performance of DWHR systems. Approaches in design and construction of DWHR systems vary based on the manufacturer, which makes the creation of a theoretical model very difficult. Figure 1-2 included three examples of commercially available designs. Due to the variations in design, DWHR system are rated experimentally using the ε-NTU method.

The effectiveness of a heat exchanger, ε, is the ratio of heat transfer, q , to the maximum possible heat transfer, $q_{\max}$, as was defined in Equation 2.1 [26].

In general, the effectiveness is dependent on the parameters shown in Equation 4.1:

$$\varepsilon = \varepsilon\left(NTU, \frac{C_{\min}}{C_{\max}}, \textit{flow arrangement} \right) \tag{4.1}$$

where NTU is the Number of Transfer Units and the flow arrangement is dependent on the type of heat exchanger (e.g. counter-flow, parallel flow, and cross-flow) [19]. *NTU* represents the magnitude of heat transfer rate relative to the rate of enthalpy change of the fluid with the smaller heat capacity rate.

Each of the dependencies in Equation 4.1 is discussed below to determine how the absolute temperature of the working fluid impacts the effectiveness of the heat exchanger.

Falling film DWHR systems operate as *Counter-Flow* heat exchangers. The flow arrangement for these devices is kept constant for the investigation; therefore it has no bearing on the impact of the absolute temperature of the working fluid on the effectiveness of the heat exchanger.

In literature, the ratio of the heat capacity rates C_c and C_h was assumed to be unity due to equal flow condition [13,14,18], in accordance with the CSA test standard. The validity of this assumption is investigated for typical temperatures within DWHR systems. Water temperatures from 5°C to 45°C are

what can be expected for DWHR systems in residential applications. In this range, the density of water varies from 1000.0 to 989.8 kg/m^3 and the specific heat of water varies from 4.20 to 4.18 $kJ/kg \cdot °C$ [26]. For clarity, C_c and C_h will be replaced with $C_{\min}$ and $C_{\max}$ in the following discussion, where $C_{\max}$ refers to the higher of the two heat capacity rates.

Under equal volumetric flow rates, the ratio of heat capacity rates can be simplified to a ratio of densities and specific heats, as shown in Equation 4.2.

$$\frac{C_{\min}}{C_{\max}} = \frac{(\dot{m}C_p)_{\min}}{(\dot{m}C_p)_{\max}} = \frac{(\rho\dot{V}C_p)_{\min}}{(\rho\dot{V}C_p)_{\max}} = \frac{(\rho C_p)_{\min}}{(\rho C_p)_{\max}} \tag{4.2}$$

To estimate the maximum expected deviation from unity, water properties at the two inlet temperatures are used in Equation 4.2. This is a more conservative approach than using the mean temperatures on the hot and cold sides. The density and specific heat for the inlet temperatures of 5°C and 45°C are used in Equation 4.3 as follows:

$$\frac{(\rho C_p)_{\min}}{(\rho C_p)_{\max}} = \frac{(\rho C_p)|_{45°C}}{(\rho C_p)|_{5°C}} = \frac{4137.2 \dfrac{kJ}{m^3 °C}}{4202.8 \dfrac{kJ}{m^3 °C}} = 98.4\% \tag{4.3}$$

This calculation predicts a maximum difference of 1.6% between $C_{\min}$ and $C_{\max}$. When DWHR systems are rated, this ratio is assumed to be unity due to the equal flow conditions, which means this small bias exists in the rated values for all systems. However, the small magnitude of this bias, even at the worst case scenario, supports the validity of this assumption. As a result, it is safe to assume that for DWHR systems operating under equal volumetric flow:

$$\frac{C_{\min}}{C_{\max}} \cong 1 \tag{4.4}$$

CSA standards use the unity assumption to define Equation 2.3, which is used to rate DWHR systems for equal flow conditions [9].

Although the unity assumption introduces minor innacuracies for effectiveness calculations, the assumption does not fully explain the effectiveness changes with inlet temperatures.

The final term from Equation 4.2 to consider is the Number of Transfer Units, NTU, which is defined in Equation 4.5:

$$NTU = \frac{UA}{C_{\min}} \tag{4.5}$$

where U is the overall heat transfer coefficient and A is the heat transfer area [19].

The value of $C_{\min}$ is mainly influenced by the flow rate since the changes in density and specific heat of water are on the order of 1% over the range of operating temperatures. This suggests that the UA product must have a substantial dependence on absolute temperatures.

In order to analytically study the UA product for DWHR systems, it was necessary to closely look at their construction. Typically, the coils are wrapped under tension around the drain pipe and no thermal adhesive is used. To confirm this, a 10.2 cm diameter pipe was cut open to expose the interface between the coils and the drain pipe. The leftmost image in Figure 4-1 shows a top view of the system without a cut through the coil wrap, illustrating the very tight wrap of the coil around the drain pipe. The center image shows a cut section of the coil and the right image shows a closeup of the contact interface between the coil and the drain pipe.

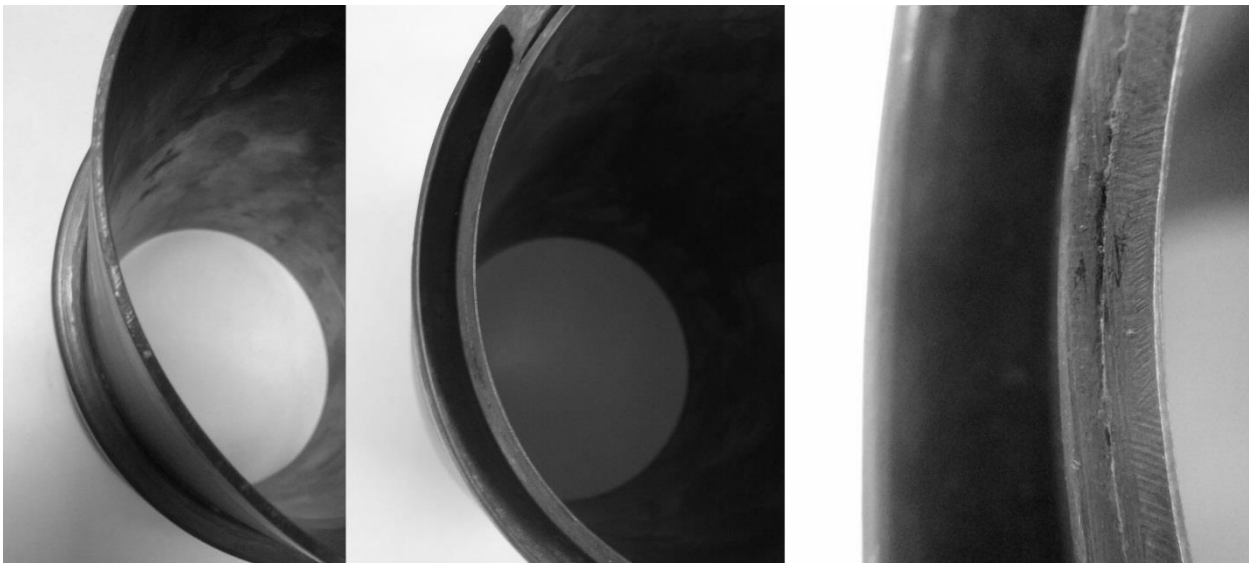

Figure 4-1 Typical construction of a 10.2 cm DWHR system, where the leftmost picture shows the coils wrapped around the drain pipe, the picture in the middle shows a coil that was cut and the rightmost picture shows the contact interface between the coil and the drain pipe.

A schematic of a typical DWHR system's construction is shown in Figure 4-2. The top view shown in the figure corresponds to the perspective from Figure 4-1 and the side view shows the coils' cross section. Surface temperature notations are identified on the schematic, along with corresponding distances to the center of the drain pipe. The effects of heat exchanger fouling, evaporation and heat losses to the environment were neglected in the development of this schematic.

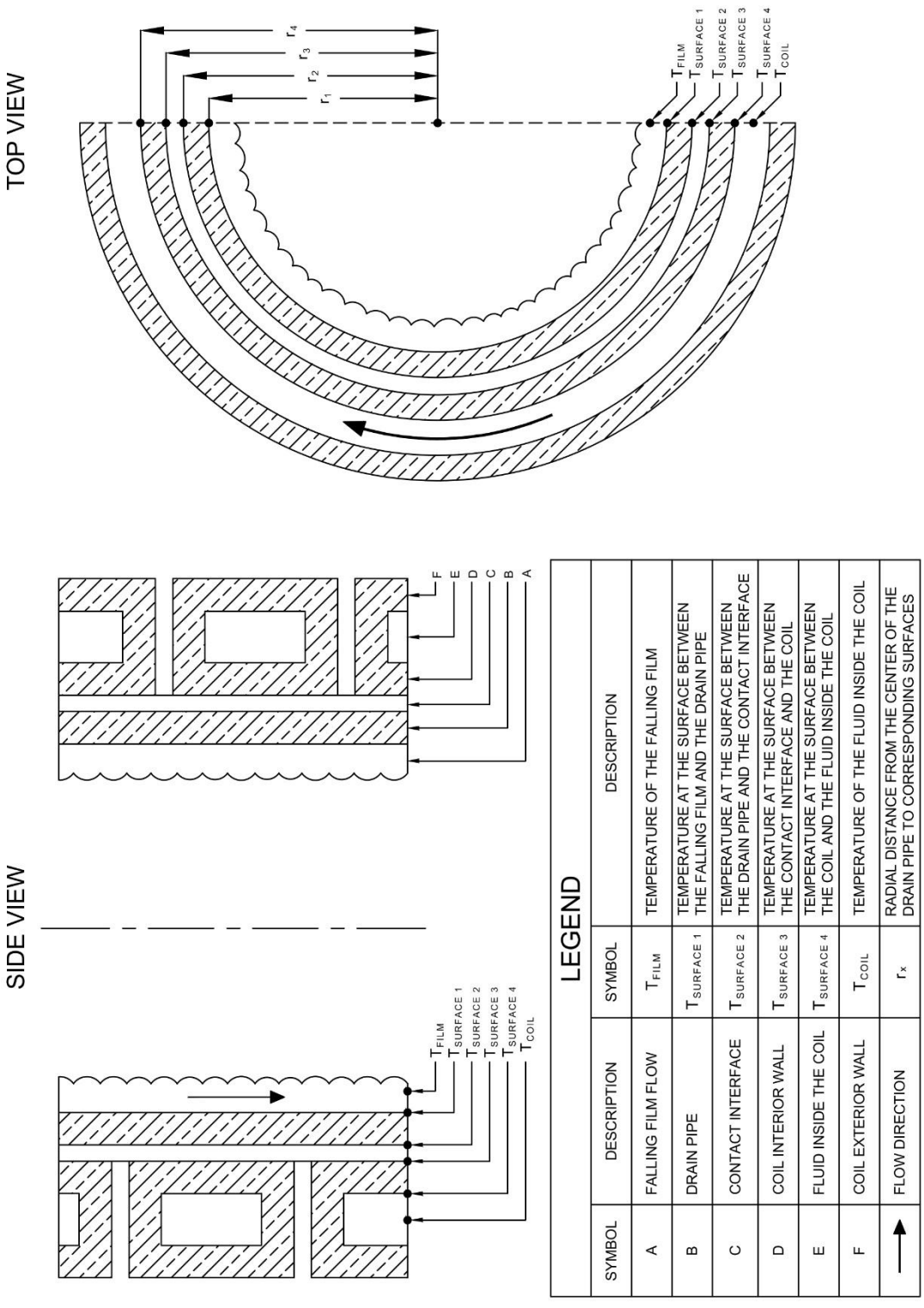

Figure 4-2 Schematic of heat transfer surfaces and temperatures within a DWHR system.

The heat transfer schematic can be represented by a network of thermal resistors, $R_{\#}$, as shown in Figure 4-3.

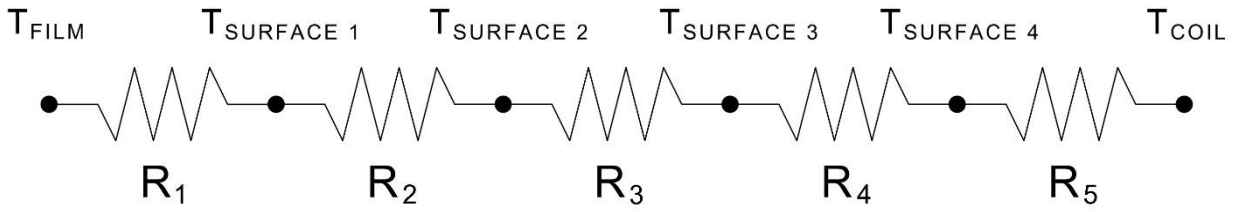

Figure 4-3 Thermal resistor network used to analytically estimate the UA product for DWHR systems.

The overall heat transfer coefficient for a DWHR system is expressed in Equation 4.6 based on the addition of the resistors in series [26].

$$\frac{1}{UA} = R_{Total} = R_1 + R_2 + R_3 + R_4 + R_5 \tag{4.6}$$

Resistors are discussed individually to analyze the temperature dependency.

Resistor R_1 corresponds to the convective heat transfer between the falling film and the drain pipe, defined by Equation 4.7:

$$R_1 = \frac{1}{h_{film} \times 2\pi \times r_1 \times L} \tag{4.7}$$

Where h_{film} is the falling film's convective heat transfer coefficient, r_1 is the radius as depicted in Figure 4-2, and L is the length of the drain pipe.

Correlations for estimating h_{film} in copper pipes have been developed by McAdams et al. [27] and improved by Prost et al. [28]. The correlation from [28] is used, as defined by Equation 4.8:

$$h_{film} = 0.01(\mathrm{Re}_D)^{\frac{1}{3}}(\mathrm{Pr})^{\frac{1}{3}}\left(\frac{k^3 g\rho^2}{\mu^2}\right)^{\frac{1}{3}} \tag{4.8}$$

where Re_D is the Reynolds number, Pr is the Prandtl number, k is the thermal conductivity, g is the gravity constant, ρ is the density, and μ is the fluid's dynamic viscosity.

This correlation was developed for turbulent falling films of water inside vertical copper tubes and is valid for $1{,}600 < \mathrm{Re}_D < 50{,}000$. It assumes the falling film remains undisturbed, and fully covers the entire surface area of the drain pipe. This correlation was chosen since it was developed for copper tubes, which is the most common material in the construction of DWHR systems. Also, the range of Reynolds numbers listed is broad enough to include all DWHR systems operating under typical conditions.

Resistor R_2 represents the conductive heat transfer that occurs through the thickness of the drain pipe, as shown in Equation 4.9:

$$R_2 = \frac{\ln\left(\frac{r_2}{r_1}\right)}{2\pi \times L \times k_C} \tag{4.9}$$

where r_1 and r_2 are radii as depicted in Figure 4-2, L is the length of the drain pipe, and k_C is the thermal conductivity of the drain pipe material, in this case copper.

Resistor R_3 corresponds to the conductive heat transfer that occurs through the contact interface between the drain pipe and the coils, as shown in Equation 4.10:

$$R_3 = \frac{\ln\left(\frac{r_3}{r_2}\right)}{2\pi \times L_{Coil} \times k_{interface}} \tag{4.10}$$

where r_2 and r_3 are radii as depicted in Figure 4-2, L_{Coil} is the length of the drain pipe that is wrapped with coils $\left(L_{Coil} < L\right)$ and $k_{interface}$ is the thermal conductivity of the interface.

Resistor R_4 represents the conductive heat transfer that occurs through the walls of the coils, as shown in Equation 4.11:

$$R_4 = \frac{\ln\left(\frac{r_4}{r_3}\right)}{2\pi \times L_{Coil} \times k_C} \tag{4.11}$$

where r_3 and r_4 are radii as depicted in Figure 4-2, L_{Coil} is the length of the drain pipe that is wrapped with coils, and k_C is the thermal conductivity of the copper coils.

Resistor R_5 represents the convective heat transfer that occurs inside the coils, as shown in Equation 4.12:

$$R_5 = \frac{1}{h_{coil} \times 2\pi \times r_4 \times L_{Coil}} \tag{4.12}$$

where h_{coil} is the convective heat transfer coefficient for the fluid flowing through the coils, r_4 is the radius as depicted in Figure 4-2, and L_{Coil} is the length of the drain pipe that is wrapped with coils.

Estimating h_{coil} is difficult due to the variety of DWHR designs. Depending on the number of coils, the flow could be either laminar or turbulent, which affects the heat transfer coefficient appreciably. Also, correlations in the literature have been developed for helical coils of *circular cross section*, whereas coils

wrapped around DWHR systems typically have a rectangular cross-section. As a result, the correlations presented for calculating h_{coil} are not to be used for design purposes; they are presented here to identify the influence of temperature on the heat transfer coefficient.

For laminar flow, a Nusselt number correlation developed by Dravid et al. [29] was used, which is shown in Equation 4.13:

$$Nu = \left(0.76 + 0.65\sqrt{De}\right)\mathrm{Pr}^{0.175} \tag{4.13}$$

Equation 4.14 shows the expression for De which is the Dean number for the coil:

$$De = \mathrm{Re}_D \sqrt{\frac{d}{D}} \tag{4.14}$$

where variables d and D represent the tube diameter and mean coil diameter, respectively, as labeled in Figure 4-4.

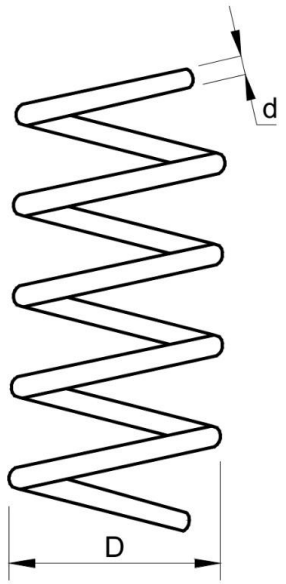

Figure 4-4 Diagram of a helical tube. Adapted from Incropera et al. [26].

Equation 4.15 shows the heat transfer coefficient determined using the Nusselt number correlation from Equation 4.13.

$$h_{coil} = Nu\left(\frac{k}{d}\right) = \left(0.76 + 0.65\sqrt{De}\right)\mathrm{Pr}^{0.175}\left(\frac{k}{d}\right) \tag{4.15}$$

Equation 4.16 has been proposed by Shah and Joshi [30] to identify the critical Reynolds number for transition to turbulent flow in a helical coil:

$$\mathrm{Re}_{critical} = 2100\left[1 + 12\sqrt{\frac{d}{D}}\right] \tag{4.16}$$

This correlation was developed for helical coils of circular cross section; therefore, it may have limitations in predicting the critical Reynolds numbers for rectangular cross sections.

For turbulent flow, a Nusselt number correlation developed by Rogers et al. [31] is used, as shown in Equation 4.17.

$$Nu = 0.023\mathrm{Re}_D^{0.85}\,\mathrm{Pr}^{0.4}\left(\frac{d}{D}\right)^{0.1} \tag{4.17}$$

The heat transfer coefficient can be calculated using the Nusselt number correlation, as shown in Equation 4.18:

$$h_{coil} = Nu\left(\frac{k}{d}\right) = 0.023\mathrm{Re}_D^{0.85}\,\mathrm{Pr}^{0.4}\left(\frac{d}{D}\right)^{0.1}\left(\frac{k}{d}\right) \tag{4.18}$$

An experimental study was performed to investigate the temperature dependence behavior predicted in this section and quantify the change in effectiveness. Based on the experimental results, a technique was developed to correct for the impact of inlet temperatures on effectiveness.

4.3 Method

DWHR systems of various diameters and from the same manufacturer were tested at various temperatures to determine the impact on effectiveness. Two 7.6cm diameter systems with lengths of 122 and 153cm, two 10.2cm diameter systems with lengths of 122 and 153cm and one 5.1cm diameter system with a length of 122cm were used for this study. Tests were performed under equal flow conditions at flow rates of 5.5, 9.5 and 14 liters per minute (LPM), encompassing the range of flow rates specified in the CSA standard [9].

The inlet temperatures chosen for the tests were 25, 30, 35, 40 and 45°C on the drain-side and 5, 10, 15 and 20°C on the mains-side. The goal was to maintain a temperature difference of at least 10°C across the heat exchanger to represent realistic operating conditions.

All tests were performed at equal flow condition and as such, the effectiveness of the systems at each condition was calculated using Equation 2.4 as perscribed by the CSA standards [9].

Tests were performed to evaluate if the change in effectiveness is affected significantly by insulating the DWHR system and capping the system to minimize losses to the environment. Unless otherwise stated, the presented results are for an uncapped, uninsulated DWHR system.

4.4 Results

The raw data used to create the figures in this chapter are presented in tabular form in Appendix C.

The first set of tests were performed on the 7.6cm diameter, 122cm long DWHR system. Figure 4-5 shows the results at a flow rate of 9.5 LPM. The effectiveness of the system increased with $T_{c,i}$ while $T_{h,i}$ was kept constant. The effectiveness also increased with $T_{h,i}$ while $T_{c,i}$ was kept constant. The results showed that increasing the inlet temperature on either side of the DWHR system would result in a higher effectiveness value. The horizontal error bars for temperature are within ±0.1°C of the points

which are barely visible on the graph. The vertical error bars are calculated based on Moffat's method [24] at the worst case scenarios as per Appendix B.

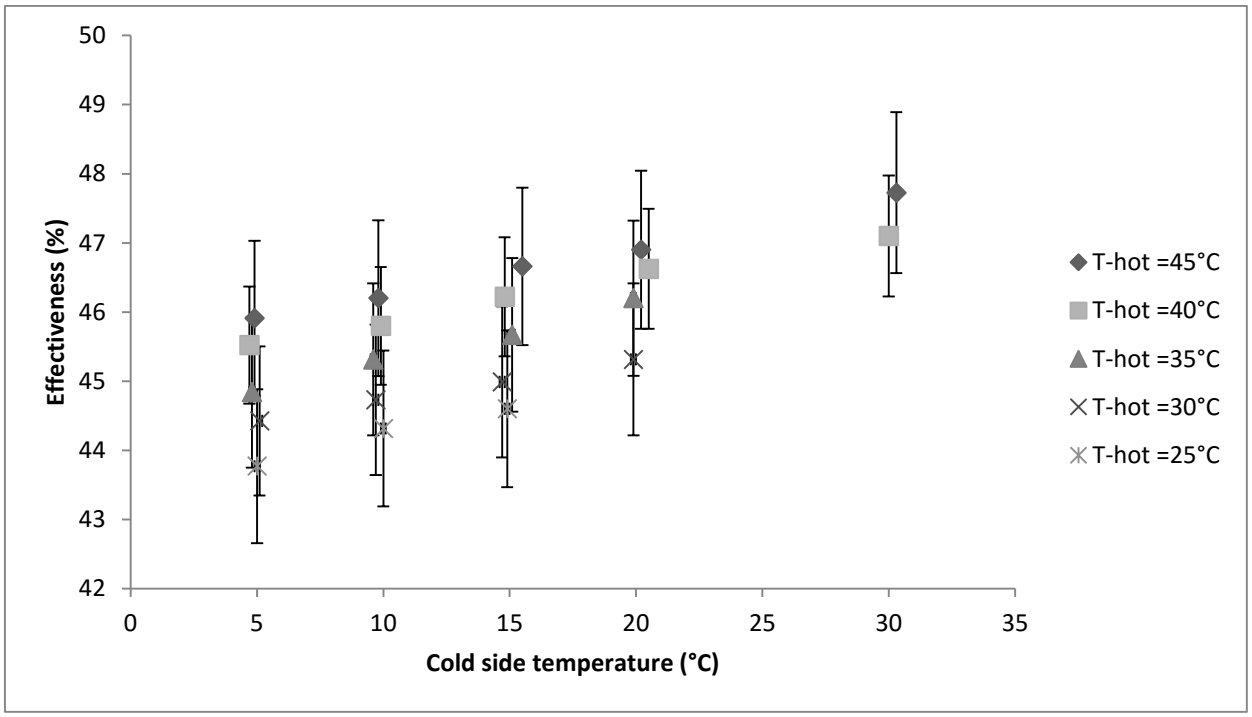

Figure 4-5 Measured effectiveness values for the 7.6cm diameter, 122cm long system tested at 9.5 LPM.

These results showed that the measured effectiveness for this DWHR system varied from about 44% to 48% depending on the inlet temperatures. The effectiveness varied with the temperature difference between the inlets, but also for different inlet temperatures when the temperature difference remained constant.

The remaining three DWHR systems produced results at 9.5 LPM similar to what was shown in Figure 4-5, and are shown in Figure 4-6, Figure 4-7 and Figure 4-8. The results of the tests performed at 5.5 and 14 LPM also generated graphs with similar trends, which are shown in Figure 4-9 through Figure 4-14.

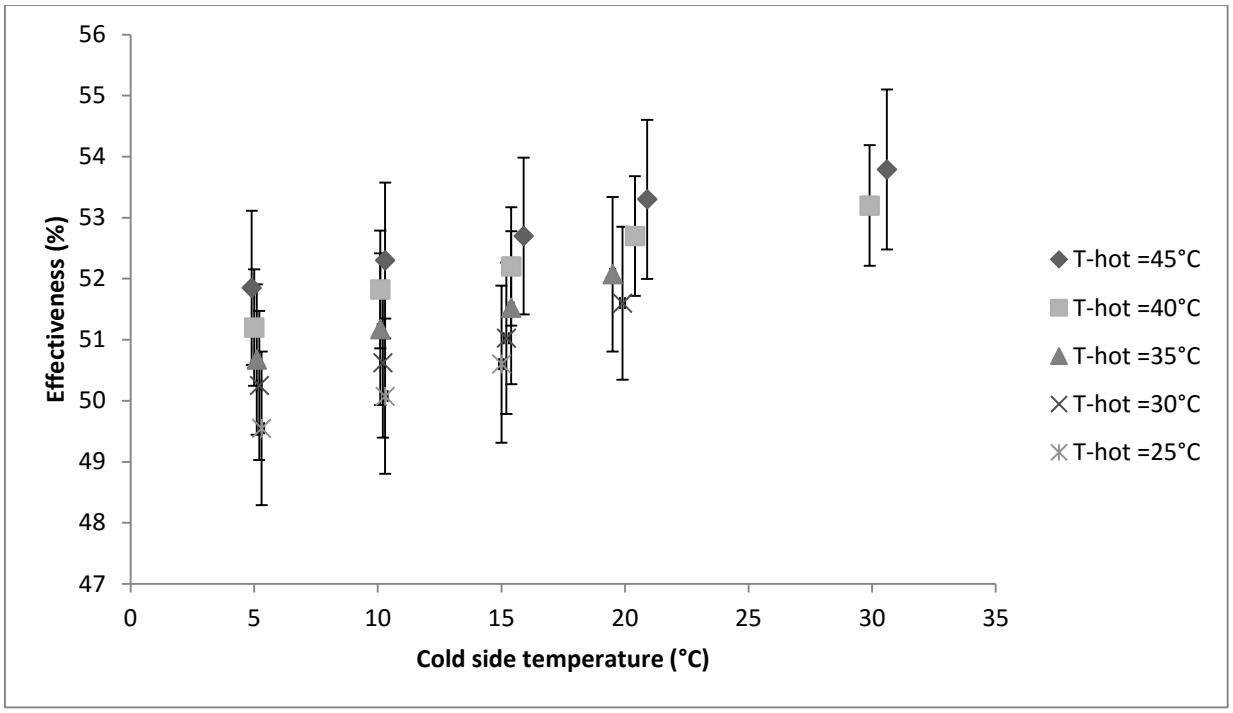

Figure 4-6 Measured effectiveness values for the 7.6cm diameter, 153cm long system tested at 9.5 LPM.

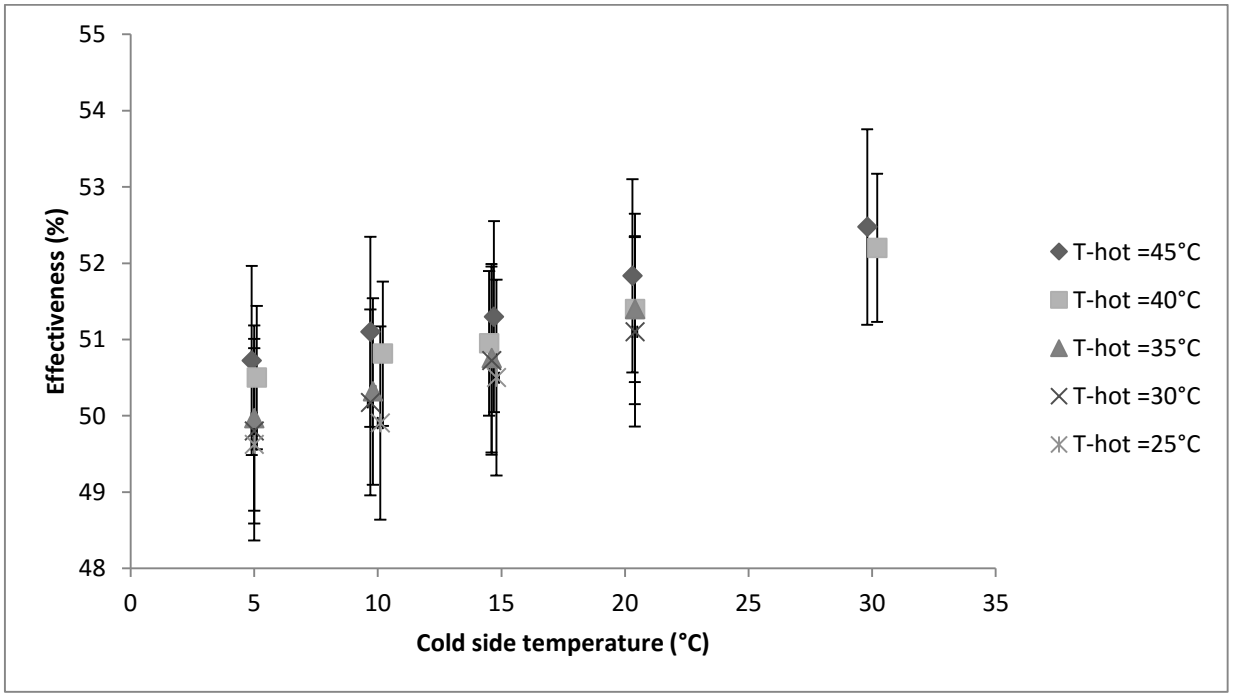

Figure 4-7 Measured effectiveness values for the 10.2cm diameter, 122cm long system tested at 9.5 LPM.

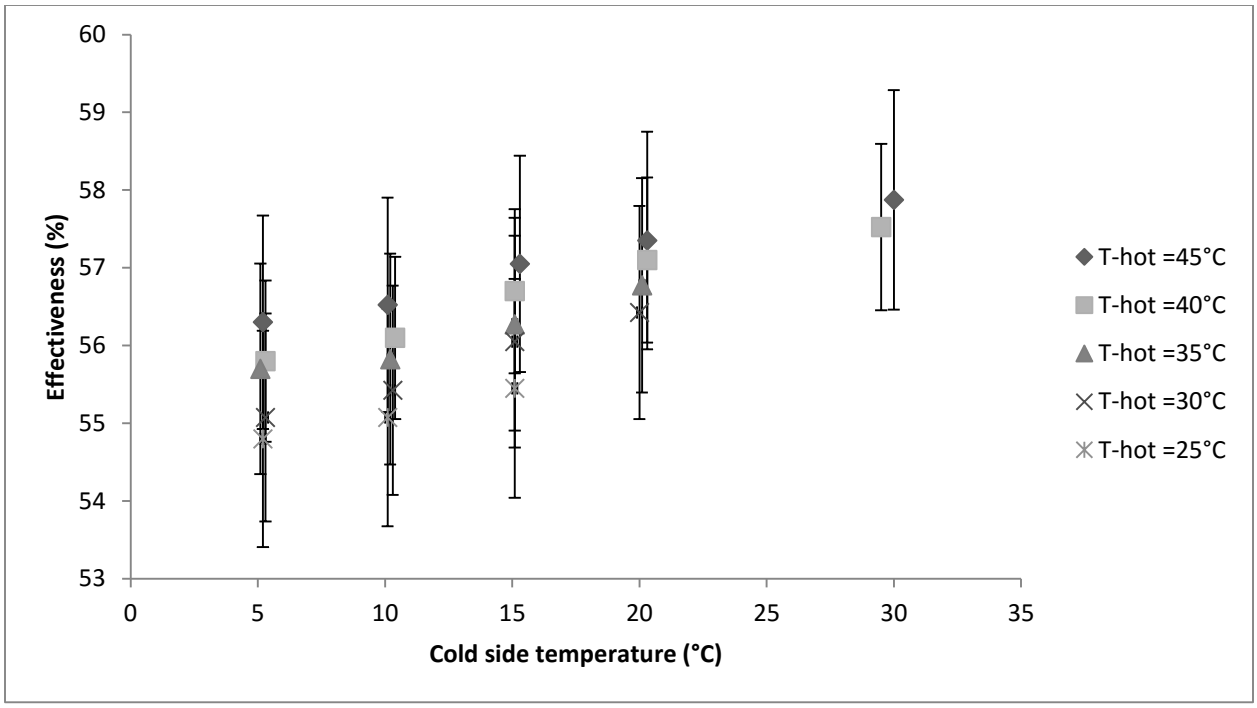

Figure 4-8 Measured effectiveness values for the 10.2cm diameter, 153cm long system tested at 9.5 LPM.

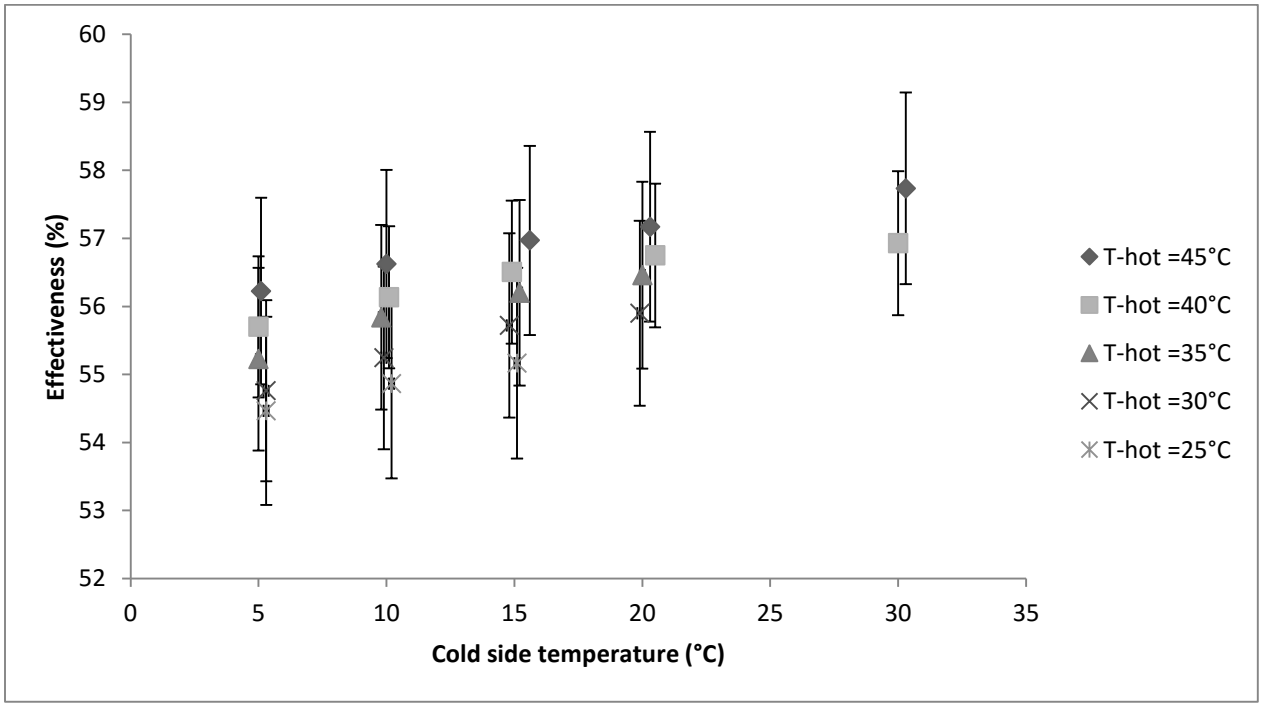

Figure 4-9 Measured effectiveness values for the 7.6cm diameter, 122cm long system tested at 5.5 LPM.

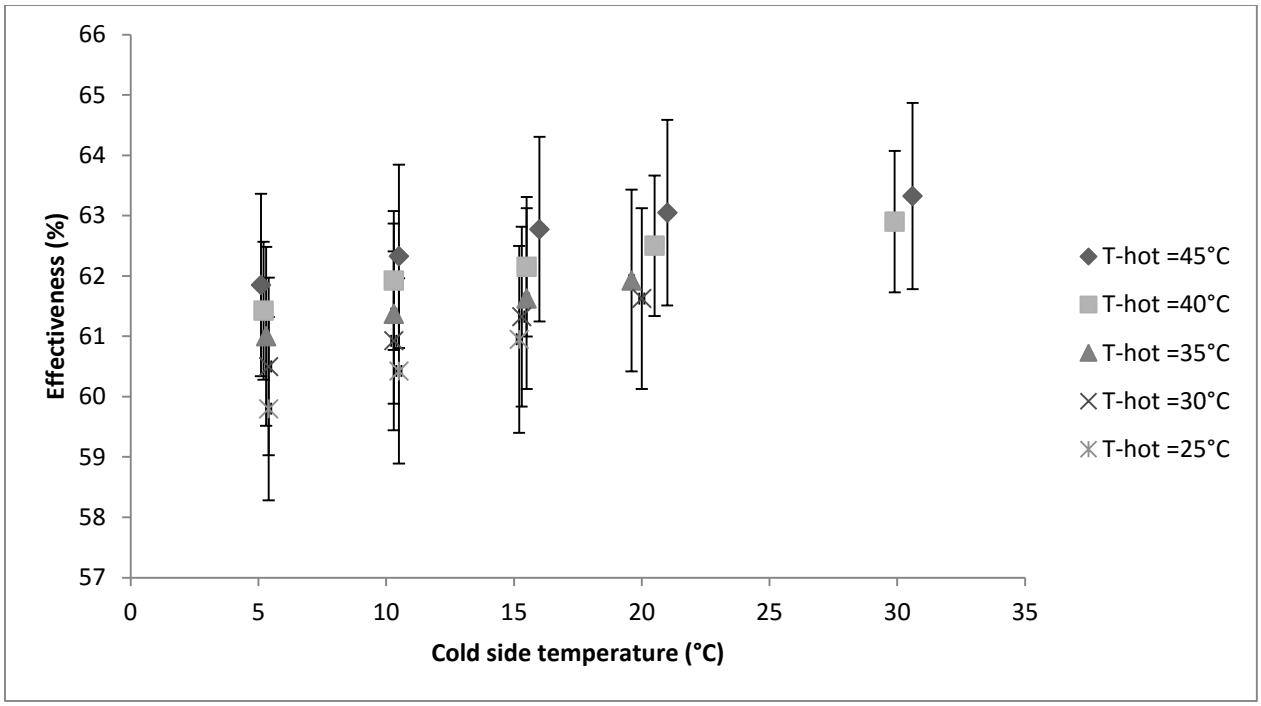

Figure 4-10 Measured effectiveness values for the 7.6cm diameter, 153cm long system tested at 5.5 LPM.

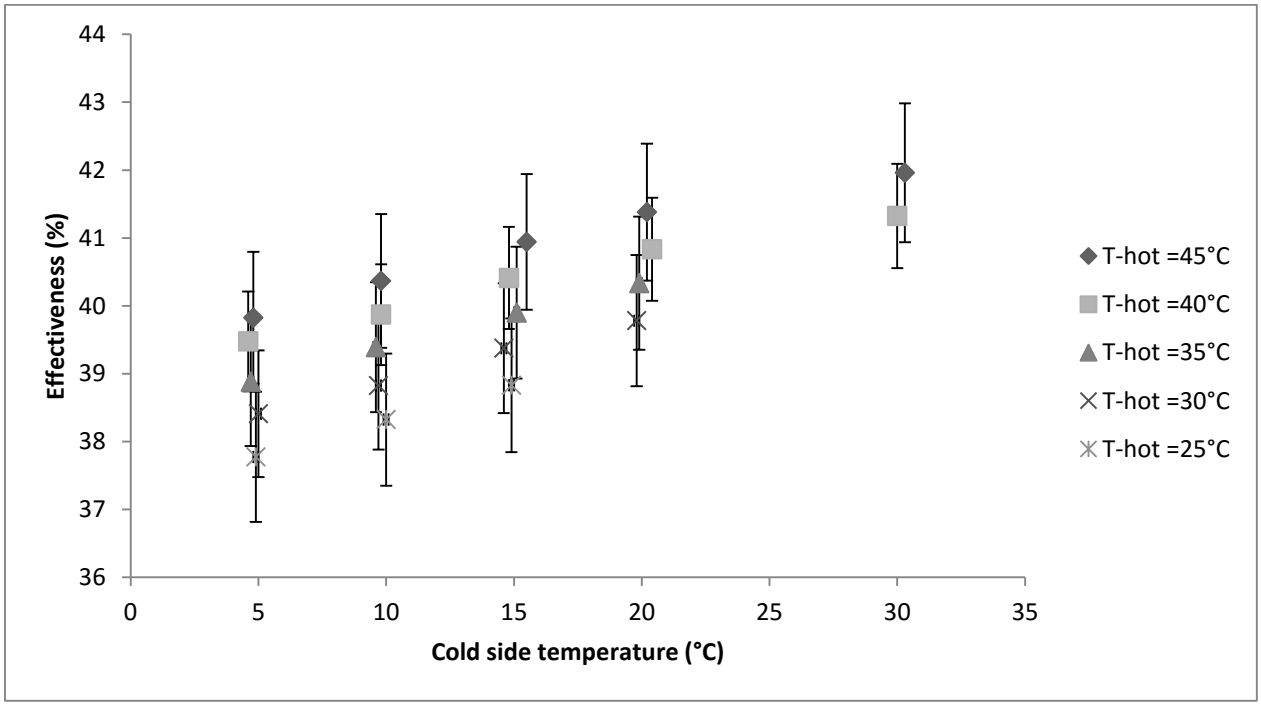

Figure 4-11 Measured effectiveness values for the 7.6cm diameter, 122cm long system tested at 14 LPM.

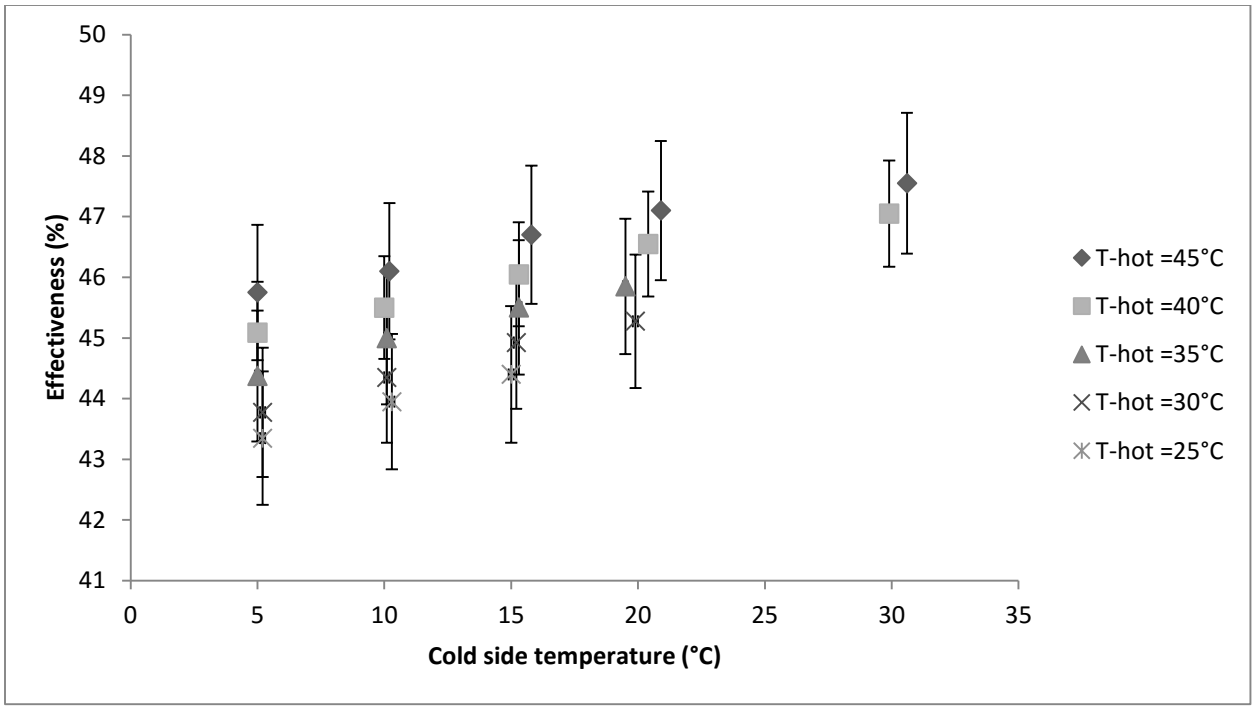

Figure 4-12 Measured effectiveness values for the 7.6cm diameter, 153cm long system tested at 14 LPM.

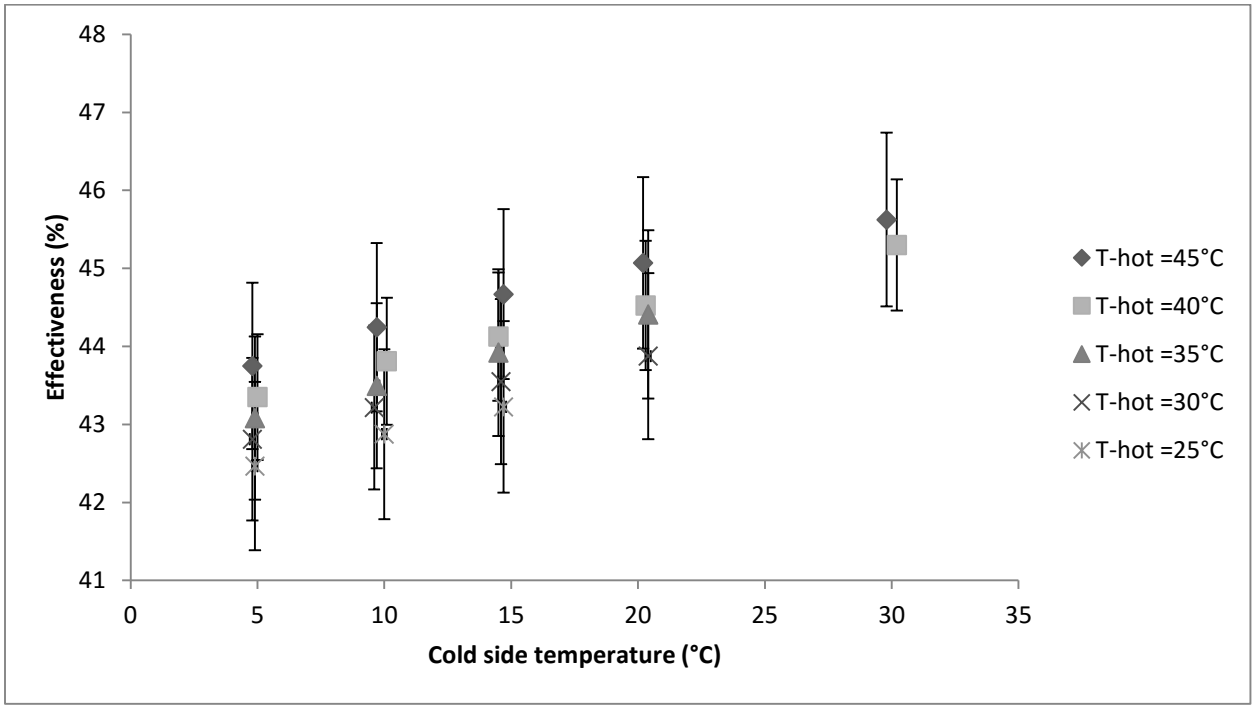

Figure 4-13 Measured effectiveness values for the 10.2cm diameter, 122cm long system tested at 14 LPM.

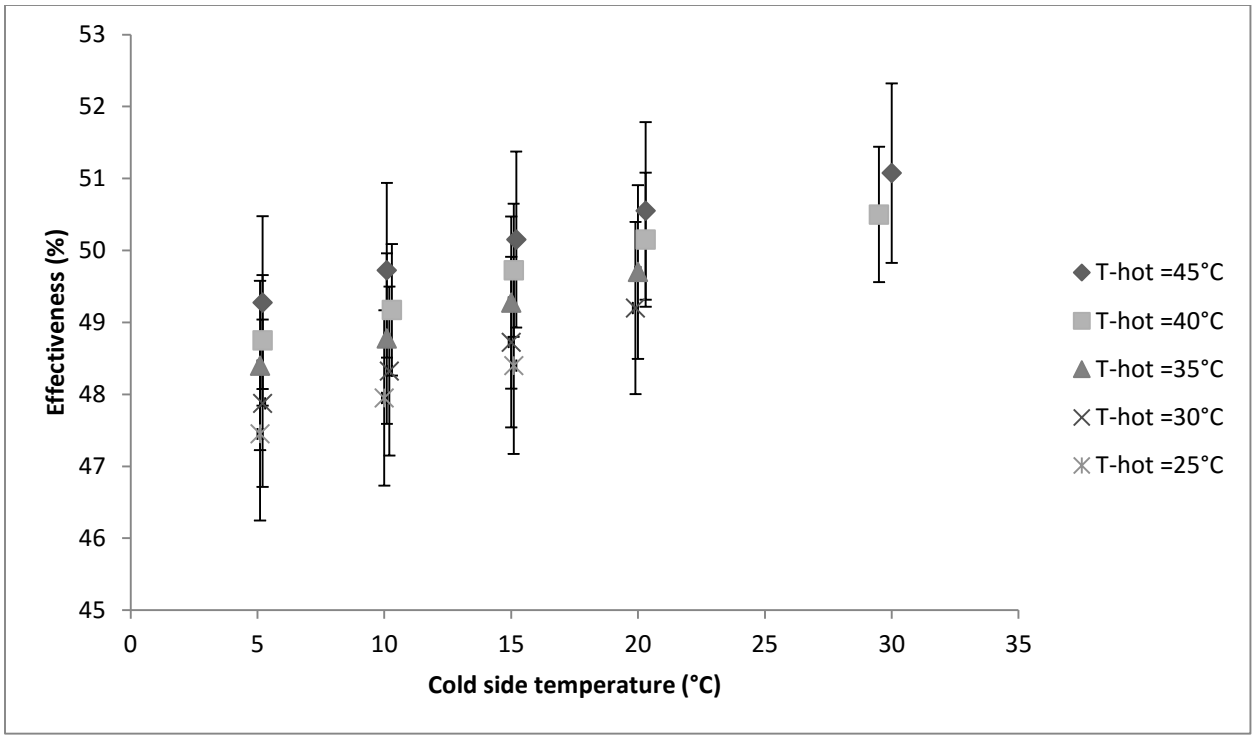

Figure 4-14 Measured effectiveness values for the 10.2cm diameter, 153cm long system tested at 14 LPM.

It was worthwhile to check if the change in effectiveness was due to evaporative and/or thermal losses from the system. To determine the effect of evaporation, the 7.6cm diameter, 122cm long DWHR system was capped to minimize evaporative losses. The effectiveness of the system was measured at multiple cold side temperatures for a flow rate of 9.5 LPM at $T_{h,i}$ = 45°C. To evaluate the effect of thermal losses , the system was wrapped with insulation of RSI = 0.25 $m^2°C/W$, and its effectiveness was measured at various cold side temperatures for a flow rate of 9.5 LPM at $T_{h,i}$ = 45°C. The ambient temperature for all tests was 20±1°C. Figure 4-15 shows the results for the evaporative and thermal loss tests performed, plotted against the results from an uninsulated, uncapped system.

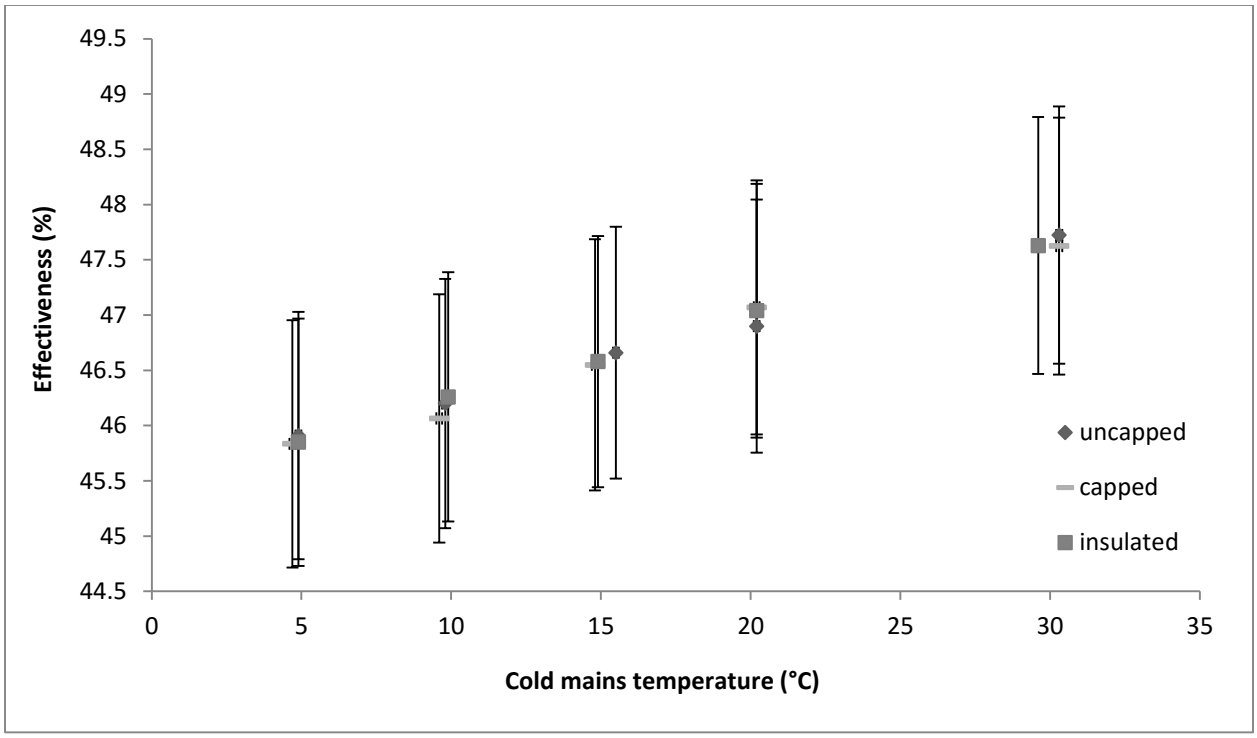

Figure 4-15 Measured effectiveness values for uncapped/uninsulated, capped and insulated 7.6cm diameter, 122cm long DWHR system tested at a flow rate of 9.5 LPM and a constant drain-side temperature of 45°C.

It was observed that increasing $T_{c,i}$ would result in higher effectiveness values regardless of whether or not the system was capped or insulated. The results from the three different sets of tests were very close in magnitude; therefore, it was confirmed that the losses from the system are negligible. As a result, it was hypothesized that the change in effectiveness is primarily due to the change in the convective heat transfer coefficients on either side of the DWHR system.

To enable designers to estimate the change in effectiveness of a DWHR system based on inlet temperatures, a correlation was developed based on the experimental results of this study. A practical method of achieving this was to establish a reference point based on inlet temperatures to normalize effectiveness.

The reference point was chosen to be at $T_{h,i}$ = 40°C and $T_{c,i}$ = 10°C, which are closest to the typical temperatures of the CSA test standard and the Europian standards [9,25]. The effectiveness at other temperatures are represented as a ratio to the reference point, as shown in Equation 4.19.

$$F_C = \frac{\varepsilon_{Corrected}}{\varepsilon_{Reference}} \tag{4.19}$$

In Equation 4.19, $\varepsilon_{Corrected}$ is the effectiveness at any inlet temperature and F_C is the ratio between $\varepsilon_{Corrected}$ and the effectiveness at the reference temperature, $\varepsilon_{Reference}$.

Using the above approach, the experimental results were split into two groups: one with constant drain-side inlet temperature and the second with constant mains-side inlet temeprature. Correlations were determined from each of the groups, with a linear fit found most appropriate. The two correlations were then comined for all temperatures, flow rates, and systems to produce Equation 4.20. This allows F_C to be calculated for any desired inlet temperatures, where all temperatures are in degrees Celsius.

$$F_C = \frac{2.37\times10^{-6}}{(°C)^2}\times T_{h,i}\times T_{c,i} + \frac{1.75\times10^{-3}}{°C}\times T_{h,i} + \frac{1.24\times10^{-3}}{°C}\times T_{c,i} + 0.917 \tag{4.20}$$

Using Equation 4.20, the corrected effectiveness can be calculated based on the reference effectiveness as shown in Equation 4.21.

$$\varepsilon_{Corrected} = \varepsilon_{Reference}\times F_C \tag{4.21}$$

The worst case of experimental uncertainty for effectiveness measurements was calculated to be ±2.54% of the value. Calculating experimental F_C values has an uncertainty ±3.6% of the value via Moffat's method [24] since two effectiveness measurements are required. Equation 4.20 is linear fit of

experimental data, therefore additional errors are introduced, but they are small due to a good fit of the data.

Equation 4.21 was verified by comparing its results to the experimental data. Points obtained at different inlet temperatures and flow rates were used for each DWHR tested, as shown in Table 4-1. The effectiveness for each case was predicted using Equation 4.21 and listed under column $\varepsilon_{Corrected}$. The predicted effectiveness was compared the experimentally measured effectiveness. The difference between the predicted values and the measured values are shown under the column labelled Prediction Error, with a maximum value of 0.37%.

Table 4-1 Predicted vs. measured effectiveness for several DWHR systems.

DWHR Diameter; Length	Flow Rate, LPM	$T_{h,i}$, °C	$T_{c,i}$, °C	$\varepsilon_{\text{Reference}}$, %	F_C, %	$\varepsilon_{Corrected}$, %	$\varepsilon_{measured}$, %	Prediction Error, %
7.6 cm; 122 cm	5.5	45	5	56.14	100.25	56.27	56.23	0.04
	9.5	25	10	45.80	97.37	44.60	44.32	0.28
	14	35	20	39.87	100.47	40.06	40.34	0.28
7.6 cm; 153 cm	5.5	30	15	61.93	98.92	61.25	61.63	0.37
	9.5	45	30	51.83	103.61	53.70	53.79	0.09
	14	40	5	45.50	99.37	45.21	45.09	0.12
10.2 cm; 122 cm	9.5	30	10	50.82	98.26	49.93	50.18	0.25
	14	35	5	43.81	98.49	43.15	43.08	0.07
10.2 cm; 153 cm	9.5	45	10	56.10	100.92	56.62	56.53	0.09
	14	40	20	49.18	101.37	49.85	50.15	0.30

In addition, a DWHR system which was not used for producing the temperature correlation was picked to verify the applicability of the correlation to systems with different diameters. The unit tested was a 5.1cm diameter, 122cm long DWHR system. Equation 4.21 was used to predict the effectiveness of this system under various inlet temperatures and flow rates for 6 cases. The results showed a maximum prediction error of 0.19%, which is within the expected bounds reported. This further confirmed the

validity of the correlation since it was capable of accurately predicting the temperature-dependent effectiveness for a DWHR system with a diameter different from those used to develop the correlation.

Table 4-2 Predicted vs. measured effectiveness for the 5.1cm diameter, 122cm long DWHR

Flow Rate, LPM	$T_{h,i}$, °C	$T_{c,i}$, °C	$\varepsilon_{\text{Reference}}$, %	F_C, %	$\varepsilon_{Corrected}$, %	$\varepsilon_{measured}$, %	Prediction Error, %
5.5	45	5	48.95	100.25	49.07	49.13	0.05
5.5	30	15	48.95	98.92	48.42	48.38	0.04
9.5	45	5	39.98	100.25	40.07	39.95	0.12
9.5	30	15	39.98	98.92	39.54	39.35	0.19
14	45	5	34.08	100.25	34.16	34.18	0.02
14	30	15	34.08	98.92	33.71	33.60	0.11

The correlation can also be used to correct the existing rated effectiveness of DWHR systems for temperatures different from the rating conditions. The CSA standardized test procedure is conducted at specific temperature conditions, with $T_{c,i}$ = 7-17°C and a temperature difference of $T_{h,i} - T_{c,i}$ = 28±1°C. The temperatures from the CSA data can be used to calculate F_C according to Equation 4.20, and the rated effectiveness is equivalent to $\varepsilon_{Corrected}$. Equation 4.21 can be reworked to isolate for $\varepsilon_{Reference}$, the effectiveness at reference conditions:

$$\varepsilon_{Reference} = \frac{\varepsilon_{Corrected}}{F_C} \tag{4.22}$$

With $\varepsilon_{Reference}$ known, the effectiveness can be estimated for any inlet temperatures using Equation 4.21.

This procedure enables performance of DWHR systems to be compared on a uniform basis, regardless of the absolute temperature values from the ratings.

To provide an alternative method to illustrate the effect of the temperature correction, the CSA curve for the 7.6cm diameter, 122cm long system was plotted for three different sets of inlet temperatures as shown in Figure 4-16. Higher inlet temperatures result in higher effectiveness values, even when the temperature difference between the inlets is kept constant.

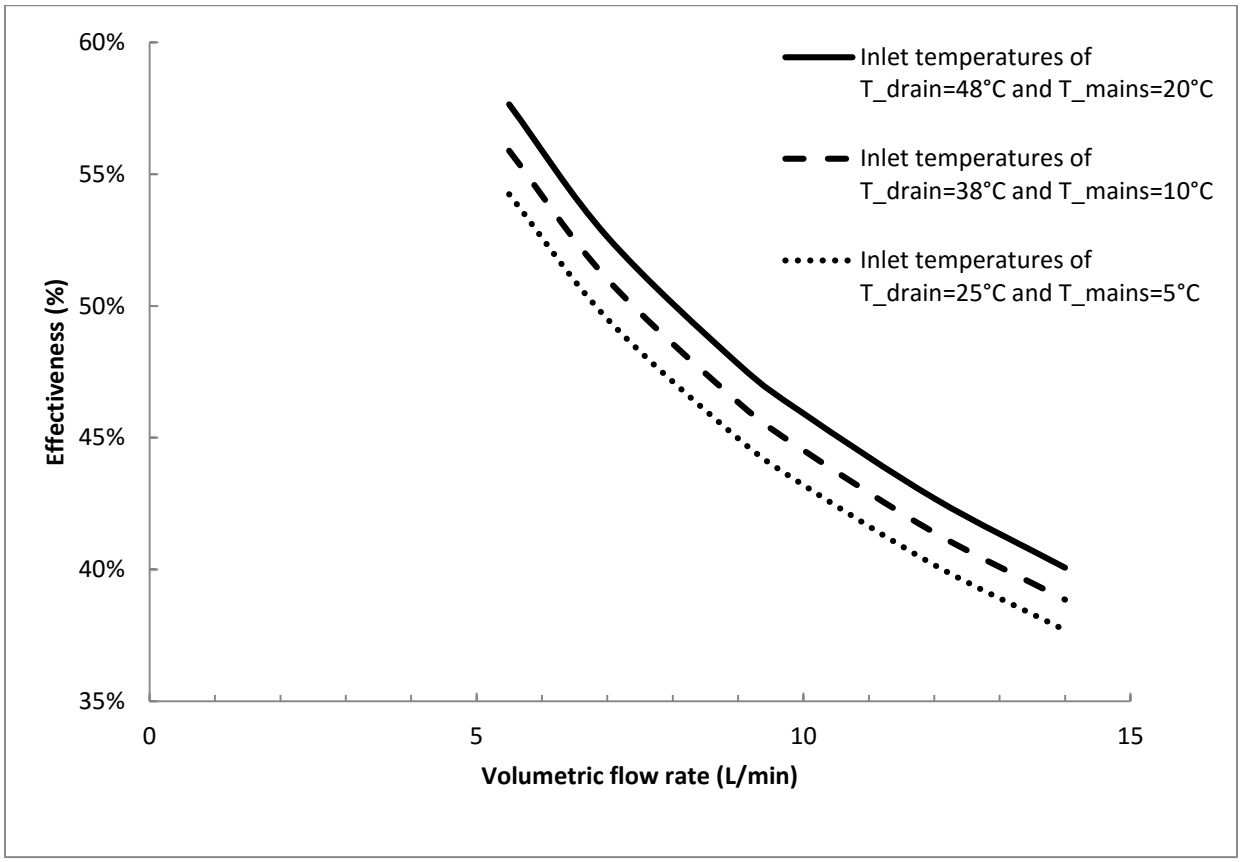

Figure 4-16 Characteristic effectiveness vs. volumetric flow rate for the 7.6cm diameter, 122cm long DWHR system at three different sets of inlet temperatures.

To investigate the validity of the resistor network, the results for a select set of experiments are compared to the results from the theoretical approach for one of the DWHR systems tested.

The physical dimensions for the 7.6cm diameter, 122cm long DWHR system are summarized in Table 4-3.

Table 4-3 Physical dimensions for the 7.6cm diameter, 122cm long system tested.

Parameter	Value
L, m	1.22
L_{Coil}, m	1.0
d, mm	7.17
D, mm	90
r_1, mm	39.5
r_2, mm	40.75
r_3, mm	40.75
r_4, mm	42
# of coils	4

Four cases were considered: cases 1 and 2 are at a flow rate of 9.5 LPM and cases 3 and 4 are at a flow rate of 14 LPM. The experimental results are summarized in Table 4-4.

Table 4-4 Experimental results for 7.6cm diameter, 122cm long DWHR system.

	Case 1	Case 2	Case 3	Case 4
Flowrate, LPM	9.5		14.0	
Average T_{mains}, °C	33.8	9.4	33.4	8.8
Average T_{drain}, °C	41.5	20.9	42.0	21.5
Experimental ε, %	47.7	43.8	42.0	37.8
Experimental UA, W/°C	600.5	516.8	700.8	594.1

To solve the resistor network, average temperatures from the experiments were used. The properties of water used in the calculations were determined at these average temperatures. The value of R_3 is uncertain; hence, R_3 was assumed to be negligible since solving this resistor is beyond the scope of the current study.

The results of solving the resistor network for the 4 cases are summarized in Table 4-5.

Table 4-5 Analytical results for the four cases of interest for the 7.6cm diameter, 122cm long system.

	Case 1	Case 2	Case 3	Case 4
Flowrate, LPM	9.5		14.0	
Average T_{mains}, °C	33.8	9.4	33.4	8.8
Average T_{drain}, °C	41.5	20.9	42.0	21.5
h_{film}, $W/m^2\,°C$	4661.5	3405.2	5341.3	3879.6
h_{coil}, $W/m^2\,°C$	7057.3	3147.2	9773.8	3773.9
Re_{coil}, Dimensionless	9445.4	5320.6	13811.3	7703.1
$Flow_{coil}$	Turbulent	Laminar	Turbulent	Laminar
R_1, °C /W	7.08E-04	9.70E-04	6.18E-04	8.43E-04
R_2, °C /W	1.01E-05	1.01E-05	1.01E-05	1.01E-05
R_3, °C /W	0	0	0	0
R_4, °C /W	1.20E-05	1.20E-05	1.20E-05	1.20E-05
R_5, °C /W	5.37E-04	1.20E-03	3.88E-04	1.00E-03
R_{Total}, °C /W	1.27E-03	2.20E-03	1.03E-03	1.87E-03
UA, W/°C	788.91	455.36	972.61	534.93
ε, %	54.5	40.7	50.1	35.3

The experimetal results for the four cases and the theoretical predictions are compared side-by-side in Table 4-6.

Table 4-6 Comparison of experimental and analytical results for the 7.6cm diameter, 122cm long system tested.

	Case 1	Case 2	Case 3	Case 4
Flowrate, LPM	9.5		14.0	
Average T_{mains}, °C	33.8	9.4	33.4	8.8
Average T_{drain}, °C	41.5	20.9	42.0	21.5
Experimental UA, W/°C	600.5	516.8	700.8	594.1
Theoretical UA, W/°C	788.9	455.4	972.6	534.9
Experimental ε, %	47.7	43.8	42.0	37.8
Theoretical ε, %	54.5	40.7	50.1	35.3

Despite the assumptions made to produce the analytical results, they were of the same order of magnitude and relatively close to the experimental results. This exercise showed that at a constant flow

rate, temperature changes on either side of the DWHR system affect the UA product, and thereby the effectiveness of the system. Both the theoretical and experimental results strongly support this claim.

It is important to point out a limitation associated with the theoretical approach. Equation 4-16 was used to determine the critical Reynolds number associated with the laminar to turbulent transition for the flow inside the coils. This equation was originally devised for coils having circular cross sections, whereas the coils wrapped around DWHR systems are typically not circular [30]. Cases 1 and 3 in Table 4-5 and Table 4-6 were found to be turbulent based on Equation 4-16; however, when the laminar flow correlation was used to calculate the theoretical effectiveness for these cases, the results were significantly closer to the experimental values as shown in Table 4-7. Clearly, Equation 4-16 was inadequate for determining the laminar to turbulent transition. Further improvement of the theoretical approach is outside the scope of this thesis.

Table 4-7 Comparison of experimental and analytical results for the 7.6cm diameter, 122cm long system when the theoretical solutions for cases 1 and 3 are based on laminar correlations instead of turbulent.

	Case 1	Case 2	Case 3	Case 4
Flowrate, LPM	9.5		14.0	
Average T_{mains} , °C	33.8	9.4	33.4	8.8
Average T_{drain} , °C	41.5	20.9	42.0	21.5
Experimental UA, W/°C	600.5	516.8	700.8	594.1
Theoretical UA, W/°C	591.8	455.4	696.2	534.9
Experimental ε, %	47.7	43.8	42.0	37.8
Theoretical ε, %	47.4	40.7	41.8	35.3

Given the close agreement between the theoretical and experimental results, it was benefitial to take a closer look at the heat transfer coefficients involved in the resistor network to narrow down the variables that were most significantly affected by temperature. This was done through substituting arbitrary temperatures into the equations for the heat transfer coefficients to determine their sensitivity on temperature.

To determine the effect of temperature on h_{film}, the ratio of heat transfer coefficients determined at two different mean temperatures, $T_X = X$ and $T_Y = Y$, can be calculated as shown in Equation 4.23.

$$\frac{h_{film}\big|_{T_X}}{h_{film}\big|_{T_Y}} = \frac{0.01\left(\mathrm{Re}_{D,X}\right)^{\frac{1}{3}}\left(\mathrm{Pr}_X\right)^{\frac{1}{3}}\left(\frac{k_X^3 g\rho_X^2}{\mu_X^2}\right)^{\frac{1}{3}}}{0.01\left(\mathrm{Re}_{D,Y}\right)^{\frac{1}{3}}\left(\mathrm{Pr}_Y\right)^{\frac{1}{3}}\left(\frac{k_Y^3 g\rho_Y^2}{\mu_Y^2}\right)^{\frac{1}{3}}} = \left(\frac{k_X}{k_Y}\right)^{\frac{2}{3}} \times \left(\frac{\mu_Y}{\mu_X}\right)^{\frac{2}{3}} \times \left(\frac{\rho_X}{\rho_Y}\right) \times \left(\frac{C_{pX}}{C_{pY}}\right)^{\frac{1}{3}} \tag{4.23}$$

Equation 4.24 shows the result of substituting the properties of water into Equation 4.23 for T_X and T_Y of 40°C and 30°C respectively.

$$\frac{h_{film}\big|_{40°C}}{h_{film}\big|_{30°C}} = (1.023)^{\frac{2}{3}} \times (1.223)^{\frac{2}{3}} \times (0.996) \times (1.00)^{\frac{1}{3}} = 1.157 = 115.7\% \tag{4.24}$$

According to Equation 4.24, h_{film} would undergo a 15.7% increase if the mean temperature was to increase from 30°C to 40°C, mostly due to the change in the dynamic viscosity of water. This is not to say that the overall effectiveness of the DWHR system would increase by 15.7%; that would to be determined based on the entire resistor network, and not a single resistor. However, the increase in h_{film} would undoubtedly result in a decrease in R_1, thereby increasing the overall UA product for the heat exchanger. Therefore, if the mean drain-side temperature is increased, a higher DWHR system effectiveness is expected.

As for the conductive heat transfer through the copper walls over the range of 5°C to 45°C, the thermal conductivity of copper varies from $401.7\frac{W}{m°C}$ to $399.0\frac{W}{m°C}$ [32]. This shows that the thermal conductivity of copper is not a strong function of temperature for the operating range of DWHR systems. Hence, resistors R_2 and R_4 were considered to be independent of temperature.

For resistor R_3, the thermal conductivity of the interface had to be determined empirically for different DWHR constructions to produce accurate results. However; this conductivity was not expected to be a strong function of temperature, similar to what was discussed in the case of R_2 and R_4. As a result, the resistor R_3 was assumed to be independent of the inlet temperatures into the DWHR system.

To determine the effect of temperature on h_{coil} for laminar flow, the ratio of heat transfer coefficients determined at two different mean temperatures, $T_X = X$ and $T_Y = Y$, is calculated as:

$$\frac{h_{coil}\big|_{T_X}}{h_{coil}\big|_{T_Y}} = \frac{\left(0.76 + 0.65\sqrt{De_X}\right)\mathrm{Pr}_X^{0.175}\left(\frac{k_X}{d}\right)}{\left(0.76 + 0.65\sqrt{De_Y}\right)\mathrm{Pr}_Y^{0.175}\left(\frac{k_Y}{d}\right)} \tag{4.25}$$

To simplify this equation further, scale analysis was performed, finding that the magnitude of $0.65\sqrt{De_X}$ is at least 20 times larger than 0.76. Therefore, Equation 4.25 is simplified to Equation 4.26:

$$\frac{h_{coil}\big|_{T_X}}{h_{coil}\big|_{T_Y}} = \frac{\left(0.65\sqrt{De_X}\right)\mathrm{Pr}_X^{0.175}\left(\frac{k_X}{d}\right)}{\left(0.65\sqrt{De_Y}\right)\mathrm{Pr}_Y^{0.175}\left(\frac{k_Y}{d}\right)} = \left(\frac{k_X}{k_Y}\right)^{0.825} \times \left(\frac{\mu_Y}{\mu_X}\right)^{0.325} \times \left(\frac{\rho_X}{\rho_Y}\right)^{0.5} \times \left(\frac{C_{pX}}{C_{pY}}\right)^{0.175} \tag{4.26}$$

Equation 4.27 showed the result of substituting the properties of water into Equation 4.26 for T_X and T_Y of 20°C and 10°C, respectively.

$$\frac{h_{coil}\big|_{20°C}}{h_{coil}\big|_{10°C}} = (1.027)^{0.825} \times (1.293)^{0.325} \times (0.998)^{0.5} \times (0.998)^{0.175} = 1.110 = 111.0\% \tag{4.27}$$

Based on the results of Equation 4.27, h_{coil} would increase by approximately 11.0% if the mean water temperature inside the coils was to increase from 10°C to 20°C, mostly due to the change in the dynamic

viscosity of water. As was discussed before, this would not translate to an increase in the overall effectiveness of the DWHR system by 11.0%; that would to be determined based on the entire resistor network. Nonetheless, this increase in h_{coil} would decrease the value of R_5, thereby increasing the UA product for the heat exchanger.

Similar to the above approach, the ratio of heat transfer coefficients for turbulent flow inside the coils was determined at two different mean temperatures, $T_X = X$ and $T_Y = Y$, as shown in Equation 4.28.

$$\frac{h_{coil}\big|_{T_X}}{h_{coil}\big|_{T_Y}} = \frac{0.023\mathrm{Re}_D^{0.85}\,\mathrm{Pr}^{0.4}\left(\frac{d}{D}\right)^{0.1}\left(\frac{k}{d}\right)}{0.023\mathrm{Re}_D^{0.85}\,\mathrm{Pr}^{0.4}\left(\frac{d}{D}\right)^{0.1}\left(\frac{k}{d}\right)} = \left(\frac{k_X}{k_Y}\right)^{0.6} \times \left(\frac{\mu_Y}{\mu_X}\right)^{0.45} \times \left(\frac{\rho_X}{\rho_Y}\right)^{0.85} \times \left(\frac{C_{pX}}{C_{pY}}\right)^{0.4} \tag{4.28}$$

Using the properties of water at T_X and T_Y of 20°C and 10°C, respectively, the impact of temperature on the heat transfer coefficient of the coil was predicted from Equation 4.29:

$$\frac{h_{coil}\big|_{20°C}}{h_{coil}\big|_{10°C}} = (1.027)^{0.6} \times (1.293)^{0.45} \times (0.998)^{0.85} \times (0.998)^{0.4} = 1.138 = 113.8\% \tag{4.29}$$

This predicted an increase of 13.8% in the magnitude of h_{coil} under turbulent flow conditions, which was again mostly due to the change in dynamic viscosity. Again, a 13.8% increase in h_{coil} would not mean an increase in effectiveness by the same magnitude. This increase in h_{coil} would decrease R_5, which increases the overall UA product for the heat exchanger.

Based on the above sensitivity analyses, it was clear that an increase in the mean temperatures on either side of the heat exchanger would lead to increased heat transfer coefficients. It was also clear that the main contributing factor to the variations in the heat transfer coefficients was the changes in the dynamic viscosity of water.

It is important to note that the mean temperatures on either side of the DWHR system were impacted by each other. As for any other heat exchanger, increasing the mean temperature on one side results in an increase in the mean temperature on the other side. For example, changing the inlet temperature for drain-side in a DWHR system would not only change the mean drain-side temperature, but also the mean temperature through the coils. Table 4-8 summarizes the expected impacts of increasing temperatures, with 'up arrows' indicating an increase, 'down arrows' indicating a decrease, and dashes indicating no change. T_{mains} and T_{drain} refer to the average temperatures through the mains-side and drain-side, respectively.

Table 4-8 Expected impacts of increasing temperatures on DWHR system performance.

Increasing Variable	Impact on Heat Transfer Parameters							
	R_1	R_2	R_3	R_4	R_5	UA	NTU	ε
T_{mains}	↓	–	–	–	↓	↑	↑	↑
T_{drain}	↓	–	–	–	↓	↑	↑	↑

Chapter 5 Performance of DWHR Systems under Unequal Flow Conditions

5.1 Theory

The resistor network developed in Chapter 4 can be used to form some initial expectations about how unequal flow rates would affect the performance of DWHR systems. To do so, a condensed version of Table 4-5 is shown here as Table 5-1. As a reminder, the values in the table show the convective heat transfer coefficients for the film and the coil as well as their corresponding resistances, where R_1 and R_5 correspond to the heat transfer by the film and coils, respectively.

Table 5-1 A condensed version of Table 4-5, showing the analytical results for the four cases of interest for the 7.6cm diameter, 122cm long system tested.

	Case 1	Case 2	Case 3	Case 4
Flowrate, LPM	9.5		14.0	
Average T_{mains}, °C	33.8	9.4	33.4	8.8
Average T_{drain}, °C	41.5	20.9	42.0	21.5
h_{film}, $W/m^2\,°C$	4661.5	3405.2	5341.3	3879.6
h_{coil}, $W/m^2\,°C$	7057.3	3147.2	9773.8	3773.9
R_1, °C /W	7.08E-04	9.70E-04	6.18E-04	8.43E-04
R_5, °C /W	5.37E-04	1.20E-03	3.88E-04	1.00E-03

The purpose of showing this table here was to direct the reader's attention towards the orders of magnitude for the heat transfer coefficients as well as the resistance values. The analytical results indicated that these values are of the same order of magnitude for the film and the coils, which means that neither one was dominating the other under equal flow conditions. This implies that if a correlation is to be developed, it has to be a function of both flow rates, and not just one.

Before doing any experiments, the correct formula for calculating effectiveness had to be developed for unequal flow conditions. Under equal flow conditions, the ratio of $\frac{C_{\min}}{C_{\max}} \cong 1$, which simplified the formula to what was shown in Equation 2.3. This simplification is no longer valid, and the correct formulas are discussed below.

It is important to clarify that for DWHR systems, the cold side of the heat exchanger (i.e. the coils) is the only side that is of interest from the perspective of heat recovery. Therefore, all the formulas developed and used in this chapter are based on the cold side of the heat exchanger.

For the case where the flow rate of the falling film, $\dot{V}_h$, is higher than the flow rate through the coils, $\dot{V}_c$, the effectiveness and heat transfer equations are as follows:

$$\varepsilon_c = \frac{q}{q_{\max}} = \frac{C_c\left(T_{c,o} - T_{c,i}\right)}{C_{\min}\left(T_{h,i} - T_{c,i}\right)} = \frac{\left(\dot{m}C_p\right)_c\left(T_{c,o} - T_{c,i}\right)}{\left(\dot{m}C_p\right)_c\left(T_{h,i} - T_{c,i}\right)} = \frac{\left(T_{c,o} - T_{c,i}\right)}{\left(T_{h,i} - T_{c,i}\right)} \tag{5.1}$$

$$q_c = C_c\left(T_{c,o} - T_{c,i}\right) = \left(\dot{m}C_p\right)_c\left(T_{c,o} - T_{c,i}\right) = \left(\rho\dot{V}C_p\right)_c\left(T_{c,o} - T_{c,i}\right) = \left(\rho\dot{V}C_p\right)_c\left(T_{c,o} - T_{c,i}\right) \tag{5.2}$$

For simplicity, the density and specific heat of water are assumed to be constant and their corresponding values are shown in Equations 5.3 and 5.4.

$$\rho = 1000\frac{kg}{m^3} \tag{5.3}$$

$$C_p = 4.18\frac{kJ}{kgK} \tag{5.4}$$

Hence, Equation 5.2 simplifies to:

$$q_c = \frac{\left(4180 \times \dot{V}_c\right)\left(T_{c,o} - T_{c,i}\right)}{60000} \tag{5.5}$$

where $\dot{V}_c$ is in LPM, temperatures are in °C and q_c is in kW.

For the case where the flow rate of the falling film, $\dot{V}_h$, is lower than the flow rate through the coils, $\dot{V}_c$, the heat transfer rate can be calculated using Equation 5.5 and effectiveness equation is as follows:

$$\varepsilon_c = \frac{q}{q_{\max}} = \frac{C_c\left(T_{c,o} - T_{c,i}\right)}{C_{\min}\left(T_{h,i} - T_{c,i}\right)} = \frac{\left(\dot{m}C_p\right)_c\left(T_{c,o} - T_{c,i}\right)}{\left(\dot{m}C_p\right)_h\left(T_{h,i} - T_{c,i}\right)} = \frac{\dot{V}_c\left(T_{c,o} - T_{c,i}\right)}{\dot{V}_h\left(T_{h,i} - T_{c,i}\right)} \tag{5.6}$$

The goals of this chapter include measuring the effectiveness and heat transfer rates for DWHR systems operating under unequal flow rates encompassing the full range of flow rates specified by the CSA standard [9]. The results are presented in terms of the equations above.

5.2 Method

A total of five DWHR systems were tested in this study, as listed in Table 5-2. Not all of the systems tested were manufactured by the same company. The manufacturers are referred to as Manufacturer A and B in this chapter to uphold their anonymity. DWHR systems by different manufacturers have different coil designs as shown in Figure 5-1.

Table 5-2 Diameters and lengths of DWHR systems studied.

System #	Manufacturer	Diameter (cm)	Length (cm)
1	A	5.1	122
2	B	7.6	102
3	A	7.6	122
4	A	7.6	153
5	A	10.2	122

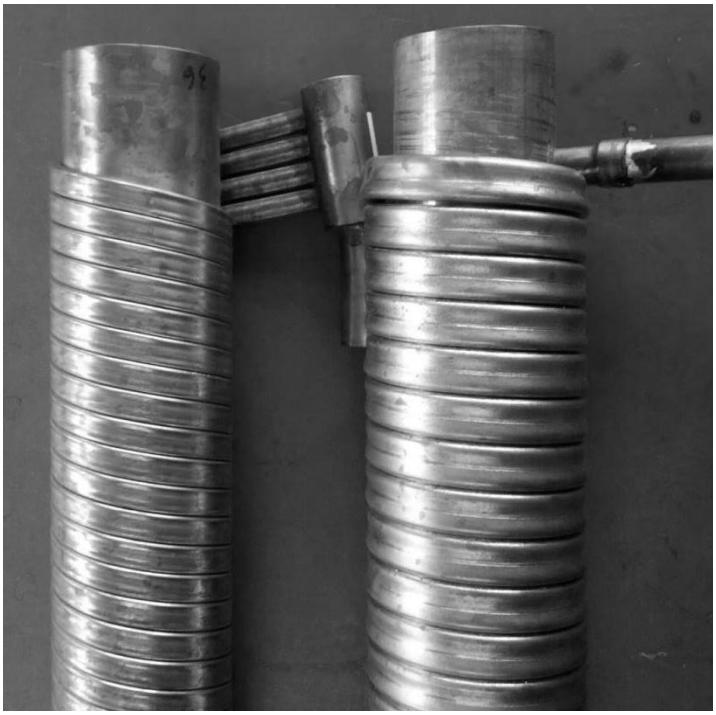

Figure 5-1 DWHR systems with coil design by manufacturer A on the left, and manufacturer B on the right.

Tests were performed at inlet temperatures of 38±1°C and 10±1°C on the drain-side and the mains-side respectively. As mentioned in the previous chapters, the CSA standard requires DWHR systems to be rated under equal flow rates of 5.5, 7, 9, 10, 12 and 14 LPM. To maintain a connection between the results produced in this study and the CSA standard, the flow rates chosen for the unequal flow tests were all the possible combination of the flow rates depicted by the CSA standard, which add up to a total of 36 conditions, including the 6 conditions with equal flow rates. Note that for the 10.2cm diameter system, conditions having a flowrate of 5.5 LPM are not considered.

For all tests peformed, the volumetric flowrate on the drain-side is initially raised to a high value of 20 LPM and then gradually lowered to the desired flow rates. This ensures that the entire inner surface area of the pipe is wetted for a given flowrate, which produces repeatable results.

5.3 Results

The data used to create the figures in this chapter are presented in tabular form in Appendix C.

The plots for effectiveness vs. volumetric flow rate of the falling film (hot side) for the five DWHR systems are shown in Figure 5-2 through Figure 5-6. The curves on each figure correspond to a different constant volumetric flow rates through the coils (cold side). Note that the curves for the 10.2cm diameter, 122cm long DWHR system do not contain data for a flow rate of 5.5 LPM because the inconsistency in the film caused non-repeatable results, as was discussed in Chapter 3. The uncertainties associated with the results presented in this section are calculated based on Moffat's constant odds method [24] as described in Appendix B.

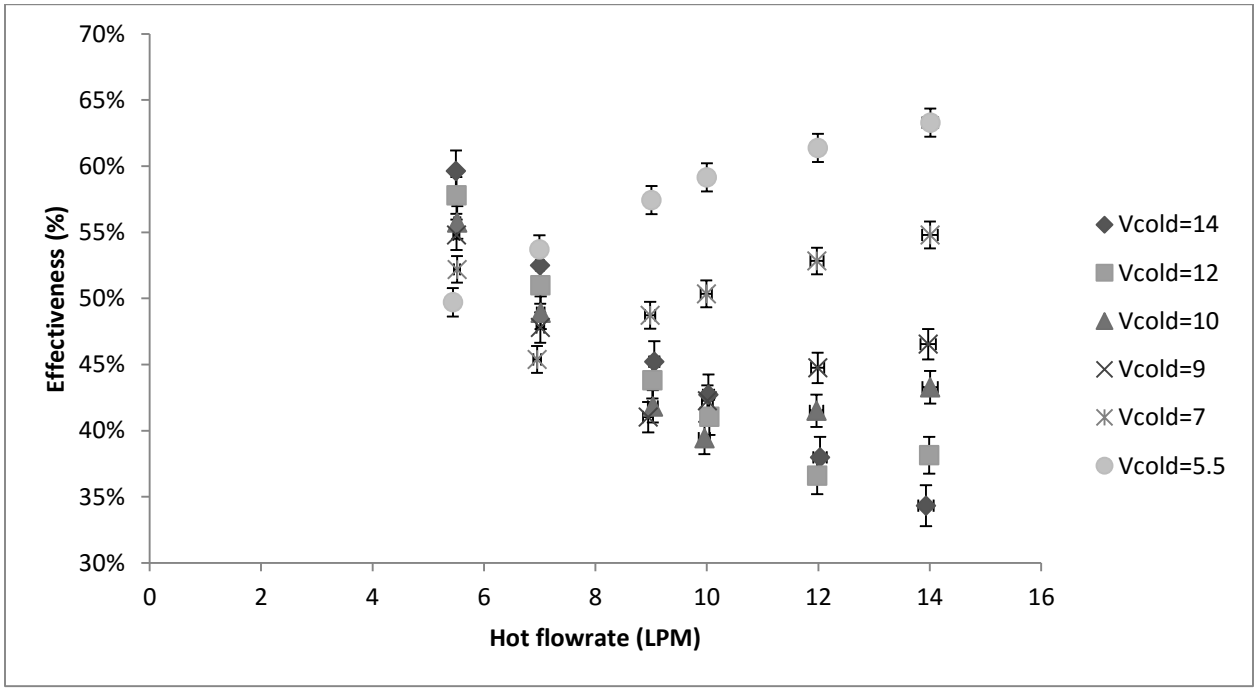

Figure 5-2 The effectiveness vs volumetric flow rate of the falling film for 6 different constant flow rates through the coils for the 5.1cm diameter, 122cm long DWHR system by manufacturer A.

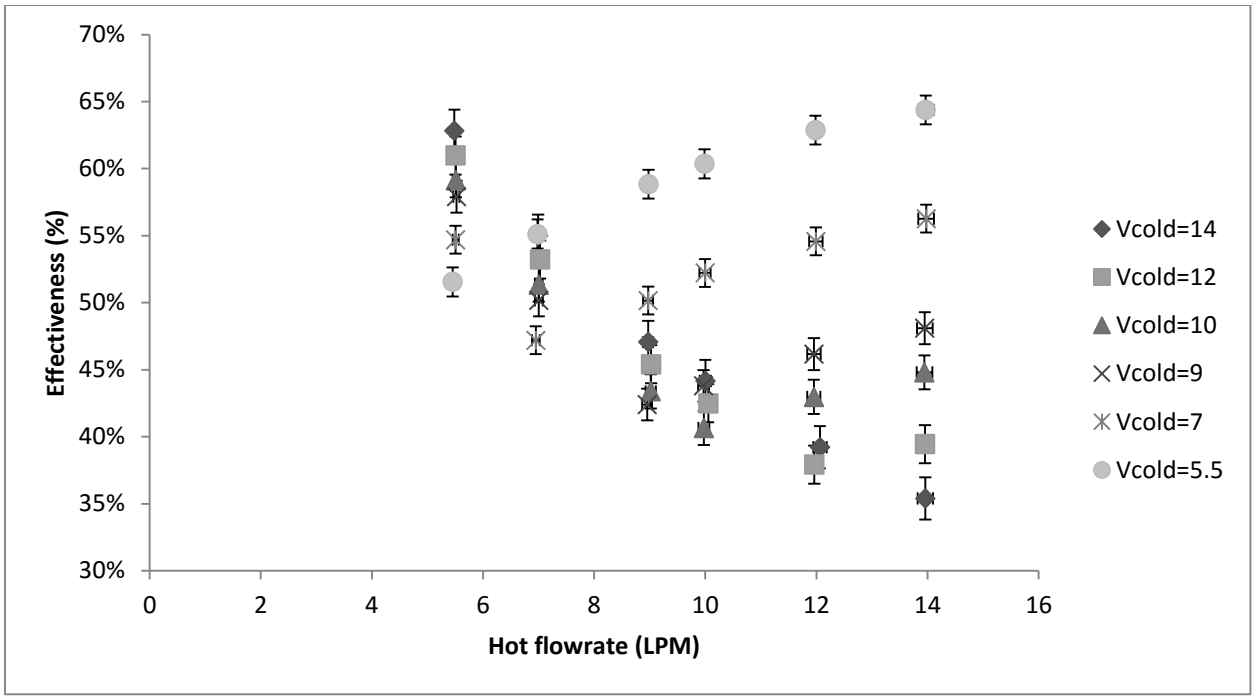

Figure 5-3 The effectiveness vs volumetric flow rate of the falling film for 6 different constant flow rates through the coils for the 7.6cm diameter, 102cm long DWHR system by manufacturer B.

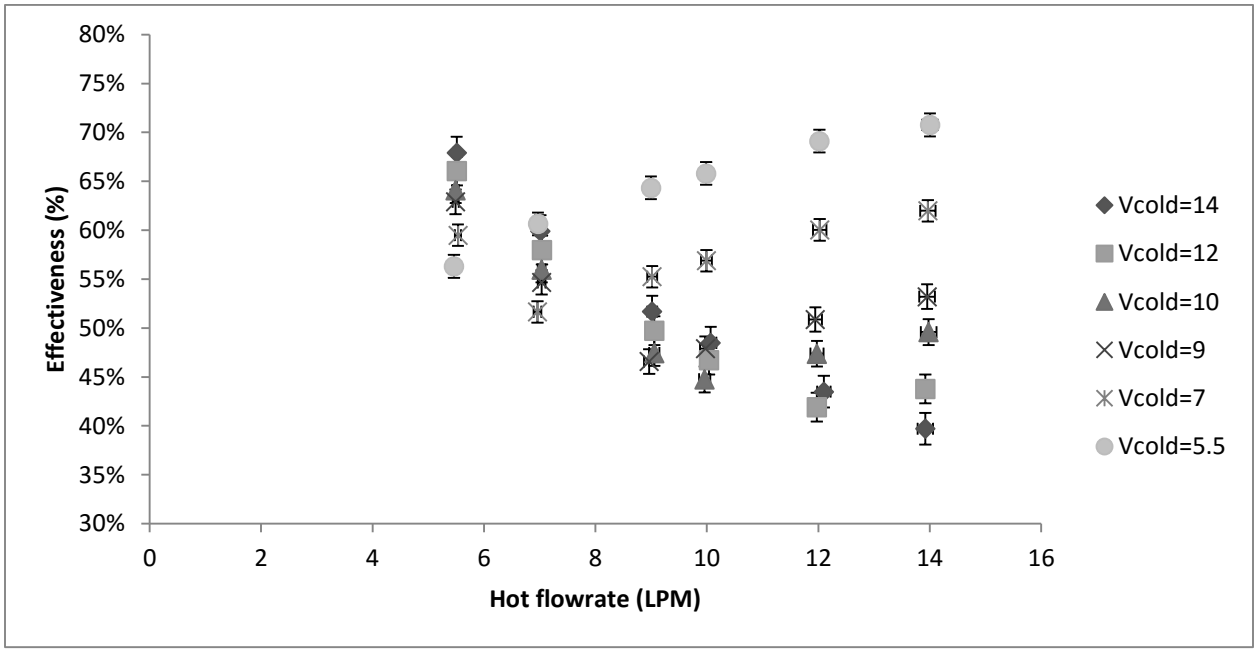

Figure 5-4 The effectiveness vs volumetric flow rate of the falling film for 6 different constant flow rates through the coils for the 7.6cm diameter, 122cm long DWHR system by manufacturer A.

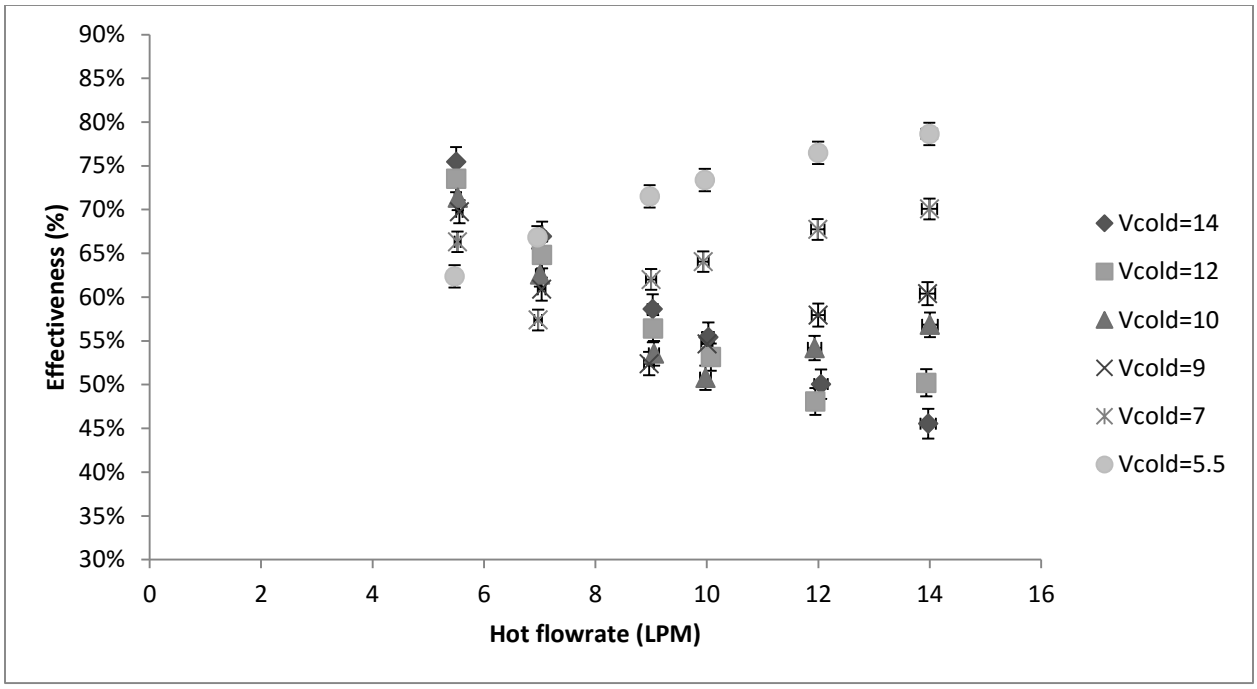

Figure 5-5 The effectiveness vs volumetric flow rate of the falling film for 6 different constant flow rates through the coils for the 7.6cm diameter, 153cm long DWHR system by manufacturer A.

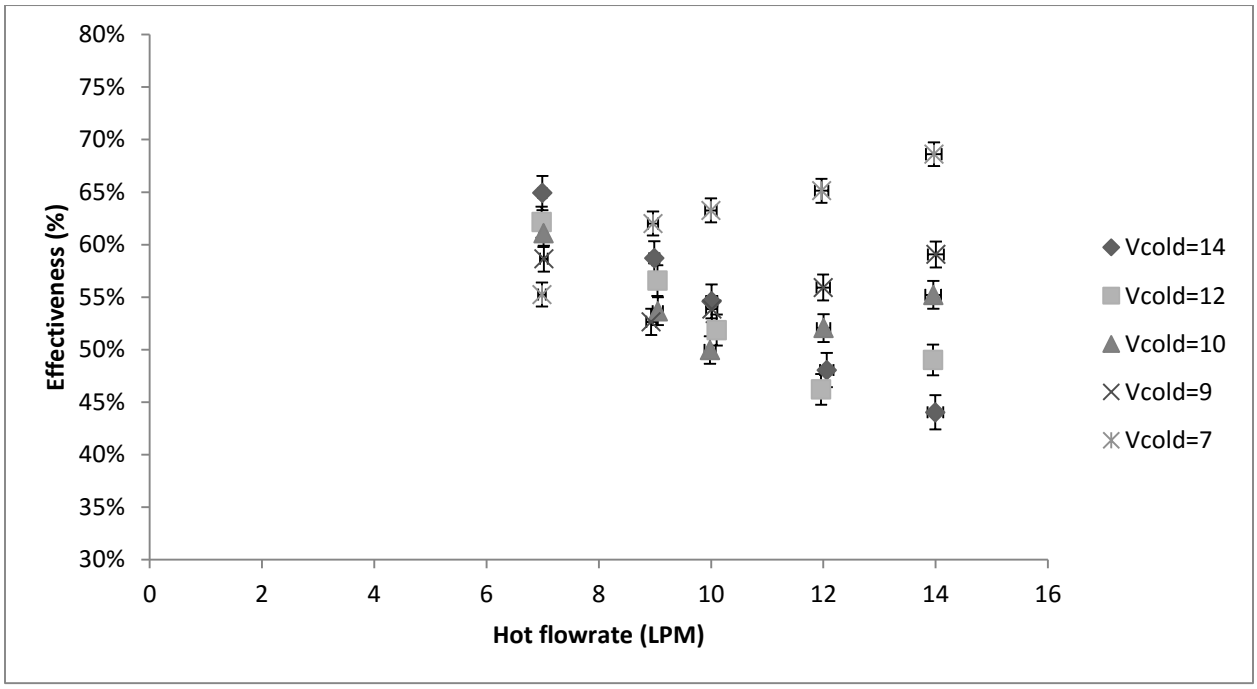

Figure 5-6 The effectiveness vs volumetric flow rate of the falling film for 5 different constant flow rates through the coils for the 10.2cm diameter, 122cm long DWHR system by manufacturer A.

Upon visual inspection, it was clear that the curves represented in each figure were very similar to the curves shown in other figures, at similar conditions. It was also observed that an inflection point exists on the curves for constant cold side flow rates of 7, 9, 10 and 12 LPM. For example, in Figure 5-2, by inspecting the curve for a constant cold flow rate of 10, it was evident that the effectiveness was at its highest value at a hot flow rate of 5.5 LPM, gradually decreased until the inflection point at 10 LPM, and then it increased for higher flow rates.

Although the curves produced for different systems were very similar, the existence of an inflection point made it difficult to devise a correlation based on effectiveness. It is also worth noting that the data was only indicative of the existence of this inflection point, and was insufficient for determining the exact flow rate at which it occurred. As a result, it was decided to look at the heat transfer rate vs. volumetric flow rate curves to determine if they are more practical for the purpose of creating a consistent correlation.

The plots for heat transfer vs. volumetric flow rate of the falling film (hot side) for the five DWHR systems are shown in Figure 5-7 through Figure 5-11. The curves on each figure correspond to a different constant volumetric flow rate through the coils (cold side). Note that the curves for the 10.2cm diameter, 122cm long DWHR system do not contain data for a flow rate of 5.5 LPM.

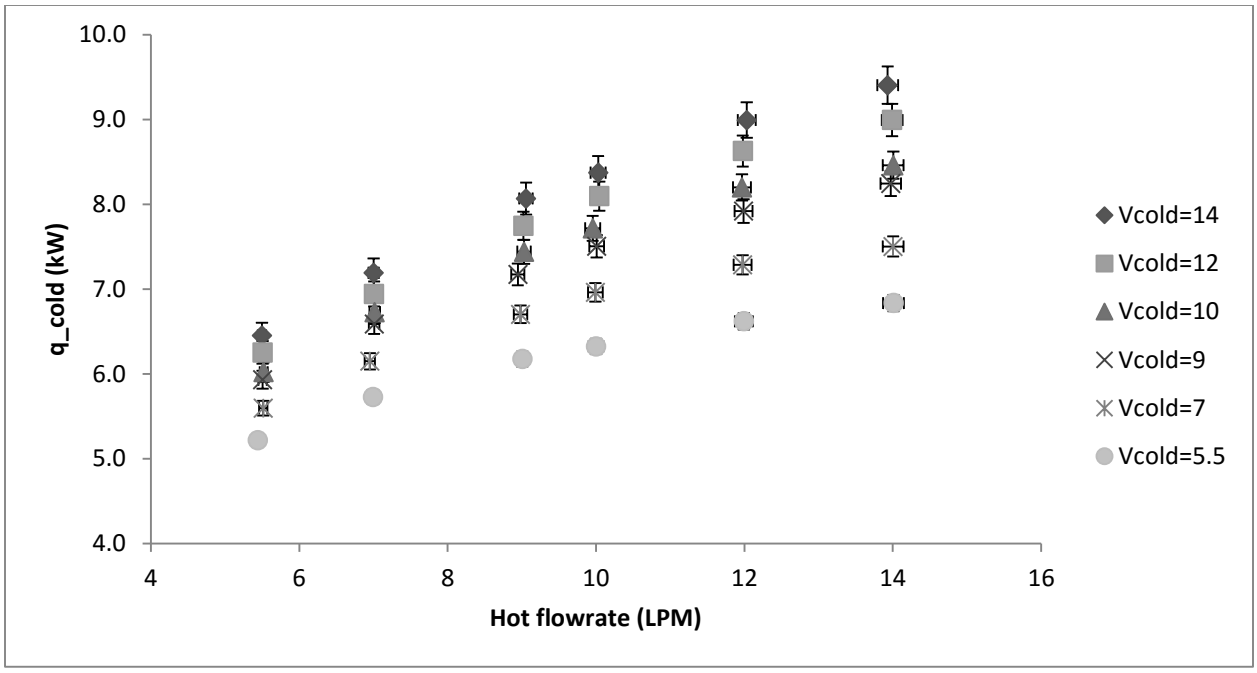

Figure 5-7 The heat transfer rate vs volumetric flow rate of the falling film for 6 different constant flow rates through the coils for the 5.1cm diameter, 122cm long DWHR system by manufacturer A.

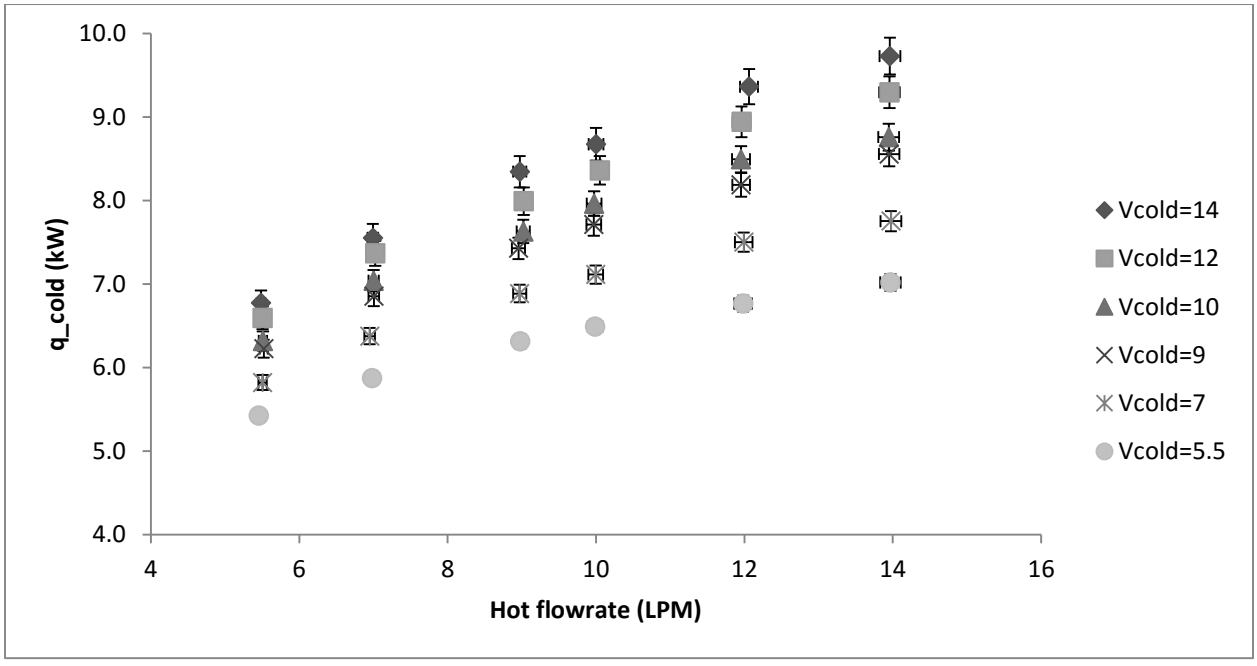

Figure 5-8 The heat transfer rate vs volumetric flow rate of the falling film for 6 different constant flow rates through the coils for the 7.6cm diameter, 102cm long DWHR system by manufacturer B.

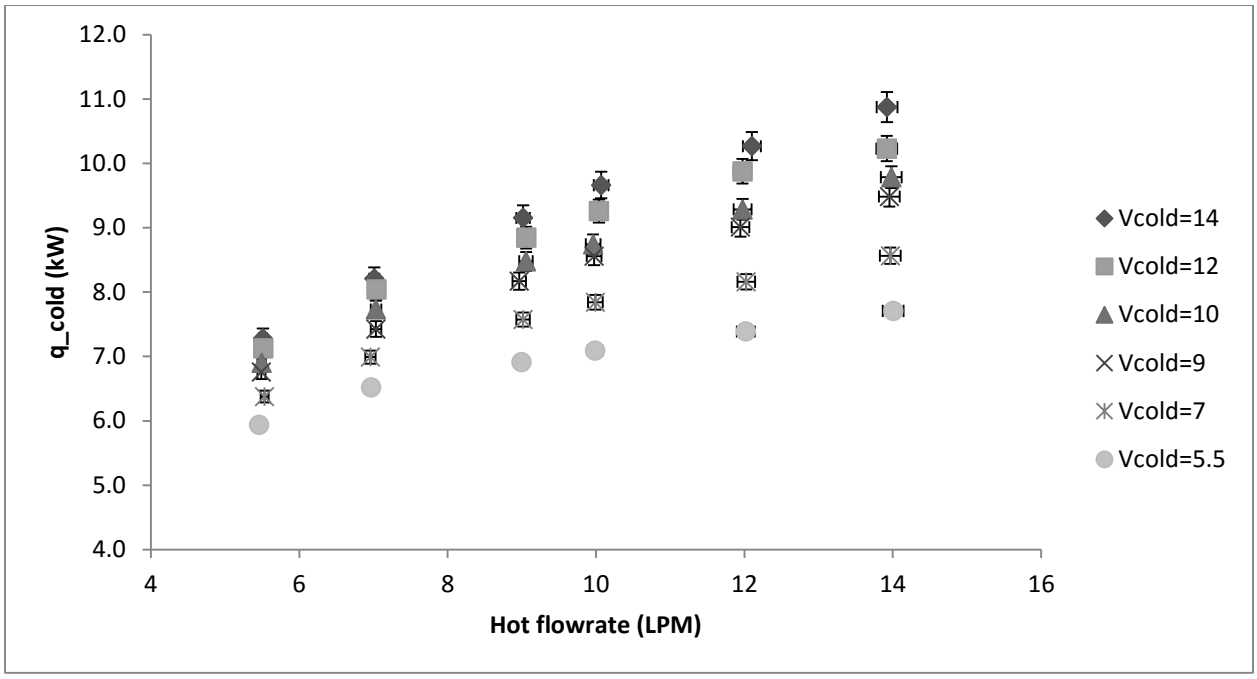

Figure 5-9 The heat transfer rate vs volumetric flow rate of the falling film for 6 different constant flow rates through the coils for the 7.6cm diameter, 122cm long DWHR system by manufacturer A.

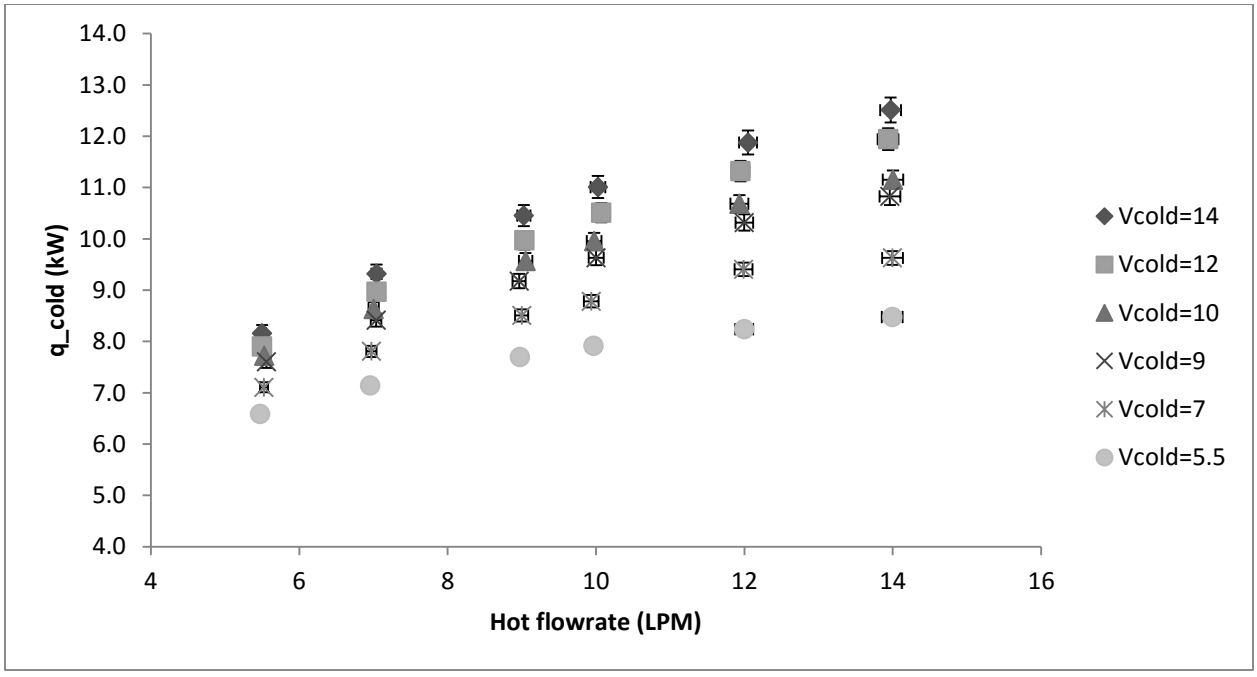

Figure 5-10 The heat transfer rate vs volumetric flow rate of the falling film for 6 different constant flow rates through the coils for the 7.6cm diameter, 153cm long DWHR system by manufacturer A.

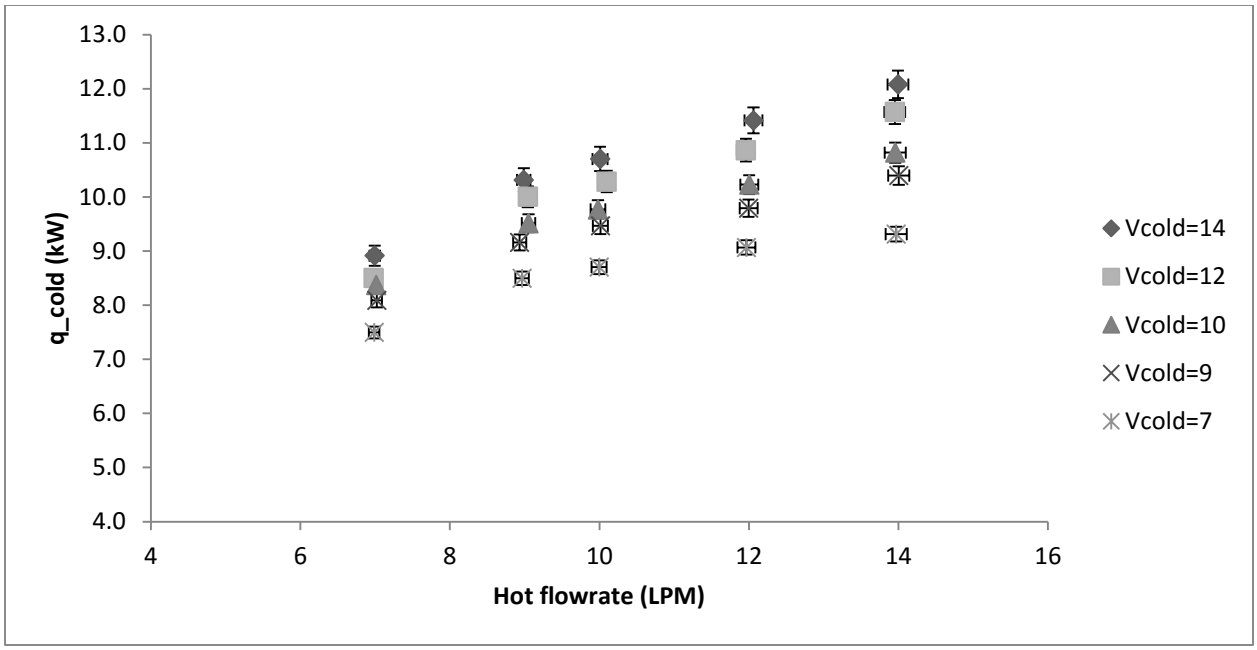

Figure 5-11 The heat transfer rate vs volumetric flow rate of the falling film for 5 different constant flow rates through the coils for the 10.2cm diameter, 122cm long DWHR system by manufacturer A.

The heat transfer plots represented a family of curves which were very similar for different DWHR systems. The heat transfer curves are logarithmic curves with no inflection points. These observations hinted at the possibility of there being a universal correlation that would allow normalization of these values and to combine them into a single curve. It was desirable for this correlation to be a function of the heat transfer rates measured at equal flow conditions, which are readily available from the CSA rating data.

After many attempts, the following correlation was created for normalizing all heat transfer curves for each DWHR system tested:

$$q_{(\dot{V}_{cold}=F1\ \&\ \dot{V}_{hot}=F2)} = q_{(\dot{V}_{cold}=\dot{V}_{hot}=F1)} \times \left[M \times ln\left(\frac{\dot{V}_{hot}=F2}{\dot{V}_{cold}=F1}\right) + N\right] \quad (5.7)$$

where $q_{(\dot{V}_{cold}=F1\ \&\ \dot{V}_{hot}=F2)}$ is the heat transfer rate measured at the unequal flow condition, $q_{(\dot{V}_{cold}=\dot{V}_{hot}=F1)}$ is the heat transfer rate measured at the equal flow condition, F1 is the flow rate through the coils, F2 is the flow rate of the falling film, and variables M and N are constants. The values for M and N are found experimentally through regression. Theoretically, the value of constant N was expected to be 1, such that Equation 5.7 would reduce to the equal flow conditions if F1 and F2 were equal. This was to be validated through regression.

Using Equation 5.7, the curves from Figure 5-7 through Figure 5-11 were normalized and represented as one curve for each DWHR system as shown in Figure 5-12 through Figure 5-16. A linear curve of best fit to represent each data set is also shown on each graph.

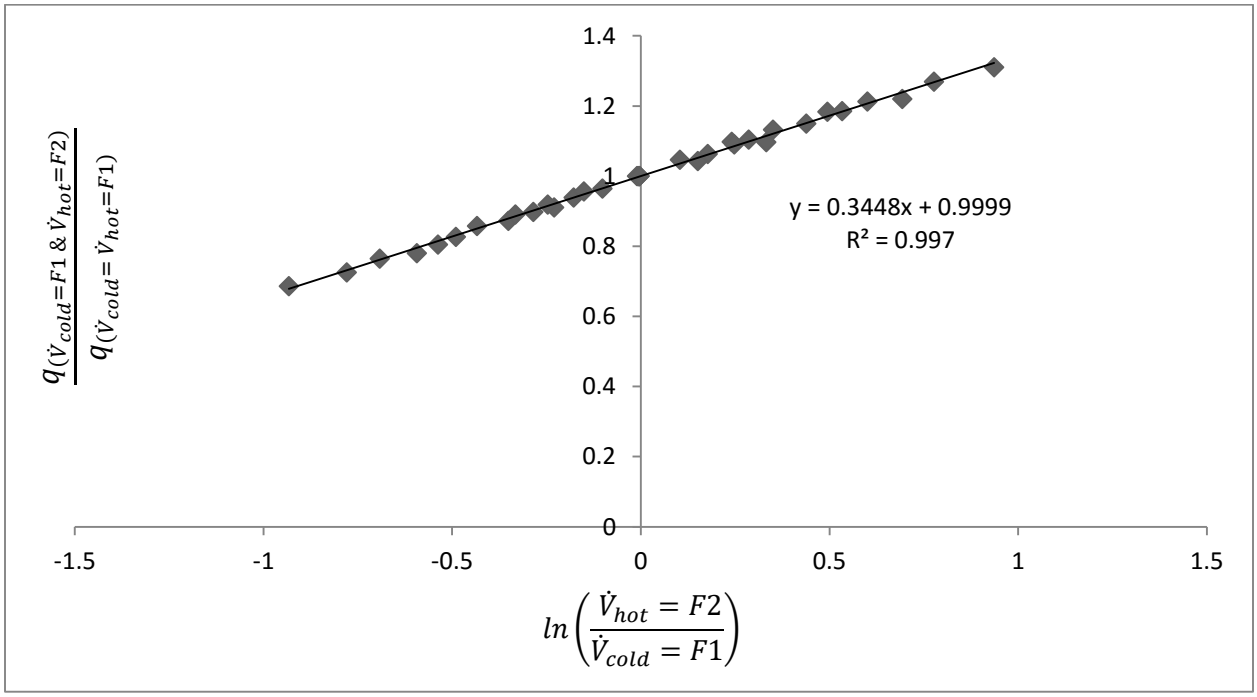

Figure 5-12 The heat transfer data normalized using Equation 5.7 for the 5.1cm diameter, 122cm long DWHR system by manufacturer A.

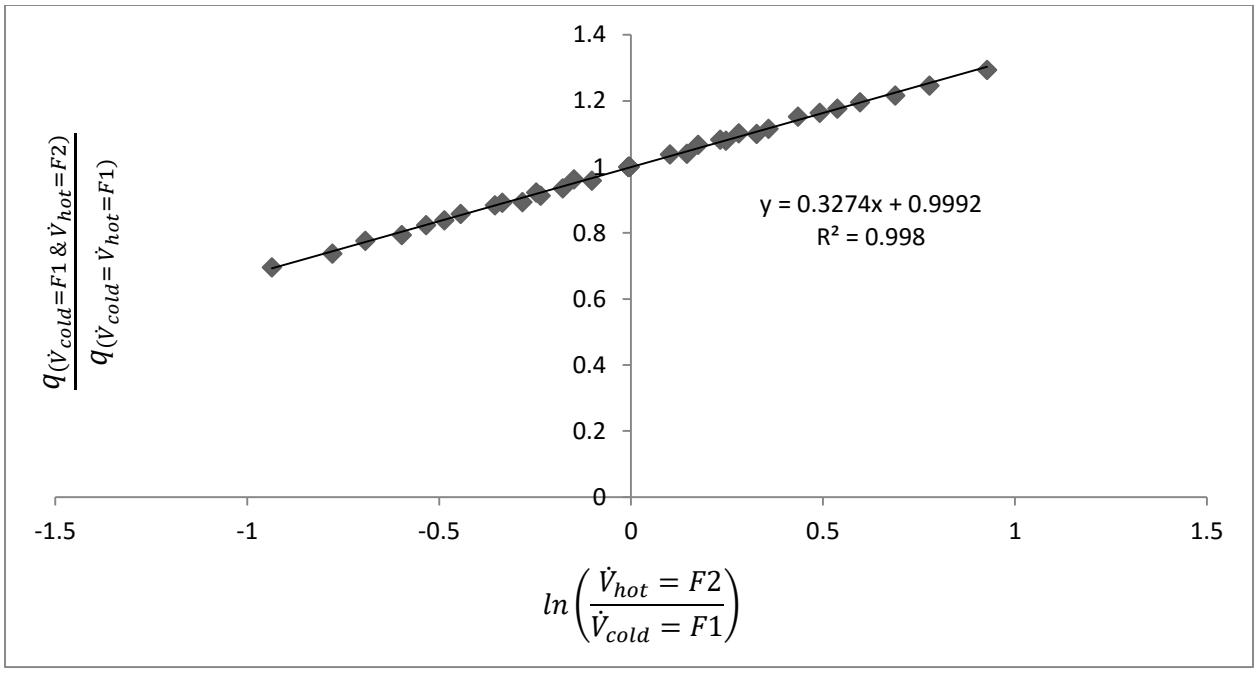

Figure 5-13 The heat transfer data normalized using Equation 5.7 for the 7.6cm diameter, 102cm long DWHR system by manufacturer B.

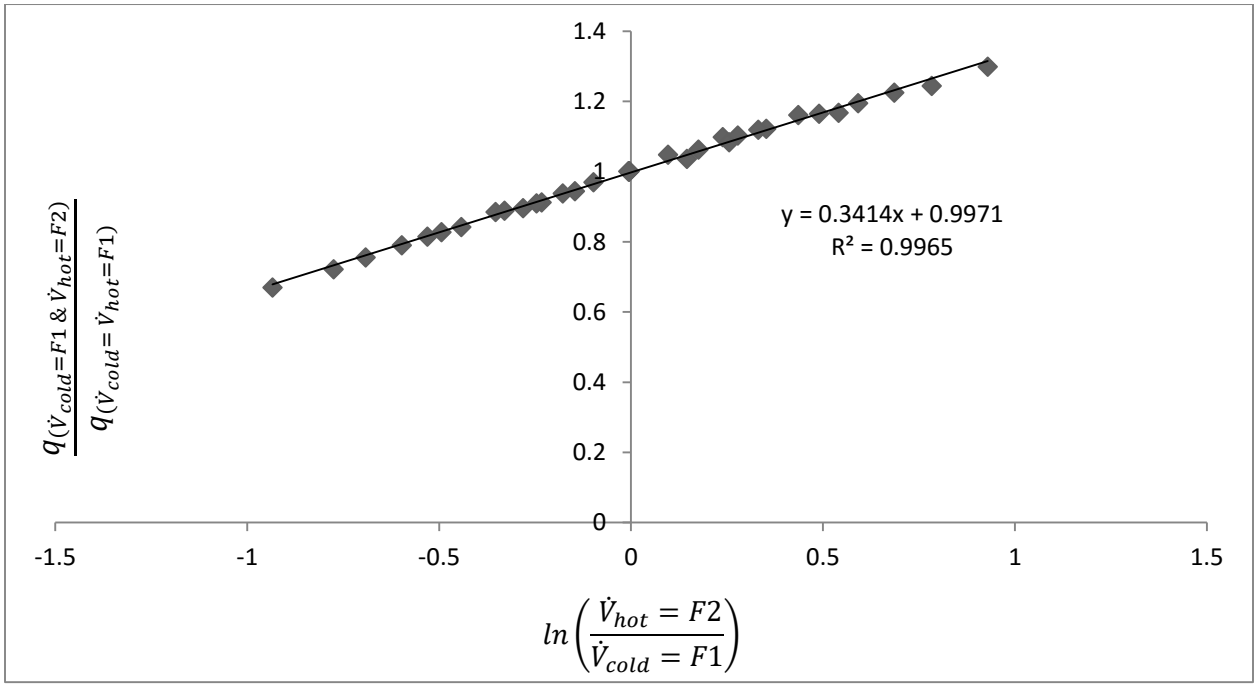

Figure 5-14 The heat transfer data normalized using Equation 5.7 for the 7.6cm diameter, 122cm long DWHR system by manufacturer A.

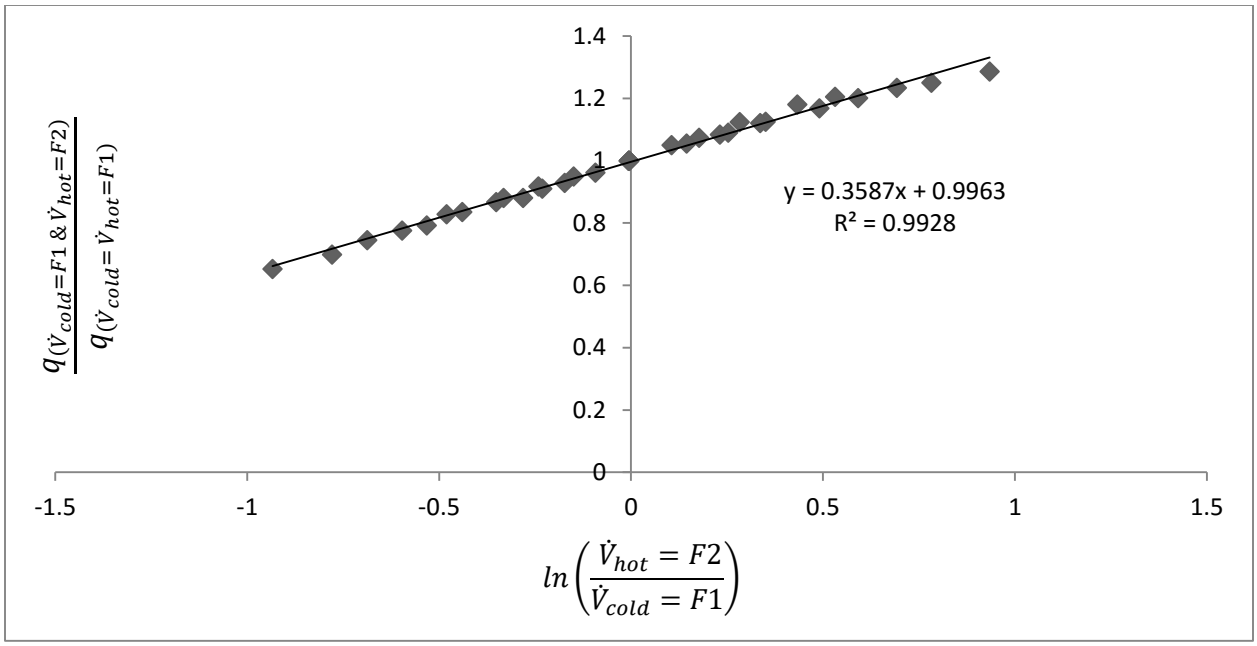

Figure 5-15 The heat transfer data normalized using Equation 5.7 for the 7.6cm diameter, 153cm long DWHR system by manufacturer A.

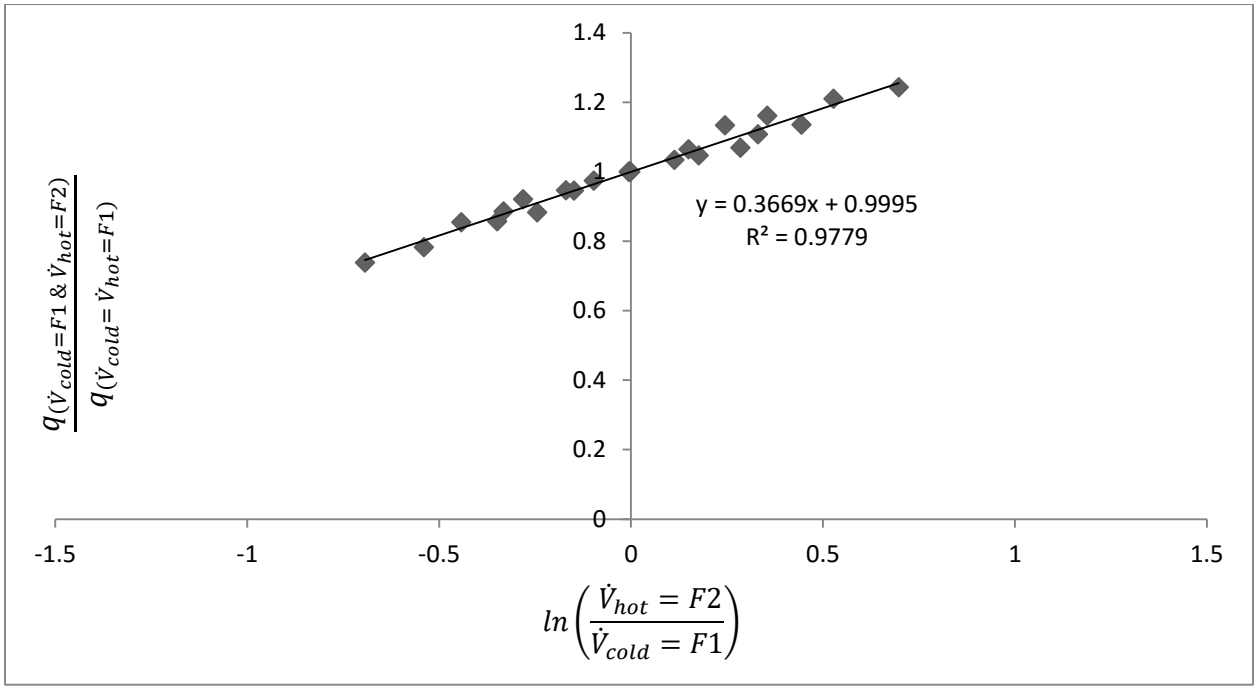

Figure 5-16 The heat transfer data normalized using Equation 5.7 for the 10.2cm diameter, 122cm long DWHR system by manufacturer A.

Based on the regression coefficients displayed on figures, Equation 5.7 could predict the heat transfer rate for individual DWHR systems very accurately. Upon closer inspection, it became clear that the constants M and N, determined using the line of best fit displayed on the figures, were very close in magnitude regardless of the length or diameter of the corresponding DWHR system. These constants are summarized in Table 5-3.

Table 5-3 Constants M and N corresponding to each DWHR system tested.

System #	Constant M	Constant N
1	0.3448	0.9999
2	0.3274	0.9992
3	0.3414	0.9971
4	0.3587	0.9963
5	0.3669	0.9995

The fact that these constants were so close in magnitude meant that a universal correlation could be created which would work for all DWHR systems with similar design. To determine constants M and N for this universal correlation, the data for all 5 DWHR systems were overlaid as shown in Figure 5-17 and a line of best fit was drawn through the entire data set.

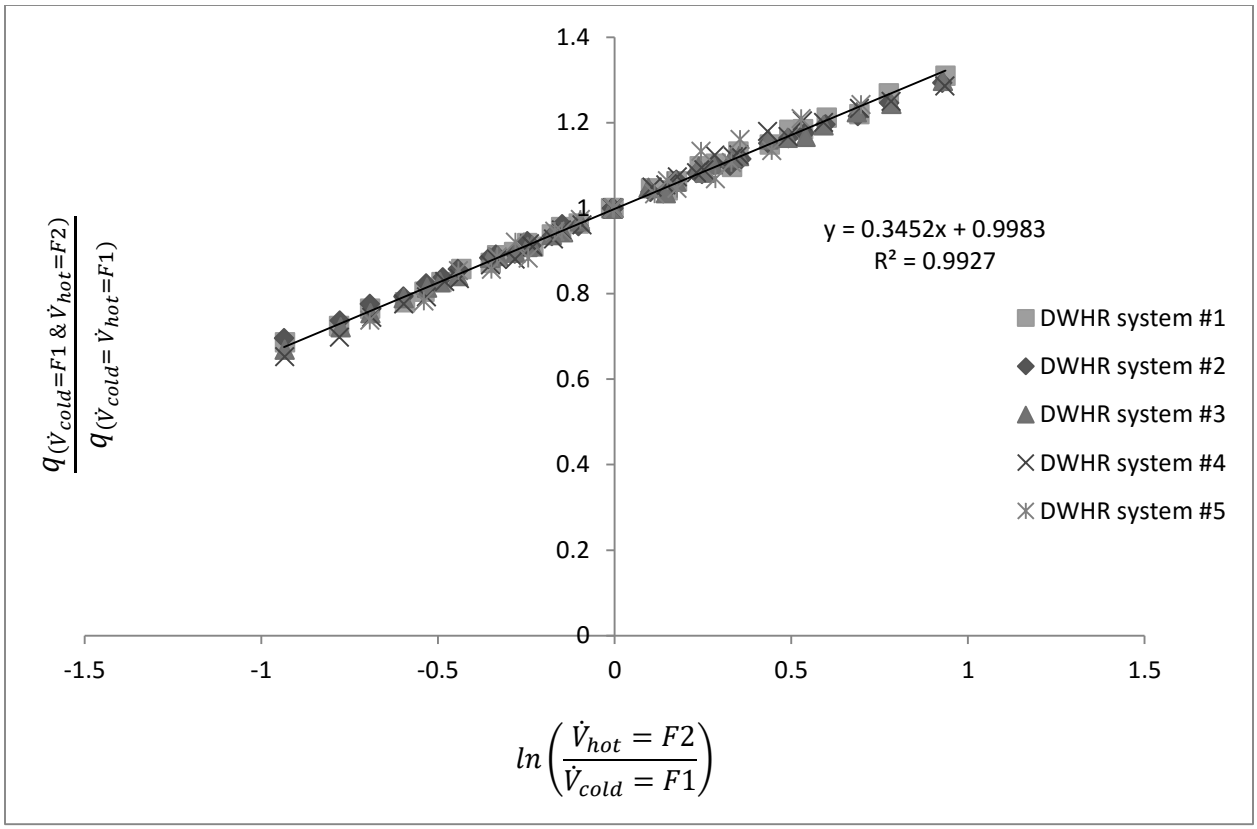

Figure 5-17 The heat transfer data normalized using Equation 5.7 for all systems.

Evidently, the data sets from different DWHR systems overlapped each other very closely; hence, the coefficients from the line of best fit on Figure 5-17 could safely be used to create Equation 5.8.

$$q_{(\dot{V}_{cold}=F1\ \&\ \dot{V}_{hot}=F2)} = q_{(\dot{V}_{cold}=\dot{V}_{hot}=F1)} \times \left[0.3452 \times ln\left(\frac{\dot{V}_{hot}=F2}{\dot{V}_{cold}=F1}\right) + 0.9983\right] \qquad (5.8)$$

As was discussed earlier, the coefficient N was expected to be equal to 1; however, due to the inaccuracies associated with the experimental results, the regression analysis determined it to be 0.9983. Since these values are almost identical, it was decided to use a value of N=1 instead. This would cause the terms inside the bracket in Equation 5.8 to reduce to 1 in the case where F1=F2, which ensures that the heat transfer rates on both sides of the equation are equal. As a result, Equation 5.9 was devised:

$$q_{(\dot{V}_{cold}=F1\ \&\ \dot{V}_{hot}=F2)} = q_{(\dot{V}_{cold}=\dot{V}_{hot}=F1)} \times \left[0.3452 \times ln\left(\frac{\dot{V}_{hot}=F2}{\dot{V}_{cold}=F1}\right) + 1\right] \quad (5.9)$$

This equation is valid for DWHR systems of any lengths and diameters, assuming they have designs similar to what was shown in Figure 5-1. As a reminder, the heat transfer rates are measured in kW and the flow rates are measured in LPM.

In order to determine the accuracy of this correlation, Equation 5.9 was used to predict the heat transfer rate for a handful of randomly selected conditions for the systems tested, in order to determine how well it could predict the performance of a given DWHR system. The measured and predicted heat transfer rates as well as the percent difference between the two are presented in Table 5-4.

Table 5-4 The results of using Equation 5.9 to predict the heat transfer rate through the coils for all DWHR systems, along with the measured values to allow comparison between the two.

DWHR system #	Cold flow rate (LPM)	Hot flow rate (LPM)	Measured heat transfer rate at equal flow condition, based on the cold flowrate (kW)	Measured heat transfer rate (kW)	Predicted heat transfer rate (kW)	Percent error
1	5.50	6.99	5.22	5.73	5.65	1.34%
	7.01	14.00	6.15	7.50	7.62	1.53%
	9.96	7.02	7.72	6.73	6.78	0.79%
	13.97	5.50	9.40	6.45	6.38	1.20%
2	5.50	9.99	5.43	6.49	6.55	0.81%
	9.03	13.95	7.43	8.56	8.54	0.15%
	9.99	7.00	7.96	7.04	6.99	0.75%
	11.99	5.50	8.94	6.60	6.54	0.85%
3	6.98	5.53	6.99	6.38	6.43	0.82%
	9.03	13.95	8.17	9.48	9.40	0.94%
	10.01	7.03	8.74	7.73	7.68	0.67%
	12.00	9.06	9.88	8.85	8.92	0.81%
4	5.49	12.00	6.59	8.24	8.37	1.54%
	8.99	5.56	9.18	7.60	7.65	0.69%
	11.99	7.04	11.32	8.97	9.24	2.94%
	14.01	9.03	12.51	10.45	10.61	1.48%
5	7.06	11.97	7.50	9.07	8.86	2.33%
	8.94	10.01	9.16	9.47	9.52	0.53%
	11.98	9.04	10.87	10.00	9.81	1.96%
	13.96	10.01	12.08	10.70	10.69	0.08%

For the 20 random cases in Table 5-4, the maximum percent error was 2.94%. The small magnitude of this percent error should be enough to show the practicality of Equation 5.9, and how it could be used for DWHR systems with different designs, lengths and diameters. At the time this chapter was written, no correlations were found in the literature to predict the performance of DWHR systems at unequal flow rates and as such, Equation 5.9 was an important development for incorporating DWHR systems into building simulation models.

5.4 Unequal Flow Model

It is helpful to summarize the results discussed so far in this chapter to create a simple procedure for predicting the performance of DWHR systems at unequal flow conditions based on the data available from CSA tests.

The CSA standard provides data for DWHR performance measured under equal flow conditions for flow rates of 5.5, 7, 9, 10, 12 and 14 LPM. This data can be used to create the characteristic effectiveness vs. flow rate curve for the DWHR system of interest. As was discussed in Chapter 3, curves of best fit in the form of Equation 3.4 are the most suitable for representing this data set. Note that for DWHR systems with diameters of 10.2cm, the effectiveness at 5.5 LPM must be excluded when developing the characteristic curves.

This curve can readily be used to predict the effectiveness at flow rates between 5.5 and 14 LPM. The next step is to find the effectiveness for the desired flow rate using this effectiveness curve. Lastly, the effectiveness value can easily be converted into a heat transfer rate using Equation 5.10 for the desired flow rate.

$$q_c = \frac{4180 \times \dot{V} \times \varepsilon \left(T_{h,i} - T_{c,i} \right)}{60000} \tag{5.10}$$

where $\dot{V}_c$ is in LPM, temperatures are in °C and q_c is in kW. Note that Equation 5.10 contains temperatures at which the CSA tests were done and assumes that the condition of interest has the same temperatures.

This heat transfer rate corresponds to the equal flow condition and it is the only unknown required to be plugged into Equation 5.10 in order to find the heat transfer rate under unequal flow rates between

5.5 and 14 LPM. The simplicity of this method allows it to be easily implemented into building simulation software, requiring no input except the existing data from the CSA ratings.

As for any experimental model, Equation 5.9 has its limitations. It cannot be applied to flow rates lower than 5.5 LPM since irregularities and non-uniform thickness of the falling film result in non-repeatable performance values. For a 10.2cm diameter DWHR system, the irregularities also occur at a flow rate of 5.5 LPM, which means that this model cannot be applied to them. Furthermore, the DWHR systems tested for creating this correlation have a similar design of a copper drain pipe wrapped with smaller tubes. The correlation developed in this study is intended to be used for DWHR systems with similar designs to those tested. The designers are asked to keep these limitations in mind when using Equation 5.9.

Chapter 6 Combined Model and Validation

6.1 Introduction

DWHR systems are rated based on their steady-state effectiveness at specific conditions listed by the CSA standards [9]. The rated effectiveness values are intended to provide designers with a means to distinguish between different commercially available products. The conditions at which DWHR systems would operate in a house could be very different than the conditions used to rate them. This means that the rated effectiveness values, by themselves, are not a necessarily a good representation of the actual performance of DWHR systems.

Throughout this thesis, different procedures and correlations have been developed to take the rated performance of a DWHR system and use it to predict the performance under particular conditions. However, each chapter only looked at the change in one variable at a time, namely the inlet temperatures and flow rates through different sides. This chapter aims to develop a procedure to combine all the correlations developed as part of this thesis and to perform experiments to determine how well the heat transfer rate can be predicted.

6.2 Universal Procedure

The step by step procedure to estimate the heat transfer rate through the coils is explained in detail in the following 9 steps.

Step ①:

Refer to the CSA rating data for the DWHR system of interest, where the effectiveness of the system was measured under equal flow conditions at flow rates of 5.5, 7, 9, 10, 12 and 14 LPM. The data set should also contain the temperatures at which the CSA tests were performed.

Step ②:

For DWHR systems with diameters of 5.1 and 7.6cm, the data from all 6 flow rates must be used. However, for 10.2cm diameter systems, the effectiveness measured at 5.5 LPM must be discarded.

Fit a curve of best fit to CSA data to produce the characteristic effectiveness vs. flow rate curve for the DWHR system. This curve is of the form shown in Equation 6.1.

$$\varepsilon = \frac{1}{G \times (\dot{V}_{cold}=F1) + H} \tag{6.1}$$

where G and H are constants determined by regression and F1 is the flow rate of cold water through the coils measured in LPM.

Step ③:

Use the curve fit from Equation 6.1 to calculate the effectiveness at the desired flow rate based on the cold side of the DWHR system (e.g. if the analysis is being done on a DWHR system operating at a cold side flow rate of 6 LPM and a hot side flow rate of 11 LPM, estimate the effectiveness at 6 LPM).

Step ④:

This step only applies to situations where the flow rate through the cold side is higher than 14 LPM. In such cases, the curve fit equation from step ③ must be used to estimate a rough effectiveness value for the desired flow rate. The estimated value should then be corrected using Equation 6.2 which was developed in Chapter 3:

$$\varepsilon_{corrected} = \varepsilon_{predicted} \times C_{Flow} = \varepsilon_{predicted} \times \left(\frac{A \times (\dot{V}_{cold}=F1) + B}{L} + 1\right) \tag{6.2}$$

where A and B are constants based on the system's diameter and L is the length of the system in meters. These constants are listed in Table 6-1.

Table 6-1 Correlation constants for Equation 6.2 determined for systems with different diameters.

Correlation Constants	⌀ 5.1cm systems	⌀ 7.6cm systems	⌀ 10.2cm systems
A (m/LPM)	5.80E-03	1.27E-02	7.10E-03
B (m)	-7.96E-02	-1.67E-01	-9.14E-02

Step ⑤:

If the inlet temperatures at the condition of interest are the same as the temperatures from the CSA tests, skip steps ⑤, ⑥ and ⑦. Otherwise, calculate $F_{C,CSA}$ using Equation 6.3 based on the temperatures at which the CSA tests were performed. These temperatures are in degrees Celsius.

$$F_{C,CSA} = \frac{2.37\times10^{-6}}{(°C)^2}\times T_{h,i}\times T_{c,i} + \frac{1.75\times10^{-3}}{°C}\times T_{h,i} + \frac{1.24\times10^{-3}}{°C}\times T_{c,i} + 0.917 \qquad (6.3)$$

Step ⑥:

The effectiveness value calculated in step ③ or ④ must now be converted to a reference effectiveness value using Equation 6.4. As was discussed in Chapter 5, this reference point is at inlet temperatures of 40°C and 10°C on the drain side and mains side respectively.

$$\varepsilon_{Reference} = \frac{\varepsilon_{Step3\,or\,4}}{F_{C,CSA}} \qquad (6.4)$$

As a reminder, the CSA test procedure is conducted at specific temperature conditions, with mains inlet temperatures ranging from $T_{c,i}$ = 7 to 17°C and a temperature difference of $T_{h,i} - T_{c,i}$ = 28±1°C. This range is too broad and the purpose of this step is to convert the effectiveness values to a reference condition since the CSA tests could have been done anywhere in the above range.

Step ⑦:

With $\varepsilon_{Reference}$ known, the effectiveness can be corrected for the desired inlet temperatures. To do so, F_C needs to be calculated using Equation 6.5 at the desired inlet temperatures. Then the temperature-corrected effectiveness value can be calculated using Equation 6.6.

$$F_C = \frac{2.37\times10^{-6}}{(°C)^2}\times T_{h,i}\times T_{c,i} + \frac{1.75\times10^{-3}}{°C}\times T_{h,i} + \frac{1.24\times10^{-3}}{°C}\times T_{c,i} + 0.917 \tag{6.5}$$

$$\varepsilon_{Temperature-Corrected} = \varepsilon_{Reference}\times F_C \tag{6.6}$$

Step ⑧:

This is the final step for systems operating under equal flow conditions. Calculate the cold side heat transfer rate using Equation 6.7. This heat transfer rate corresponds to equal flow conditions. Note that this equation was developed in Chapter 6 based on constant properties for water.

$$q_c = \frac{4180\times(\dot{V}_{cold}=F1)\times\varepsilon_{temperature-corrected}\times(T_{h,i}-T_{c,i})}{60000} \tag{6.7}$$

where $\dot{V}_{cold}$ is in LPM, temperatures are in °C and q_c is in kW.

Step ⑨:

This step only applies to systems operating under unequal flow conditions. The heat transfer rate calculated in step ⑧ can be represented as shown in Equation 6.8. This value can be plugged into Equation 6.9 to calculate the cold side heat transfer rate for the desired flow rate through the hot side.

$$q_C = q_{(\dot{V}_{cold}=\dot{V}_{hot}=F1)} \tag{6.8}$$

$$q_{(\dot{V}_{cold}=F1\,\&\,\dot{V}_{hot}=F2)} = q_{(\dot{V}_{cold}=\dot{V}_{hot}=F1)} \times \left[0.3452 \times ln\left(\frac{\dot{V}_{hot}=F2}{\dot{V}_{cold}=F1}\right) + 1\right] \quad (6.9)$$

where F1 is the flow rate through the coils and F2 is the flow rate of the falling film.

The procedure was to be validated experimentally to determine how well it can predict the heat transfer rates for various DWHR systems.

6.3 Method

A total of four DWHR systems were tested in this study, as listed in Table 6-2. The systems were made by different manufacturers, referred to as Manufacturer A and B. DWHR systems by different manufacturers have different coil designs as shown in Figure 6-1.

Table 6-2 Diameters and lengths of DWHR systems studied.

System #	Manufacturer	Diameter (cm)	Length (cm)
1	A	5.1	92
2	A	7.6	122
3	B	7.6	102
4	B	10.2	122

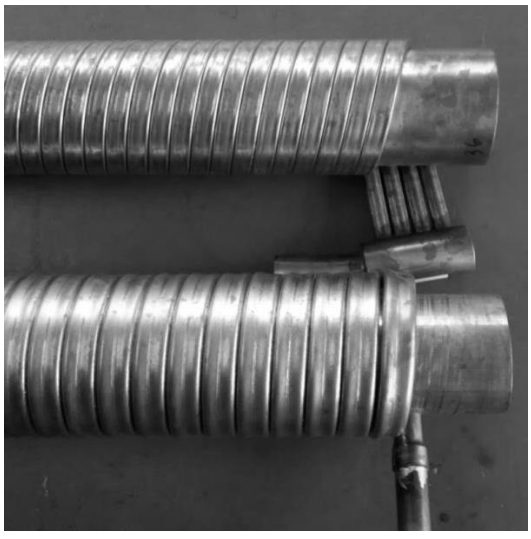

Figure 6-1 DWHR systems with coils designed by manufacturer A (top) and B (bottom).

Each of the DWHR systems were tested at flow rates of 5.5, 7, 9, 10, 12 and 14 LPM in order to produce the CSA data at inlet temperatures of 38±1°C and 10±1°C on the drain side and the mains side, respectively. Each system was then tested at random conditions with varying temperatures and flow rates through either side of the system. The effectiveness and heat transfer rates were measured in each case. The intent was to use the universal procedure described in the introduction to predict the heat transfer rates and compare them to the measured values.

6.4 Results

The raw data used to create the tables in this chapter are presented in tabular form in Appendix C.

6.4.1 System#1

The CSA data generated for system #1 are presented in Table 6-3. This system was tested under a total of six random cases. The variables of interest, as well as the effectiveness and the heat transfer rates for these cases are shown in Table 6-4.

Table 6-3 The CSA data for system #1 gathered at inlet temperatures of 38±1°C and 10±1°C on the drain side and the mains side, respectively.

$\dot{V}_c$ (LPM)	ε_c	q_c (kW)
5.50	49.78%	5.28
6.99	45.33%	6.22
8.98	41.18%	7.26
10.01	39.41%	7.83
12.03	36.64%	8.75
14.03	34.46%	9.54

Table 6-4 The results from the random tests performed on system#1.

Case #	$T_{c,i}$ (°C)	$T_{h,i}$ (°C)	$\dot{V}_c$ (LPM)	$\dot{V}_h$ (LPM)	ε_c	q_c (kW)
1	9.7	37.5	16.97	14.98	34.48%	10.03
2	9.4	38.0	16.10	19.03	33.75%	10.81
3	9.4	37.9	8.01	15.00	51.18%	8.13
4	10.7	42.6	9.97	6.04	53.95%	7.25
5	3.5	28.2	7.47	13.01	50.18%	6.45
6	3.5	27.9	5.49	11.48	59.19%	5.53

Using the results from Table 6-3 and Table 6-4, the heat transfer rates for each case were calculated using the universal procedure. However, before presenting the final results in a tabulated form, the calculations for case#1 are presented in detail to provide an example for the readers as to how the procedure is used. These calculations are presented below for Case #1.

Step ① and ②:

System #1 has a diameter of 5.1cm; hence, the effectiveness measured at 5.5 LPM must be included when generating the characteristic effectiveness vs. flow rate curve. This curve was generated using results from Table 6-3 and is shown in Figure 6-2.

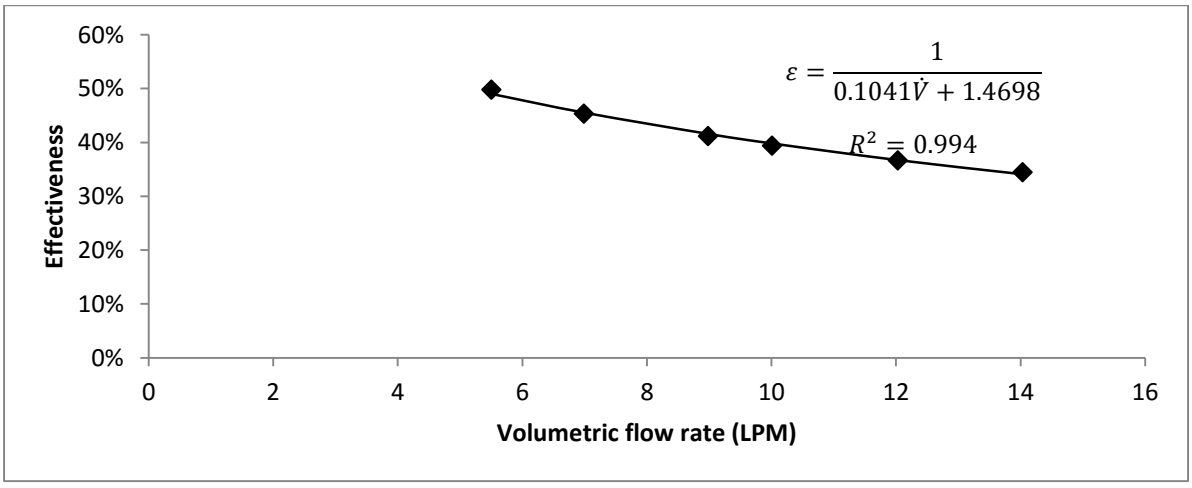

Figure 6-2 Characteristic effectiveness vs. volumetric flow rate curve for system#1.

Therefore, the characteristic equation for this system is:

$$\varepsilon = \frac{1}{\frac{0.1041\times(\dot{V}_{cold}=F1)}{(LPM)}+1.4698} \tag{6.10}$$

where $\dot{V}_{cold}$ is in LPM.

Step ③:

The flow rate through the mains side for this case was 16.97 LPM, which is outside the range covered by step ③. Therefore, step ④ had to be followed.

Step ④:

The corrected effectiveness at 16.97 LPM was calculated using Equation 6.2 as follows:

$$\varepsilon_{corrected} = \frac{1}{0.1041\times(16.97)+1.4698} \times \left(\frac{5.80E-03\times(16.97)-7.96E-02}{1.22} + 1\right) \tag{6.11}$$

$$\therefore \varepsilon_{corrected} = 31.38\%$$

Steps ⑤⑥⑦:

The inlet temperatures for this particular case closely match the temperatures at which the CSA tests were done. Hence, these steps were skipped.

Step ⑧:

The heat transfer rate corresponding to the equal flow conditions at 16.97 LPM is calculated as follows:

$$q_c = \frac{4180\times(16.97)\times(31.38\%)\times(37.5-9.7)}{60000} = 10.34\ kW \tag{6.12}$$

For case #1, the flow rate through the drain side was 14.98 LPM, which meant that the results from this step were not final and Step ⑨ had to be followed.

Step ⑨:

The heat transfer rate under this unequal flow condition was calculated using Equation 6.9 as follows:

$$q_{(\dot{V}_{cold}=16.97\ \&\ \dot{V}_{hot}=14.98)} = q_{(\dot{V}_{cold}=\dot{V}_{hot}=16.97\ )} \times \left[0.3452 \times ln\left(\frac{\dot{V}_{hot}=14.98}{\dot{V}_{cold}=16.97}\right) + 1\right] \qquad (6.13)$$

$$\rightarrow q_{(\dot{V}_{cold}=16.97\ \&\ \dot{V}_{hot}=14.98)} = 10.34\ kW \times \left[0.3452 \times ln\left(\frac{14.98}{16.97}\right) + 1\right]$$

$$\therefore q_{(\dot{V}_{cold}=16.97\ \&\ \dot{V}_{hot}=14.98)} = 9.90\ kW$$

Therefore, the procedure predicted a heat transfer rate of 9.90 kW under the conditions for case #1. The measured heat transfer rate for this case was 10.03 kW. The percent difference between these two values was 1.37%, which showed how effective the procedure was at predicting the actual heat transfer rate for case #1 based solely on the existing CSA data.

The final predicted values for all cases for system #1 are presented in Table 6-5. The maximum percent difference between the measured and predicted values was 2.81%. Although this number may seem large, it only translated to 0.23 kW, which was not a large enough error to discredit the results.

Table 6-5 The measured and predicted heat transfer rates for system#1.

Case #	$T_{c,i}$ (°C)	$T_{h,i}$ (°C)	$\dot{V}_c$ (LPM)	$\dot{V}_h$ (LPM)	Measured q_c (kW)	Predicted q_c (kW)	Percent Difference
1	9.7	37.5	16.97	14.98	10.03	9.90	1.37%
2	9.4	38.0	16.10	19.03	10.81	10.90	0.75%
3	9.4	37.9	8.01	15.00	8.13	8.36	2.81%
4	10.7	42.6	9.97	6.04	7.25	7.32	0.92%
5	3.5	28.2	7.47	13.01	6.45	6.59	2.20%
6	3.5	27.9	5.49	11.48	5.53	5.56	0.49%

6.4.2 System#2

The CSA data generated for system #2 are presented in Table 6-6. This system was tested under a total of four random cases. The variables of interest, as well as the effectiveness and the heat transfer rates for these cases are shown in Table 6-7.

Table 6-6 The CSA data for system #2 gathered at inlet temperatures of 38±1°C and 10±1°C on the drain side and the mains side, respectively.

$\dot{V}_c$ (LPM)	ε_c	q_c (kW)
5.50	49.55%	5.26
7.00	44.28%	6.01
9.01	39.39%	6.96
10.01	37.68%	7.38
12.02	35.01%	8.27
14.02	32.94%	9.11

Table 6-7 The results from the random tests performed on system#2.

Case #	$T_{c,i}$ (°C)	$T_{h,i}$ (°C)	$\dot{V}_c$ (LPM)	$\dot{V}_h$ (LPM)	ε_c	q_c (kW)
1	14.6	44.9	12.98	10.53	39.91%	8.87
2	14.7	44.6	7.96	6.03	51.51%	6.47
3	4.8	35.1	7.99	13.50	47.48%	8.01
4	4.8	34.9	6.02	10.97	54.47%	6.88

The results from Table 6-6 and Table 6-7 were used to predict the heat transfer rates at the four cases using the procedure. The final predicted values for all cases are presented in Table 6-8. The maximum percent difference between the measured and predicted values was 3.53%, which translated into 0.29 kW.

Table 6-8 The measured and predicted heat transfer rates for system#2.

Case #	$T_{c,i}$ (°C)	$T_{h,i}$ (°C)	$\dot{V}_c$ (LPM)	$\dot{V}_h$ (LPM)	Measured q_c (kW)	Predicted q_c (kW)	Percent Difference
1	14.6	44.9	12.98	10.53	8.87	8.74	1.51%
2	14.7	44.6	7.96	6.03	6.47	6.45	0.31%
3	4.8	35.1	7.99	13.50	8.01	8.30	3.53%
4	4.8	34.9	6.02	10.97	6.88	7.05	2.40%

6.4.3 System#3

The CSA data generated for system #3 are presented in Table 6-9. This system was tested under a total of eighteen random cases. The variables of interest, as well as the effectiveness and the heat transfer rates for these cases are shown in Table 6-10.

Table 6-9 The CSA data for system #3 gathered at inlet temperatures of 38±1°C and 10±1°C on the drain side and the mains side, respectively.

$\dot{V}_c$ (LPM)	ε_c	q_c (kW)
5.45	51.55%	5.43
6.95	47.20%	6.38
8.95	42.41%	7.43
9.97	40.66%	7.96
11.96	37.93%	8.94
13.96	35.40%	9.73

Table 6-10 The results from the random tests performed on system#3.

Case #	$T_{c,i}$ (°C)	$T_{h,i}$ (°C)	$\dot{V}_c$ (LPM)	$\dot{V}_h$ (LPM)	ε_c	q_c (kW)
1	10.5	38.1	25.28	24.83	27.83%	13.30
2	10.5	37.9	16.04	15.92	33.51%	10.21
3	9.6	38.1	22.06	21.78	29.42%	12.70
4	9.6	37.9	19.32	19.05	31.23%	11.74
5	9.7	38.0	19.18	7.07	57.67%	8.04
6	9.7	37.9	15.95	9.00	48.24%	8.54
7	9.8	38.0	12.09	16.05	40.86%	9.72
8	9.7	38.0	10.01	19.02	48.47%	9.56
9	14.6	44.9	14.02	13.93	36.35%	10.71
10	14.7	44.7	9.00	8.96	43.44%	8.16
11	14.8	44.4	5.47	5.42	52.66%	5.89
12	14.9	45.0	14.01	10.05	45.23%	9.52
13	14.9	44.8	11.97	9.03	46.62%	8.76
14	4.8	35.1	14.06	13.97	34.90%	10.29
15	4.8	35.0	9.00	8.92	41.85%	7.85
16	5.1	34.8	5.49	5.44	51.16%	5.77
17	4.8	35.1	9.03	13.99	47.34%	9.02
18	4.8	35.0	7.03	9.99	51.03%	7.55

The results from Table 6-9 and Table 6-10 were used to predict the heat transfer rates at the eighteen cases using the universal procedure. The final predicted values for all cases are presented in Table 6-11. The maximum percent difference between the measured and predicted values was 3.25%, which translated into 0.45 kW.

Table 6-11 The measured and predicted heat transfer rates for system#3.

Case #	$T_{c,i}$ (°C)	$T_{h,i}$ (°C)	$\dot{V}_c$ (LPM)	$\dot{V}_h$ (LPM)	Measured q_c (kW)	Predicted q_c (kW)	Percent Difference
1	10.5	38.1	25.28	24.83	13.30	13.75	3.25%
2	10.5	37.9	16.04	15.92	10.21	10.33	1.19%
3	9.6	38.1	22.06	21.78	12.70	13.06	2.75%
4	9.6	37.9	19.32	19.05	11.74	11.94	1.65%
5	9.7	38.0	19.18	7.07	8.04	7.88	2.02%
6	9.7	37.9	15.95	9.00	8.54	8.55	0.10%
7	9.8	38.0	12.09	16.05	9.72	9.73	0.11%
8	9.7	38.0	10.01	19.02	9.56	9.51	0.50%
9	14.6	44.9	14.02	13.93	10.71	10.54	1.63%
10	14.7	44.7	9.00	8.96	8.16	8.21	0.65%
11	14.8	44.4	5.47	5.42	5.89	5.79	1.67%
12	14.9	45.0	14.01	10.05	9.52	9.30	2.34%
13	14.9	44.8	11.97	9.03	8.76	8.69	0.77%
14	4.8	35.1	14.06	13.97	10.29	10.23	0.61%
15	4.8	35.0	9.00	8.92	7.85	7.96	1.33%
16	5.1	34.8	5.49	5.44	5.77	5.67	1.79%
17	4.8	35.1	9.03	13.99	9.02	9.30	2.96%
18	4.8	35.0	7.03	9.99	7.55	7.71	2.14%

6.4.4 System#4

The CSA data generated for system #4 are presented in Table 6-12. This system was tested under a total of eight random cases. The variables of interest, as well as the effectiveness and the heat transfer rates for these cases are shown in Table 6-13.

Table 6-12 The CSA data for system #4 gathered at inlet temperatures of 38±1°C and 10±1°C on the drain side and the mains side, respectively.

$\dot{V}_c$ (LPM)	ε_c	q_c (kW)
5.50	56.15%	5.97
6.99	52.83%	7.15
9.01	50.25%	8.83
10.01	48.33%	9.46
12.02	44.88%	10.57
14.06	42.29%	11.65

Table 6-13 The results from the random tests performed on system#4.

Case #	$T_{c,i}$ (°C)	$T_{h,i}$ (°C)	$\dot{V}_c$ (LPM)	$\dot{V}_h$ (LPM)	ε_c	q_c (kW)
1	9.6	38.1	18.03	13.01	47.72%	12.33
2	9.5	37.9	17.00	8.05	62.98%	10.03
3	9.7	38.1	9.02	18.97	60.40%	10.76
4	9.7	38.0	10.95	16.01	51.81%	11.18
5	12.2	37.1	12.99	9.50	54.03%	8.90
6	12.2	36.9	9.98	8.07	55.65%	7.73
7	7.1	34.8	10.53	13.49	49.95%	10.14
8	7.0	34.2	8.51	12.46	56.15%	9.05

The results from Table 6-12 and Table 6-13 were used to predict the heat transfer rates at the eight cases using the procedure. The final predicted values for all cases are presented in Table 6-14. The maximum percent difference between the measured and predicted values was 3.13%, which translated into 0.35 kW.

Table 6-14 The measured and predicted heat transfer rates for system#4.

Case #	$T_{c,i}$ (°C)	$T_{h,i}$ (°C)	$\dot{V}_c$ (LPM)	$\dot{V}_h$ (LPM)	Measured q_c (kW)	Predicted q_c (kW)	Percent Difference
1	9.6	38.1	18.03	13.01	12.33	12.45	1.00%
2	9.5	37.9	17.00	8.05	10.03	9.99	0.40%
3	9.7	38.1	9.02	18.97	10.76	11.11	3.13%
4	9.7	38.0	10.95	16.01	11.18	11.37	1.70%
5	12.2	37.1	12.99	9.50	8.90	8.81	1.09%
6	12.2	36.9	9.98	8.07	7.73	7.66	0.88%
7	7.1	34.8	10.53	13.49	10.14	10.30	1.58%
8	7.0	34.2	8.51	12.46	9.05	9.11	0.66%

6.5 Conclusions

Four different DWHR systems were tested at a total of 36 random cases as a part of this study. The universal procedure was used to predict the heat transfer rates for these cases and the predicted values were in good agreement with the experimental results. The percent errors between the predicted and measured heat transfer rates among all the 36 cases were always less than 4%. This was a clear indication of how effective the procedure was at predicting the heat transfer rates, based solely on the CSA rating data.

6.5.1 Limitations

As for any experimental model, there are limitations that apply to the procedure presented in this chapter. This section summarizes those limitations to prevent any misuse of the procedure.

Most importantly, every correlation that was developed in this thesis only applies to DWHR recovery systems that consist of a large copper pipe wrapped with smaller tubes, operating in a counter-flow arrangement. There are different variations of designs for DWHR systems that could deviate significantly from the design described above, and as such, the correlations from this thesis may not be used to predict their performance.

There are flow rates for which the model would not work. As was mentioned previously, the above procedure cannot be used to predict the performance of 10.2 cm diameter systems for flow rates below 7 LPM. As for systems with smaller diameters, the procedure cannot be used for flow rates below 5.5 LPM. This limitation is rooted in the problems with partial wetting described in Chapter 3. It is also important to point out that the test equipment used for producing the results in this thesis was only capable of supplying flow rates up to 25 LPM; hence, the procedure could not be tested for flow rates above 25 LPM to determine its validity. As a result, it is ill-advised to use the procedure to predict the heat transfer rates for flow rates above 25 LPM.

Lastly, the temperatures correction factors were developed for inlet temperatures of $5°C < T_{c,i} < 20°C$ and $30°C < T_{h,i} < 45°C$. The test apparatus could not be used to evaluate the performance of DWHR outside of the temperature ranges listed above. Therefore, the procedure is not guaranteed to work for operating temperatures outside the above ranges.

Chapter 7 Conclusions and Recommendations

This thesis focused on devising methods and correlations for predicting performance of DWHR systems under different situations including equal-flow condition, unequal flow condition and variable inlet temperatures. The combination of these correlations was made into a universal procedure, which was verified experimentally to always predict the heat transfer rates to within 4% of the measured values. The only inputs required for this universal procedure are the pre-existing rating data from the CSA tests.

Now that general procedure for determining the steady state heat transfer for DWHR systems has been developed, it is important to point out the steps that need to be taken in the future to complement the outcomes of this thesis.

The procedure can easily be programmed. In Chapter 6, the procedure was programmed into Excel, which was used to produce the results in the tables throughout the chapter. Due to its simplicity, it could very easily be programmed into software such as TRNSYS, in order to perform building simulation analysis with realistic temperatures and water draws.

This thesis was solely based on results collected during steady state operation of DWHR systems; however, in reality, there are transient effects associated with the operation of such systems. For example, once a shower tap is turned on, the system would take a finite period of time before warming up and reaching steady state. In other words, DWHR systems are 'first order' systems and further research needs to be done to quantify the 'time-constant' for such systems. This period of time is likely to be a function of many variables including the pipe dimensions, inlet flow rates and temperatures.

Another potentially significant factor neglected in this thesis was heat exchanger fouling. DWHR systems are installed downstream of shower drains. Over time, accumulation of soap, hair and other unwanted materials is expected to occur on the inside surface of these systems. Fouling is known to reduce the

performance of heat exchangers, and DHWR systems are not exempt from this. In fact, the fouling inside the drain pipe could change the behavior of the falling film. It could cause non-uniformities in the film thickness or at the worst case scenario, prevent the formation of a film altogether, which would mean a significant drop in performance. Field studies are required to determine the effect of fouling on DWHR systems.

Once enough information is known about the transient effects and fouling, they could be combined with the procedure developed in this thesis to create a reliable building simulation model for DWHR systems.

Lastly, the theoretical approach developed in Chapter 4 could be further improved based on experimental analysis to allow designers to adjust variables such as length or diameter to optimize performance of DWHR systems at the design stage.

References

[1] U.S. Energy Information Administration, "International Energy Outlook," 2013.

[2] D&R International Ltd. (2012, March) Buildings Energy Data Book. [Online]. http://buildingsdatabook.eren.doe.gov/docs%5CDataBooks%5C2011_BEDB.pdf

[3] Office of Energy Efficiency & Renewable Energy. (2013, March) U.S. Department of Energy. [Online]. http://energy.gov/eere/buildings/articles/hot-showers-fresh-laundry-clean-dishes

[4] Natural Resources Canada. (2012) www.nrcan.gc.ca; Residential Sector Secondary Energy Use and GHG Emissions by End-Use. [Online]. http://oee.nrcan.gc.ca/corporate/statistics/neud/dpa/data_e/downloads/comprehensive/Excel/2012/res_ca_2_e.xls

[5] I.E. Smith, "Recovery and utilisation of heat from domestic waste water," *Applied Energy*, vol. 1, pp. 205-214, 1975.

[6] G. Proskiw, "Design and analysis of a residential greywater heat recover system," Ottawa, 1995.

[7] Ministry of Municipal Affairs and Housing Building and Development Branch, "2006 Building Code - Supplimentary Standards," in *Supplimentary Standard SB-12 Energy Efficiency for Housing*. Toronto: Queen's Printer Ontario, 2013, pp. 22,.

[8] Government of Manitoba. (2015, April) Manitoba Building Code Amendment; The Buildings and Mobile Homes Act. [Online]. http://web2.gov.mb.ca/laws/regs/annual/2015/052.pdf

[9] CSA Standards, "Test method for measuring efficiency and pressure loss of drain water heat recovery units," Mississauga , Standard 2012.

[10] RenewABILITY Energy Inc. (2015) Renewability. [Online]. http://www.renewability.com/uploads/documents/en/home_retrofit.pdf

[11] Watercycles Energy Recovery Inc. (2015) Watercycles. [Online]. http://www.watercycles.ca/index.php/i-m-a-contractor

[12] EcoInnovation Technologies. (2015) Ecoinnovation. [Online]. http://ecoinnovation.ca/s/Installation-guide-TD-English-R7-2013.pdf

[13] Michael R. Collins, Gerald W. E. Van decker, and Joel Murray, "Characteristic effectiveness curves for falling-film drain water heat recovery systems," *HVAC&R Research*, vol. 19, no. 6, pp. 649-662, 2013.

[14] Charles Zaloum, John Gusdorf, and Anil Parekh, "Performance Evaluation of Drain Water Heat Recovery Technology at the Canadian Centre for Housing Technology," Sustainable Buildings and Communities, National Resources Canada, Ottawa, 2007.

[15] Parham Eslami-nejad and Michel Bernier, "Impact of Grey Water Heat Recovery on the Electrical Demand of Domesic Hot Water Heaters," in *Eleventh International IBPSA Conference*, Glasgow, 2009, pp. 681-687.

[16] Daniel Słyś and Sabina Kordana, "Financial Analysis of the Implementation of a Drain Water Heat Recovery Unit in Residential Housing," *Energy and Buildings*, vol. 71, pp. 1-11, March 2014.

[17] J. J. Tomlinson, "Heat Recovery from Wastewater using a Gravity-Film Heat Exchanger," Oak Ridge National, 2001.

[18] R. Schuitema , N. C. Sijpheer , and E. J. Bakker , "Energy Performance of a Drainwater Heat Recovery System," in *European Conference and Cooperation Exchange on Sustainable Energy*, Vienna, 2005.

[19] W. M. Kays and A. L. London, "Compact Heat Exchangers," in *Compact Heat Exchangers*. Stanford: McGraw-Hill Book Company, 1984, pp. 14-20.

[20] Omega Engineering. (2015) ECONOMICAL LIQUID TURBINE FLOWMETERS. [Online]. http://www.omega.com/Green/pdf/FTB1400_Series.pdf

[21] Omega Engineering Inc. (2013, June) Omega Engineering. [Online]. http://www.omega.com/Temperature/pdf/P-Ultra_RTD.pdf

[22] Omega Engineering Inc. (2013, June) Omega Engineering. [Online]. http://www.omega.com/Pressure/pdf/PX309.pdf

[23] Go Tankless. (2013, March) Go Tankless website. [Online]. http://gotankless.ca/achieving-the-best-water-heater-efficiency/2013

[24] R.J. Moffat, "Contributions to the Theory of Single-Sample Uncertainty Analysis," *Transactions of the ASME*, no. 104, pp. 250-258, 1982.

[25] NEN, "NEN 5128:2004+A1:2009; Energy performance of residential functions and residential buildings - Determination method," 2009.

[26] Frank P. Incropera, David P. DeWitt, Theodore L. Bergman, and Adrienne S. Lavine, *Fundamentals of Heat and Mass Transfer*, 6th ed.: Wiley, 2007.

[27] W. H. McAdams, T. B. Drew, and G. S. Bays, "Heat Transfer to Falling-Water Films," *Transactions of the A.S.M.E.*, pp. 627-631, October 1940.

[28] J. S. Prost, M. T. González, and M. J. Urbicain, "Determination and correlation of heat transfer coefficients in a falling film evaporator," *Journal of Food Engineering*, vol. 73, no. 4, pp. 320-326, April 2006.

[29] A. N. Dravid, K. A. Smith, E. W. Merrill, and P. L.T. Brian, "Effect of Secondary Fluid Motion on Laminar Flow Heat Transfer in Helically Coiled Tubes," *AIChE* , vol. 17, pp. 1114-1122, September 1971.

[30] R. K. Shah and S. D. Joshi, "Convective Heat Transfer In Curved Ducts," in *Handbook of Single-Phase Convective Heat Transfer*. United States of America: John Wiley & Sons Inc., 1987, ch. 5, pp. 1-46.

[31] G. F.C. Rogers and Y. R. Mayhew, "Heat Transfer and Pressure Loss in Helically Coiled Tubes with Turbulent Flow," *International Journal of Heat and Mass Transfer*, vol. 7, pp. 1207-1216, March 1964.

[32] J Panayiotis Karditsas and Marc-Jean Baptiste. (2011, February) ARIES Program Public Information Site. [Online]. http://www-ferp.ucsd.edu/LIB/PROPS/PANOS/cu.html

Appendix A - Performance of DWHR Systems under Small Tilt Angles with respect to Vertical[2]

Introduction

The performance of DWHR systems relies on water falling as an annular film that wets the inner surface of the drain pipe. This phenomenon results in high heat transfer rates on the drain-side of the system. Heat transfer surface area is maximized and the water film thickness which resists conduction is minimized. DWHR systems are designed to be installed vertically, which allows water to fall as a relatively uniform thin film [10,11,12].

In new construction, proper care can enable accurate vertical installation of DWHR systems. However, an accurate vertical installation may not be possible in many retrofit applications. Several building designers and DWHR system manufacturers have shown interest in estimating the reduction of DWHR performance for non-vertical installations. Straying from a perfectly vertical orientation will likely cause the film to be non-uniform around the drain pipe's inner circumference, reducing the performance of the heat exchanger. This study will identify how sensitive DWHR systems are to tilt angles away from vertical, and provide insight on what installation angles are acceptable.

Method

For this study, six DWHR systems of various lengths and diameters were chosen as listed in Table A-1.

[2] The contents of this Appendix have been accepted for publication in the Energy and Buildings journal under the title of "Impact of Small Tilt Angles on the Performance of Falling Film Drain Water Heat Recovery Systems"

Table A-1 Diameters and lengths of DWHR systems studied.

Pipe #	Diameter (cm)	Length (cm)
1	5.1	122
2	7.6	92
3	7.6	122
4	7.6	153
5	10.2	122
6	10.2	153

The thermal effectiveness of each DWHR system was measured at flow rates of 5.5, 9.5, and 14 LPM, and at tilt angles from vertical of 0, 2, 5, 10, and 15 degrees. The cold and hot-side temperatures of 10±0.5°C and 38±0.5°C were maintained for the mains-side inlet and drain-side inlet respectively. To achieve the maximum wetting area in the pipes, each test is started with a high flow rate of 20 LPM and gradually lowered to achieve the desired flow rate. The drain-side flow was photographed to observe the behavior of the falling film.

The CSA test standard requires DWHR systems to be installed at no more than 2° from vertical orientation during testing [9]. The test platform meets this angular requirement, but also allows testing of DWHR systems at angles further from vertical. The performance at tilt angles away from vertical is assessed to evaluate variations to be expected in standardized tests and service installations, both of which can never be perfectly vertical.

The tilt angle measurement was performed using a plumb-bob and linear measurement, with trigonometry used to calculate the angle. The experimental setup and measurement method are depicted Figure A-1. This method results in significantly less error than using an inclinometer, which would have an uncertainty of at least ±0.5° due to least count on a protractor scale. Given the distance between the two rulers, a, and horizontal displacement, d, the tilt angle away from vertical, θ_T, is calculated as:

$$\theta_T = atan\left(\frac{d}{a}\right) \qquad (A.1)$$

Using a nominal reference distance of a =1.22m and assuming linear measurements can be made to a tolerance of ±0.01m, the uncertainty for angular measurements is estimated to be ±0.02°. This calculation is based on the constant-odds method described by Moffat [24].

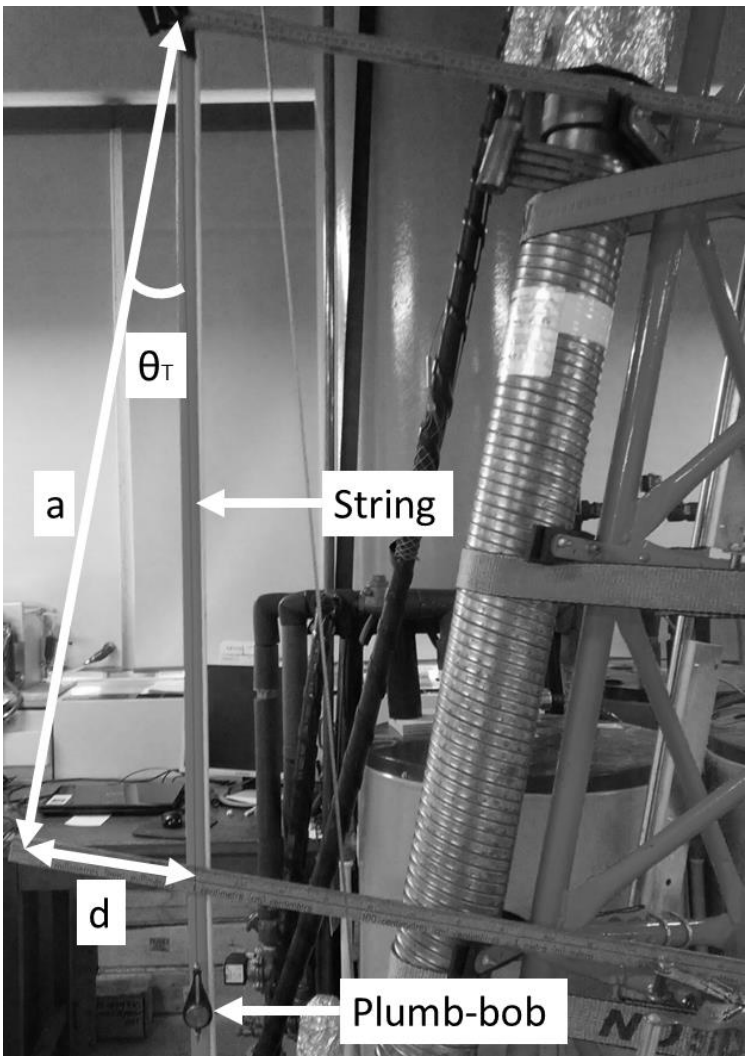

Figure A-1 Experimental apparatus and setup with DWHR system tilted.

Results and Discussion

The general expectation was that the effectiveness of a falling film DWHR system decreases as the tilt angle, θ_T, increases. In order to best represent this reduction, the results are displayed in terms of an effectiveness ratio, ε_r. This ratio is calculated by dividing the effectiveness of the DWHR system at a given angle by its effectiveness in a vertical orientation, as shown in Equation A.2. For example, at a tilt angle of 0°, ε_r would equal 100% and a gradual decrease is expected as θ_T is increased. The uncertainty associated with ε_r is calculated to be ±0.85% of full scale using the constant-odds methods described by Moffat [24] as detailed in Appendix B.

$$\varepsilon_r = \frac{Effectiveness\ at\ \theta_T}{Effectiveness\ at\ vertical} \qquad (A.2)$$

The raw data used to create the figures in this Appendix are presented in tabular form in Appendix C.

Figure A-2 contains the results of the tests performed on all six systems at a flow rate of 5.5 LPM. For a tilt angle of 2°, the performance of all systems remained almost unaffected. At worst, the ε_r value was reduced to 97%. For tilt angles greater than 2°, visual inspection revealed that the falling film became uneven, as shown in Figure A-3 and Figure A-4. For vertical orientation, a relatively uniform thin film was observed around the circumference of the drain-side pipe. For the tilted case, the film became thinner at the upper section of the circumference of the drain-side pipe since most of the water gravitated to the lower section of the circumference. The film thickness was no longer consistent as shown in Figure A-4 (A), compared to the uniform film thickness at vertical shown in Figure A-4 (B).

The non-uniformity of the film led to a certain degree of non-repeatability in the results. This phenomenon was observed in Chapter 3, where low volumetric flow rates led to disturbances in the

falling film, making the results non-repeatable. This is why the values of ε_r for different systems at tilt angles above 2° are distributed over a range of values, as shown in Table A-2 and Figure A-2.

Table A-2 Experimental data collected at a flow rate of 5.5 LPM.

θ_T (degrees)	Effectiveness Ratio					
	Pipe 1	Pipe 2	Pipe 3	Pipe 4	Pipe 5	Pipe 6
0	100.0%	100.0%	100.0%	100.0%	100.0%	100.0%
2	99.2%	97.1%	100.0%	100.0%	99.8%	98.7%
5	90.1%	90.4%	100.0%	97.0%	98.9%	96.3%
10	73.6%	76.5%	90.0%	72.5%	86.7%	80.0%
15	72.8%	69.4%	78.1%	68.2%	73.1%	67.4%

Note: These values are for specific DWHR systems and should not be used to predict performance of other products.

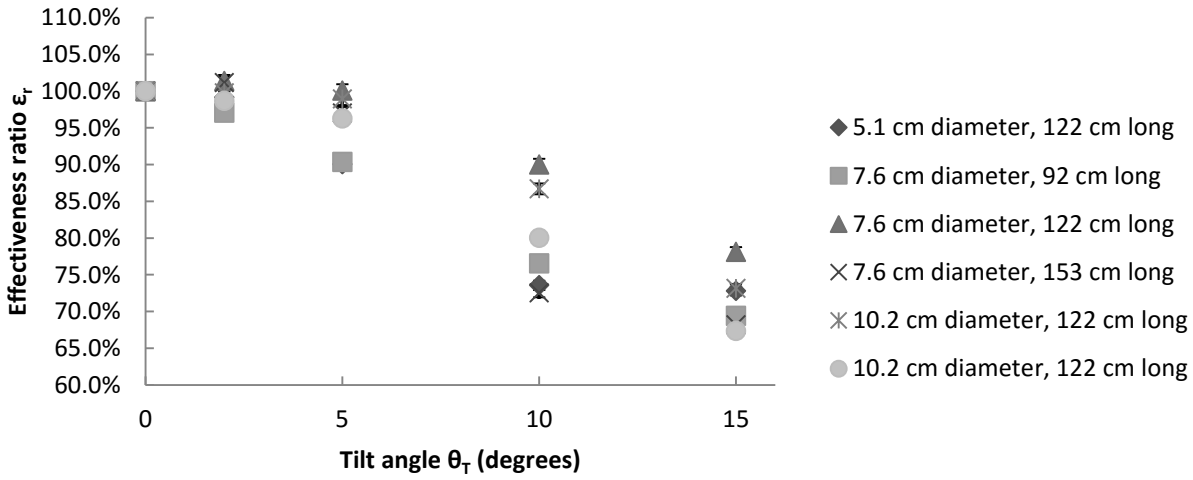

Figure A-2 The effectiveness ratio as a function of the tilt angle for all systems at 5.5 LPM.

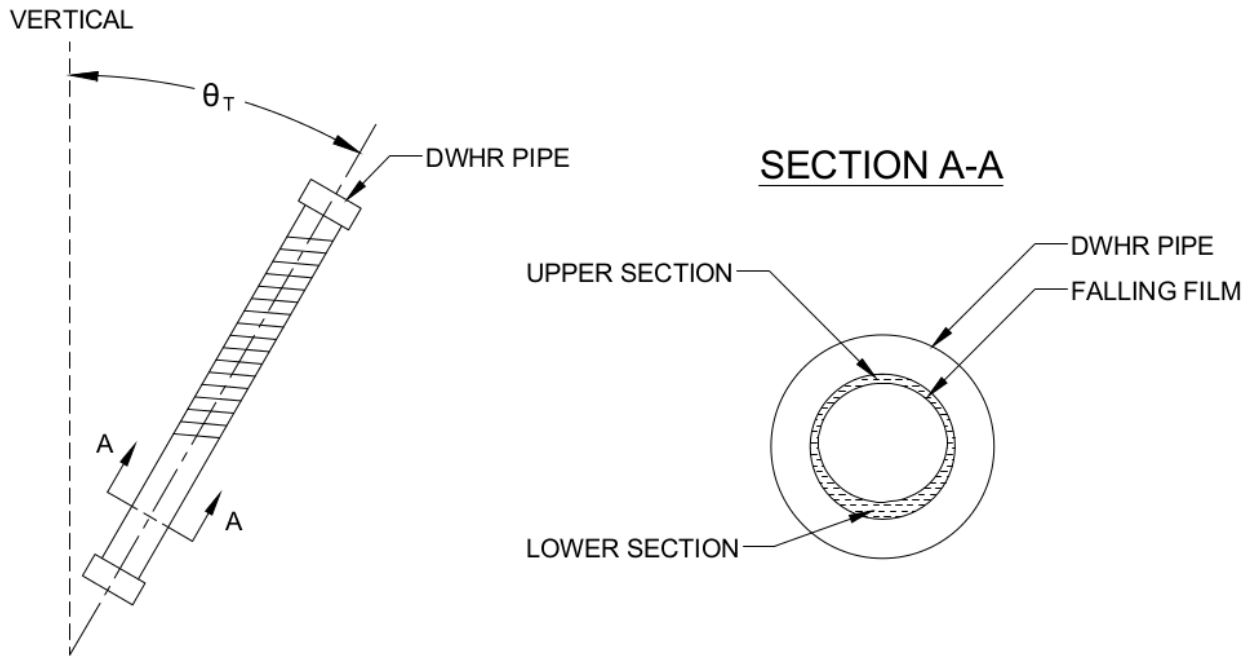

Figure A-3 The observed difference in thickness in the lower and upper sections of the DWHR system.

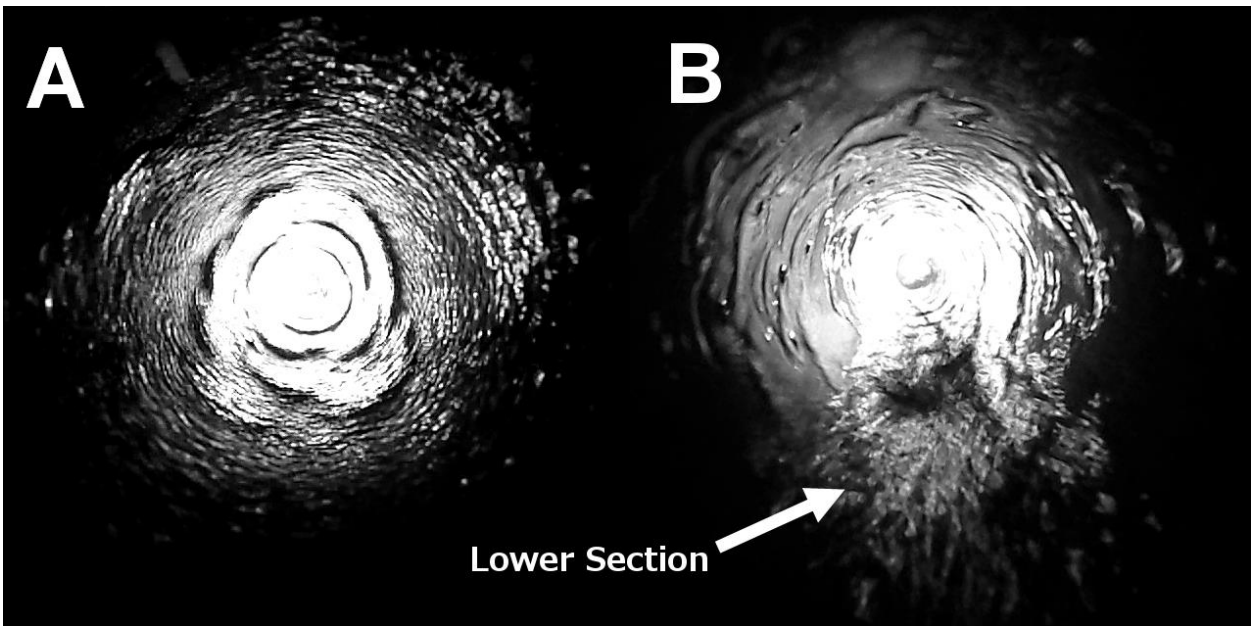

Figure A-4 The behavior of the falling film in the drain-side pipe for a vertical installation (A) vs. an installation on a 10° tilt from vertical (B) for the same DWHR system at the same volumetric flow rate.

The results for the flow rate of 9.5 LPM are shown in Table A-3 and Figure A-5, and the results for 14 LPM are shown in Table A-4 and Figure A-6. At a tilt angle of 2°, the test results indicated that the lowest ε_r value for both flow rates was 96%. Similar to the results for 5.5 LPM, ε_r values became more variable for tilt angles larger than 2°.

Table A-3 Experimental data collected at a flow rate of 9.5 LPM.

θ_T (degrees)	Effectiveness Ratio					
	Pipe 1	Pipe 2	Pipe 3	Pipe 4	Pipe 5	Pipe 6
0	100.0%	100.0%	100.0%	100.0%	100.0%	100.0%
2	99.3%	98.5%	96.6%	96.6%	99.8%	98.3%
5	92.1%	93.3%	91.5%	88.4%	98.1%	94.6%
10	77.8%	82.5%	81.4%	71.7%	91.5%	85.6%
15	74.1%	72.6%	68.0%	64.6%	82.6%	77.7%

Note: These values are for specific DWHR systems and should not be used to predict performance of other products.

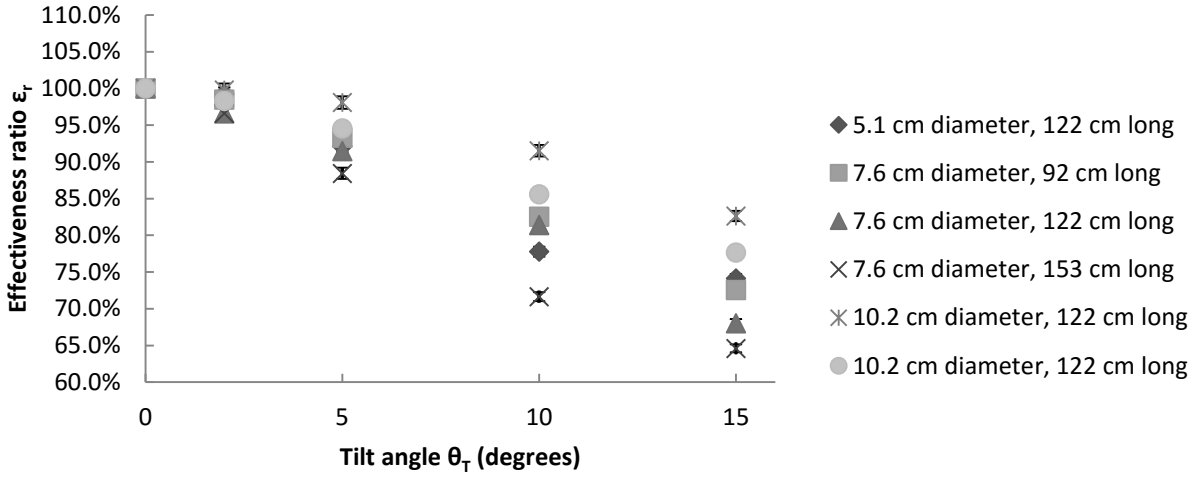

Figure A-5 The effectiveness ratio as a function of the tilt angle for all systems at 9.5 LPM.

Table A-4 Experimental data collected at a flow rate of 14 LPM.

θ_T (degrees)	Effectiveness Ratio					
	Pipe 1	Pipe 2	Pipe 3	Pipe 4	Pipe 5	Pipe 6
0	100.0%	100.0%	100.0%	100.0%	100.0%	100.0%
2	96.9%	97.9%	96.9%	95.5%	99.7%	98.4%
5	87.4%	92.2%	89.9%	84.5%	96.8%	92.9%
10	76.3%	81.2%	75.0%	69.1%	87.7%	81.4%
15	71.1%	69.0%	65.6%	61.7%	77.6%	72.0%

Note: These values are for specific DWHR systems and should not be used to predict performance of other products.

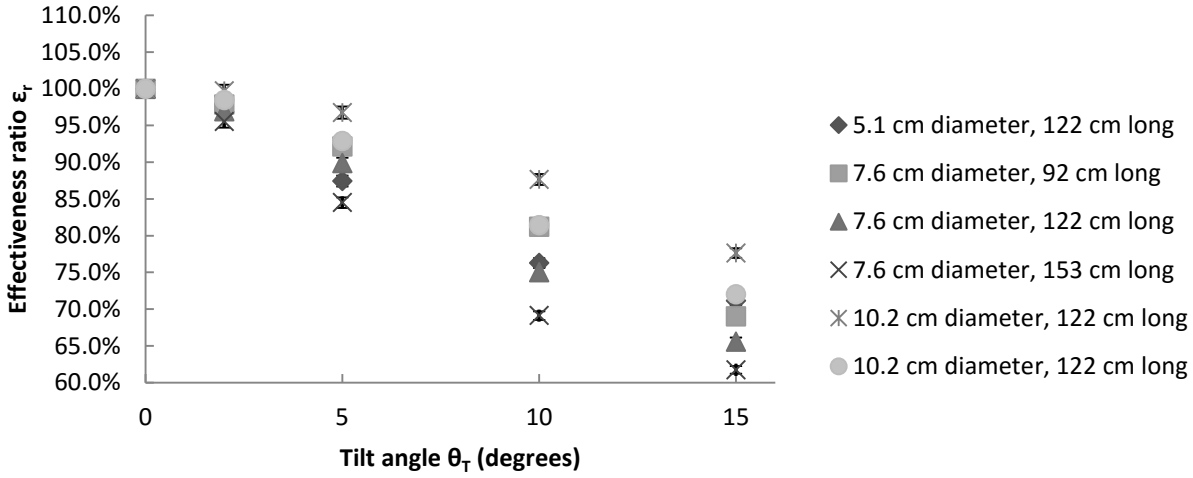

Figure A-6 The effectiveness ratio as a function of the tilt angle for all systems at 14 LPM.

The differences in film thickness at the upper and lower sections of the pipe were more pronounced for flow rates of 9.5 and 14 LPM compared to 5.5 LPM. No clear photographs could be produced to highlight the change in thickness that appeared for different flow rates; hence, Figure A-7 was created to illustrate this phenomenon. From visual inspection, it was evident that the thicker part of the film at the lower section of the circumference of the pipe had a higher velocity than the rest of the film.

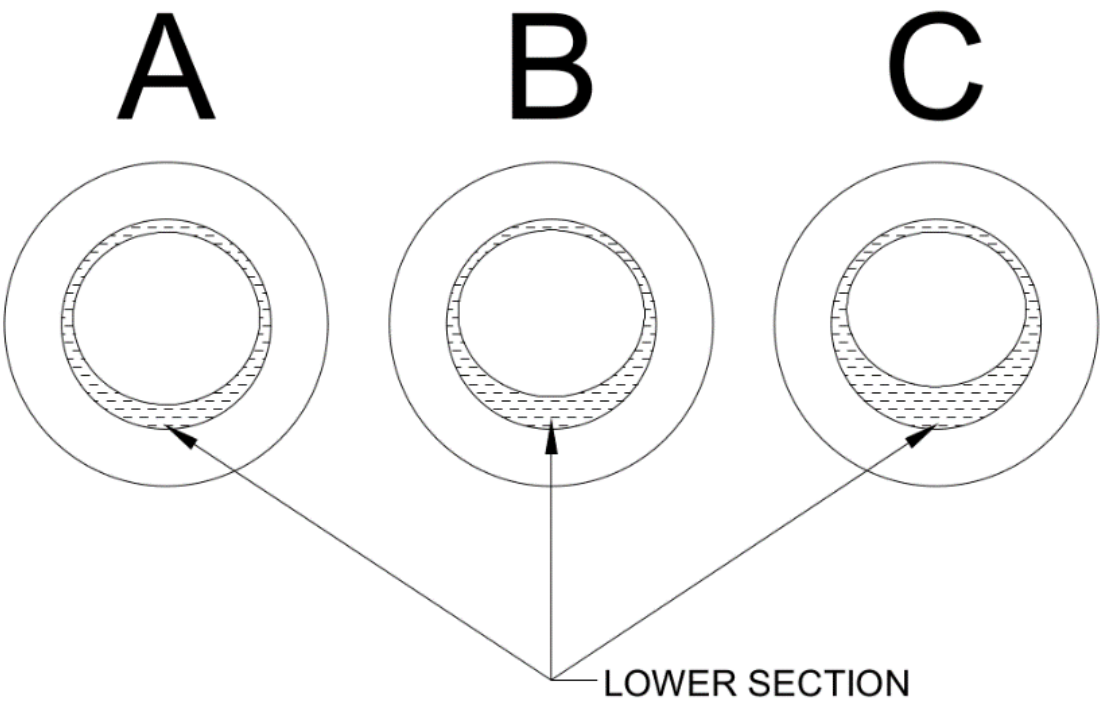

Figure A-7 The difference in thickness at the lower section of the pipe for (A) 5.5 LPM, (B) 9.5 LPM and (C) 14 LPM.

In practice, DWHR systems are designed to be installed and operated in a vertical orientation. This study shows that the effectiveness of DWHR systems is significantly decreased at tilt angles greater than 2°. Due to erratic behavior of falling films at increased tilt angles, it was deemed impractical to develop a tilt angle model representing all DWHR systems. ε_r values for all combinations tested in this study are summarized in Table A-5.

Table A-5 Range of effectiveness ratios for different tilt angles.

θ_T (degrees)	Minimum ε_r (%)	Maximum ε_r (%)
2	96	100
5	85	99
10	69	92
15	62	83

Tilt angles larger than 15° were not investigated as part of this study. The performance drop is expected to be greater for extreme tilt angles, such as 45°, since water will not fall as a film, which substantially reduces the heat transfer area. Although no experimental results for extreme angles were produced as a part of this study, it can be generalized that the current designs of falling film DWHR systems are not suitable for installations at extreme angles. Designers are strongly encouraged to only use DWHR systems in applications where a vertical installation is possible.

The overall trend of decreasing performance with increased tilt angle for falling-film heat exchangers was demonstrated by this study. It is not possible to accurately predict how a given system will perform at a particular tilt due to the unstable nature of falling films. As a result, the performance of DWHR systems installed at varied angles cannot be accurately modelled at this time. DWHR systems are designed to be installed at a vertical orientation and the results from this study show that these systems would perform much worse than intended if they are installed at an angle greater than 2° from vertical.

Appendix B - Uncertainty Calculations

This appendix focuses on explaining how the uncertainty calculations were done for the experimental results. The test instruments used to take measurements in every test are summarized in Table A-6, along with their respective accuracies. All uncertainty calculations performed in this thesis are based on Moffat's constant odds method [24].

Table A-6 The measurement accuracies for all instruments used in this thesis.

Parameter	Accuracy
RTD Temperature Probes	± 0.1 °C
Cold Water Flow Meter	± 1% Reading
Hot Water Flow Meter	± 1% Reading
Pressure Transducers	± 862.5 Pa

Uncertainty Associated With the Effectiveness Calculations

The effectiveness of a DWHR system operating under equal flow conditions is calculated using Equation A.3 below:

$$\varepsilon = \frac{T_{c,o} - T_{c,i}}{T_{h,i} - T_{c,i}} = \frac{\Delta T_{cold}}{\Delta T_{max}} \qquad (A.3)$$

The first step is to calculate the uncertainty for the ΔT_{cold} and ΔT_{max} :

$$\delta \Delta T_{cold} = \sqrt{\left(\delta T_{c,o}\right)^2 + \left(\delta T_{c,i}\right)^2} = \sqrt{(0.1℃)^2 + (0.1℃)^2} = \pm 0.14℃ \qquad (A.4)$$

$$\delta \Delta T_{max} = \delta \Delta T_{cold} = \pm 0.14℃ \qquad (A.5)$$

The uncertainty in the effectiveness calculation can now be expressed as:

$$\delta \varepsilon = \varepsilon \times \sqrt{\left(\frac{\delta \Delta T_{cold}}{\Delta T_{cold}}\right)^2 + \left(\frac{\delta \Delta T_{max}}{\Delta T_{max}}\right)^2} = \varepsilon \times \sqrt{\left(\frac{0.14℃}{\Delta T_{cold}}\right)^2 + \left(\frac{0.14℃}{\Delta T_{max}}\right)^2} \qquad (A.6)$$

As is clear from Equation A.6, the actual value of the uncertainty in effectiveness calculation varies from test to test and requires substitution of values for ε, ΔT_{cold} and ΔT_{max} .

For example, for a test data with $\varepsilon = 0.4453$, $\Delta T_{cold} = 12.51℃$ and $\Delta T_{max} = 28.1℃$, the uncertainty is calculated to be:

$$\delta\varepsilon = 0.4453 \times \sqrt{\left(\frac{0.14℃}{12.51℃}\right)^2 + \left(\frac{0.14℃}{28.1℃}\right)^2} = \pm 0.55\% \ (F.S.) \qquad (A.7)$$

The effectiveness of a DWHR system operating under unequal flow conditions is calculated using Equation A.8 below:

$$\varepsilon = \frac{\dot{V}_{cold}(T_{c,o} - T_{c,i})}{\dot{V}_{min}(T_{h,i} - T_{c,i})} = \frac{\dot{V}_{cold}\Delta T_{cold}}{\dot{V}_{min}\Delta T_{max}} \qquad (A.8)$$

The first step is to calculate the uncertainty for the numerator and the denominator as follows:

$$\frac{\delta(\dot{V}_{cold}\Delta T_{cold})}{\dot{V}_{cold}\Delta T_{cold}} = \sqrt{\left(\frac{\delta\dot{V}_{cold}}{\Delta\dot{V}_{cold}}\right)^2 + \left(\frac{\delta\Delta T_{cold}}{\Delta T_{cold}}\right)^2} = \sqrt{(1\%)^2 + \left(\frac{0.14℃}{\Delta T_{cold}}\right)^2} \qquad (A.9)$$

$$\frac{\delta(\dot{V}_{min}\Delta T_{max})}{\dot{V}_{min}\Delta T_{max}} = \sqrt{\left(\frac{\delta\dot{V}_{min}}{\Delta\dot{V}_{min}}\right)^2 + \left(\frac{\delta\Delta T_{max}}{\Delta T_{max}}\right)^2} = \sqrt{(1\%)^2 + \left(\frac{0.14℃}{\Delta T_{max}}\right)^2} \qquad (A.10)$$

Now the uncertainty in the effectiveness calculation can now be expressed as:

$$\delta\varepsilon = \varepsilon \times \sqrt{(1\%)^2 + (1\%)^2 + \left(\frac{0.14℃}{\Delta T_{cold}}\right)^2 + \left(\frac{0.14℃}{\Delta T_{max}}\right)^2} \qquad (A.11)$$

Similar to the case for the equal flow conditions, calculating the actual uncertainty in the effectiveness value requires substitution of values for ε, ΔT_{cold} and ΔT_{max} .

For example, for a test data with $\varepsilon = 0.5598$, $\Delta T_{cold} = 11.1℃$, $\Delta T_{max} = 28.2℃$,$\Delta\dot{V}_{cold} = 10\ LPM$ and $\dot{V}_{min} = 7\ LPM$, the uncertainty is calculated to be:

$$\delta\varepsilon = 0.5598 \times \sqrt{(1\%)^2 + (1\%)^2 + \left(\frac{0.14℃}{11.1}\right)^2 + \left(\frac{0.14℃}{28.2}\right)^2} = \pm 1.1\% \ (F.S.) \qquad (A.12)$$

Uncertainty Associated With the Heat Transfer Rate Calculations

The uncertainty calculation procedure for the heat transfer rate is the same for both equal and unequal flow conditions. Equation A.13 is used to calculate the heat transfer rate based on the cold side of the heat exchanger:

$$q = \frac{4180 \times \dot{V}_{cold} \times \Delta T_{cold}}{60000} \qquad (A.13)$$

The uncertainty for the heat transfer calculations can be expressed as:

$$\delta q = q \times \sqrt{\left(\frac{\delta \dot{V}_{cold}}{\Delta \dot{V}_{cold}}\right)^2 + \left(\frac{\delta \Delta T_{cold}}{\Delta T_{cold}}\right)^2} = q \times \sqrt{(1\%)^2 + \left(\frac{0.14℃}{\Delta T_{cold}}\right)^2} \qquad (A.14)$$

Again, the actual value of this uncertainty depends on the measured values for q and ΔT_{cold} .

For example, for a test data with for $q = 6.99\ kW$ and $\Delta T_{cold} = 14.34℃$, the uncertainty is calculated to be:

$$\delta q = 6.99\ kW \times \sqrt{(1\%)^2 + \left(\frac{0.14℃}{14.34℃}\right)^2} = \pm 0.097\ kW \qquad (A.15)$$

Uncertainty Associated With the Pressure Drop Calculations

The pressure drop through the coils is simply determined by calculating the difference between the inlet and outlet pressures as shown in Equation A.16:

$$\Delta P = P_{in} - P_{out} \qquad (A.16)$$

The uncertainty in ΔP can be expressed as:

$$\delta \Delta P = \sqrt{(\delta P_{in})^2 + (\delta P_{out})^2} = \sqrt{(0.8625\ kPa)^2 + (0.8625\ kPa)^2} = \pm 1.22\ kPa \qquad (A.17)$$

Appendix C - Raw Experimental Data

Experimental Data for Chapter 4

The experimental results for the 7.6cm diameter, 122cm long DWHR system used to create the corresponding plots in Chapter 4.

Table A-7 The results for the 7.6cm diameter, 122cm long system tested at different inlet temperatures.

Volumetric Flow rate of 5.5 LPM			Volumetric Flow rate of 9.5 LPM			Volumetric Flow rate of 14 LPM		
Thot-in (°C)	Tcold-in (°C)	ε (%)	Thot-in (°C)	Tcold-in (°C)	ε (%)	Thot-in (°C)	Tcold-in (°C)	ε (%)
44.8	30.3	57.74	45.0	30.3	47.73	45.1	30.3	42.0
44.9	20.3	57.17	45.0	20.2	46.90	45.2	20.2	41.4
44.9	15.6	56.97	45.1	15.5	46.66	45.1	15.5	40.9
44.8	10.0	56.63	45.1	9.8	46.20	45.2	9.8	40.4
44.8	5.1	56.23	45.0	4.9	45.91	45.1	4.8	39.8
40.0	30.0	56.93	40.2	30.0	47.10	40.3	30.0	41.3
40.0	20.5	56.75	40.2	20.5	46.63	40.3	20.4	40.8
40.0	14.9	56.51	40.1	14.8	46.22	40.2	14.8	40.4
39.8	10.1	56.14	40.1	9.9	45.80	40.2	9.8	39.9
39.8	5.0	55.70	40.1	4.7	45.52	40.2	4.6	39.5
35.1	20.0	56.46	35.2	19.9	46.20	35.3	19.9	40.3
35.0	15.2	56.20	35.2	15.1	45.67	35.3	15.1	39.9
35.0	9.8	55.84	35.2	9.6	45.32	35.2	9.6	39.4
35.0	5.0	55.23	35.2	4.8	44.84	35.3	4.7	38.9
30.2	19.9	55.90	30.3	19.9	45.32	30.3	19.8	39.8
30.2	14.8	55.72	30.2	14.7	44.99	30.3	14.6	39.4
30.0	9.9	55.25	30.2	9.7	44.73	30.2	9.7	38.8
30.1	5.3	54.76	30.2	5.1	44.43	30.3	5.0	38.4
25.3	15.1	55.17	25.3	14.9	44.60	25.4	14.9	38.8
25.2	10.2	54.87	25.3	10.0	44.32	25.4	10.0	38.3
25.3	5.3	54.47	25.3	5.0	43.77	25.4	4.9	37.8

The experimental results for the 7.6cm diameter, 153cm long DWHR system used to create the corresponding plots in Chapter 4.

Table A -8 The results for the 7.6cm diameter, 153cm long system tested at different inlet temperatures.

Volumetric Flow rate of 5.5 LPM			Volumetric Flow rate of 9.5 LPM			Volumetric Flow rate of 14 LPM		
Thot-in (°C)	Tcold-in (°C)	ε (%)	Thot-in (°C)	Tcold-in (°C)	ε (%)	Thot-in (°C)	Tcold-in (°C)	ε (%)
45.0	30.6	63.33	45.1	30.6	53.79	45.2	30.6	47.6
45.0	21.0	63.05	45.1	20.9	53.30	45.2	20.9	47.1
45.0	16.0	62.78	45.1	15.9	52.70	45.2	15.8	46.7
44.9	10.5	62.33	45.1	10.3	52.30	45.1	10.2	46.1
44.8	5.1	61.85	45.0	4.9	51.85	45.0	5.0	45.8
40.1	29.9	62.90	40.2	29.9	53.20	40.3	29.9	47.1
40.1	20.5	62.50	40.2	20.4	52.70	40.3	20.4	46.6
40.0	15.5	62.15	40.2	15.4	52.20	40.3	15.3	46.1
39.9	10.3	61.93	40.1	10.1	51.83	40.2	10.0	45.5
40.0	5.2	61.43	40.2	5.0	51.20	40.2	5.0	45.1
35.1	19.6	61.93	35.2	19.5	52.08	35.3	19.5	45.9
35.1	15.5	61.63	35.2	15.4	51.53	35.3	15.3	45.5
35.1	10.3	61.38	35.2	10.1	51.18	35.2	10.1	45.0
35.1	5.3	61.00	35.2	5.1	50.68	35.3	5.0	44.4
30.3	20.0	61.63	30.3	19.9	51.60	30.3	19.9	45.3
30.2	15.3	61.33	30.3	15.2	51.03	30.3	15.2	44.9
30.2	10.3	60.93	30.3	10.2	50.63	30.3	10.1	44.4
30.2	5.4	60.50	30.3	5.2	50.25	30.3	5.2	43.8
25.3	15.2	60.95	25.3	15.0	50.60	25.3	15.0	44.4
25.3	10.5	60.43	25.3	10.3	50.08	25.3	10.3	44.0
25.3	5.4	59.80	25.3	5.3	49.55	25.3	5.2	43.4

The experimental results for the 10.2cm diameter, 122cm long DWHR system used to create the corresponding plots in Chapter 4.

Table A-9 The results for the 10.2cm diameter, 122cm long system tested at different inlet temperatures.

Volumetric Flow rate of 9.5 LPM			Volumetric Flow rate of 14 LPM		
Thot-in (°C)	Tcold-in (°C)	ε (%)	Thot-in (°C)	Tcold-in (°C)	ε (%)
45.0	29.8	52.48	45.1	29.8	45.6
45.0	20.3	51.84	45.2	20.2	45.1
45.0	14.7	51.30	45.1	14.7	44.7
45.0	9.7	51.10	45.2	9.7	44.2
44.8	4.9	50.73	45.2	4.8	43.8
40.1	30.2	52.20	40.2	30.2	45.3
40.1	20.4	51.40	40.2	20.3	44.5
40.0	14.5	50.95	40.2	14.5	44.1
40.0	10.2	50.82	40.1	10.1	43.8
40.1	5.1	50.50	40.3	5.0	43.4
35.1	20.4	51.40	35.3	20.4	44.4
35.1	14.6	50.76	35.2	14.5	43.9
35.0	9.8	50.32	35.1	9.7	43.5
35.2	5.0	49.97	35.3	4.9	43.1
30.2	20.4	51.10	30.3	20.4	43.9
30.2	14.6	50.73	30.3	14.6	43.6
30.2	9.7	50.18	30.3	9.6	43.2
30.2	5.0	49.80	30.3	4.8	42.8
25.3	14.8	50.50	25.4	14.7	43.2
25.4	10.1	49.91	25.4	10.0	42.9
25.3	5.0	49.63	25.4	4.9	42.5

The experimental results for the 10.2cm diameter, 153cm long DWHR system used to create the corresponding plots in Chapter 4.

Table A-10 The results for the 10.2cm diameter, 153cm long system tested at different inlet temperatures.

Volumetric Flow rate of 9.5 LPM			Volumetric Flow rate of 14 LPM		
Thot-in (°C)	Tcold-in (°C)	ε (%)	Thot-in (°C)	Tcold-in (°C)	ε (%)
45.1	30.0	57.88	45.2	30.0	51.1
45.2	20.3	57.35	45.2	20.3	50.6
45.0	15.3	57.05	45.1	15.2	50.2
45.0	10.1	56.53	45.1	10.1	49.7
45.1	5.2	56.30	45.2	5.2	49.3
40.2	29.5	57.53	40.3	29.5	50.5
40.2	20.3	57.10	40.3	20.3	50.2
40.2	15.1	56.70	40.3	15.1	49.7
40.1	10.4	56.10	40.1	10.3	49.2
40.1	5.3	55.80	40.2	5.2	48.8
35.1	20.1	56.78	35.2	20.0	49.7
35.2	15.1	56.28	35.3	15.0	49.3
35.2	10.2	55.83	35.3	10.1	48.8
35.2	5.1	55.70	35.3	5.1	48.4
30.3	20.0	56.43	30.3	19.9	49.2
30.3	15.1	56.05	30.3	15.0	48.7
30.3	10.3	55.43	30.3	10.2	48.3
30.3	5.3	55.08	30.3	5.2	47.9
25.4	15.1	55.45	25.4	15.1	48.4
25.4	10.1	55.08	25.4	10.0	48.0
25.4	5.2	54.80	25.4	5.1	47.5

The experimental results for the capped 7.6cm diameter, 122cm long DWHR system used to create the corresponding plots in Chapter 4.

Table A-11 The results for the capped 7.6cm diameter, 122cm long system tested at different inlet temperatures.

Volumetric Flow rate of 5.5 LPM			Volumetric Flow rate of 9.5 LPM			Volumetric Flow rate of 14 LPM		
Thot-in (°C)	Tcold-in (°C)	ε (%)	Thot-in (°C)	Tcold-in (°C)	ε (%)	Thot-in (°C)	Tcold-in (°C)	ε (%)
44.8	30.3	57.76	45.1	30.3	47.63	45.1	30.3	42.0
44.8	20.3	57.33	45.0	20.2	47.07	45.1	20.2	41.5
44.8	14.9	57.00	45.0	14.8	46.55	45.1	14.8	41.0
44.8	9.8	56.59	45.0	9.6	46.07	45.2	9.5	40.5
44.8	4.9	56.23	45.0	4.7	45.84	45.2	4.6	40.0

The experimental results for the insulated 7.6cm diameter, 122cm long DWHR system used to create the corresponding plots in Chapter 4.

Table A-12 The results for the insulated 7.6cm diameter, 122cm long system tested at different inlet temperatures

Volumetric Flow rate of 5.5 LPM			Volumetric Flow rate of 9.5 LPM			Volumetric Flow rate of 14 LPM		
Thot-in (°C)	Tcold-in (°C)	ε (%)	Thot-in (°C)	Tcold-in (°C)	ε (%)	Thot-in (°C)	Tcold-in (°C)	ε (%)
44.8	29.6	57.79	45.1	29.6	47.63	45.2	29.6	41.9
44.8	20.3	57.40	45.0	20.2	47.04	45.2	20.2	41.3
44.8	15.0	56.98	45.0	14.9	46.58	45.1	14.8	40.8
45.0	10.1	56.62	45.1	9.9	46.26	45.3	9.8	40.4
44.7	5.3	56.16	44.9	4.9	45.85	45.1	4.8	39.9

Experimental Data for Chapter 5

The experimental results for the 5.1cm diameter, 122cm long DWHR system used to create the corresponding plots in Chapter 5.

Table A-13 Experimental results for the 5.1cm diameter, 122cm long DWHR system by Manufacturer A tested in Chapter 5.

$\dot{V}_{cold}$ (LPM)	$\dot{V}_{hot}$ (LPM)	ε	q-cold (kW)
5.49	5.44	49.7%	5.22
5.50	6.99	53.7%	5.73
5.49	9.01	57.4%	6.17
5.49	10.00	59.1%	6.32
5.52	11.99	61.4%	6.62
5.49	14.01	63.3%	6.83
6.94	5.52	52.2%	5.59
7.00	6.95	45.4%	6.15
7.01	8.98	48.7%	6.70
7.04	9.99	50.3%	6.96
7.02	11.98	52.8%	7.29
7.01	14.00	54.8%	7.50
8.99	5.51	54.8%	5.93
8.97	7.01	47.8%	6.59
9.00	8.95	41.0%	7.17
9.02	10.01	42.3%	7.50
9.01	11.99	44.7%	7.92
9.01	13.97	46.5%	8.24
9.99	5.52	55.7%	6.02
9.96	7.02	48.9%	6.73
9.99	9.03	41.8%	7.44
10.00	9.95	39.4%	7.72
10.02	11.97	41.5%	8.20
10.04	14.01	43.3%	8.46
12.01	5.50	57.8%	6.25
12.00	7.01	51.0%	6.94
11.99	9.02	43.8%	7.75
12.00	10.04	41.1%	8.10
12.02	11.98	36.6%	8.63
12.03	13.99	38.1%	8.99
13.97	5.50	59.6%	6.45
13.99	7.00	52.5%	7.19
13.98	9.06	45.2%	8.07
13.99	10.03	42.7%	8.37
13.99	12.03	38.0%	8.99
13.99	13.93	34.3%	9.40

The experimental results for the 7.6cm diameter, 122cm long DWHR system used to create the corresponding plots in Chapter 5.

Table A-14 Experimental results for the 7.6cm diameter, 122cm long DWHR system by Manufacturer A tested in Chapter 5.

$\dot{V}_{cold}$ (LPM)	$\dot{V}_{hot}$ (LPM)	ε	q-cold (kW)
5.49	5.46	56.3%	5.94
5.49	6.97	60.6%	6.52
5.51	9.00	64.3%	6.92
5.53	9.99	65.8%	7.09
5.49	12.02	69.1%	7.39
5.53	14.00	70.8%	7.71
6.98	5.53	59.5%	6.38
7.00	6.96	51.7%	6.99
6.98	9.02	55.2%	7.57
7.03	9.99	56.9%	7.84
7.00	12.02	60.0%	8.16
7.04	13.97	62.0%	8.57
8.99	5.49	62.9%	6.76
9.00	7.03	54.7%	7.43
9.02	8.96	46.6%	8.17
9.06	9.97	47.9%	8.56
9.05	11.95	50.9%	9.01
9.03	13.95	53.2%	9.48
9.98	5.49	64.1%	6.90
10.01	7.03	56.0%	7.73
9.99	9.06	47.4%	8.48
10.00	9.96	44.8%	8.74
10.05	11.98	47.4%	9.29
10.04	13.98	49.6%	9.79
11.97	5.51	66.1%	7.12
11.97	7.04	58.0%	8.04
12.00	9.06	49.7%	8.85
12.00	10.04	46.7%	9.26
12.03	11.97	41.9%	9.88
12.04	13.92	43.8%	10.23
14.02	5.51	67.9%	7.28
14.00	7.01	59.9%	8.21
14.04	9.02	51.7%	9.15
14.00	10.07	48.5%	9.66
14.00	12.10	43.5%	10.27
14.02	13.92	39.7%	10.87

The experimental results for the 7.6cm diameter, 153cm long DWHR system used to create the corresponding plots in Chapter 5.

Table A-15 Experimental results for the 7.6cm diameter, 153cm long DWHR system by Manufacturer A tested in Chapter 5.

$\dot{V}_{cold}$ (LPM)	$\dot{V}_{hot}$ (LPM)	ε	q-cold (kW)
5.50	5.47	62.4%	6.59
5.52	6.96	66.8%	7.14
5.49	8.97	71.5%	7.69
5.51	9.96	73.4%	7.91
5.49	12.00	76.5%	8.24
5.50	13.99	78.7%	8.48
6.96	5.52	66.3%	7.11
7.01	6.97	57.4%	7.81
6.99	9.00	62.0%	8.51
6.99	9.94	64.0%	8.78
7.04	11.99	67.7%	9.40
7.00	14.00	70.1%	9.63
8.99	5.56	69.8%	7.60
8.95	7.03	60.9%	8.42
9.01	8.96	52.4%	9.18
9.00	10.00	54.7%	9.63
9.04	12.00	57.9%	10.32
9.06	13.96	60.4%	10.83
10.04	5.53	71.4%	7.72
9.95	7.00	62.6%	8.63
9.93	9.05	53.6%	9.57
10.03	9.97	50.8%	9.95
10.00	11.93	54.2%	10.68
10.00	14.00	56.8%	11.15
11.98	5.50	73.5%	7.90
11.99	7.04	64.8%	8.97
11.97	9.03	56.4%	9.97
11.97	10.07	53.2%	10.51
12.01	11.95	48.1%	11.32
12.06	13.94	50.2%	11.94
13.99	5.50	75.5%	8.16
14.00	7.04	66.9%	9.32
14.01	9.03	58.6%	10.45
13.98	10.03	55.4%	11.01
14.00	12.05	50.1%	11.88
14.05	13.97	45.5%	12.51

The experimental results for the 7.6cm diameter, 153cm long DWHR system used to create the corresponding plots in Chapter 5.

Table A-16 Experimental results for the 7.6cm diameter, 102cm long DWHR system by Manufacturer B tested in Chapter 5.

$\dot{V}_{cold}$ (LPM)	$\dot{V}_{hot}$ (LPM)	ε	q-cold (kW)
5.49	5.45	51.6%	5.43
5.53	6.98	55.1%	5.88
5.49	8.98	58.8%	6.32
5.50	9.99	60.4%	6.49
5.51	11.98	62.9%	6.77
5.52	13.97	64.4%	7.02
6.97	5.51	54.7%	5.82
7.00	6.95	47.2%	6.38
7.01	8.97	50.2%	6.89
6.99	10.00	52.2%	7.11
7.00	11.99	54.6%	7.50
7.02	13.98	56.3%	7.75
8.98	5.52	57.9%	6.23
8.97	7.01	50.2%	6.86
9.01	8.95	42.4%	7.43
9.01	9.97	43.8%	7.71
9.03	11.95	46.2%	8.19
9.03	13.95	48.1%	8.56
10.01	5.51	59.1%	6.32
9.99	7.00	51.3%	7.04
9.99	9.02	43.4%	7.63
10.01	9.97	40.7%	7.96
10.03	11.95	43.0%	8.50
10.05	13.95	44.8%	8.76
11.99	5.50	61.0%	6.60
11.98	7.02	53.2%	7.37
11.97	9.02	45.4%	7.99
12.01	10.05	42.5%	8.36
12.02	11.96	37.9%	8.94
12.07	13.96	39.4%	9.30
13.98	5.48	62.8%	6.77
13.97	6.99	55.0%	7.55
13.98	8.97	47.1%	8.35
13.99	10.00	44.2%	8.68
14.00	12.06	39.2%	9.36
14.02	13.96	35.4%	9.73

The experimental results for the 10.2cm diameter, 122cm long DWHR system used to create the corresponding plots in Chapter 5.

Table A-17 Experimental results for the 10.2cm diameter, 122cm long DWHR system by Manufacturer A tested in Chapter 5.

$\dot{V}_{cold}$ (LPM)	$\dot{V}_{hot}$ (LPM)	ε	q-cold (kW)
7.00	6.99	55.2%	7.50
7.02	8.96	62.0%	8.50
7.01	10.00	63.3%	8.70
7.06	11.97	65.1%	9.07
6.96	13.97	68.6%	9.31
8.97	7.02	58.7%	8.09
8.97	8.93	52.6%	9.16
8.94	10.01	53.9%	9.47
9.02	12.00	55.9%	9.79
8.98	14.00	59.1%	10.40
9.94	7.01	61.1%	8.37
9.97	9.05	53.7%	9.52
10.01	9.98	50.0%	9.77
10.06	12.00	52.1%	10.23
10.03	13.96	55.2%	10.82
11.97	6.98	62.1%	8.51
11.98	9.04	56.6%	10.00
11.96	10.10	51.9%	10.28
12.03	11.96	46.2%	10.87
12.02	13.95	49.0%	11.57
13.98	6.99	64.9%	8.91
13.99	8.99	58.7%	10.31
13.96	10.01	54.6%	10.70
14.00	12.06	48.1%	11.42
14.04	13.99	44.0%	12.08

Experimental Data for Chapter 6

The experimental results for the 5.1 cm diameter, 122cm long DWHR system used in Chapter 6.

Table A-18 Experimental results for the 5.1cm diameter, 122cm long DWHR system by Manufacturer A tested in Chapter 6.

Tcold-in (°C)	Thot-in (°C)	Cold Flowrate (LPM)	Hot Flowrate (LPM)	ε (%)	q-cold (kW)
9.9	37.8	5.50	5.44	49.78%	5.28
9.5	37.8	6.99	6.96	45.33%	6.22
9.7	38.0	8.98	8.93	41.18%	7.26
9.4	37.9	10.01	9.98	39.41%	7.83
9.4	38.0	12.03	11.99	36.64%	8.75
9.6	38.1	14.03	13.94	34.46%	9.54
9.7	37.5	16.97	14.98	34.48%	10.03
9.4	38.0	16.10	19.03	33.75%	10.81
9.4	37.9	8.01	15.00	51.18%	8.13
10.7	42.6	9.97	6.04	53.95%	7.25
3.5	28.2	7.47	13.01	50.18%	6.45
3.5	27.9	5.49	11.48	59.19%	5.53

The experimental results for the 7.6 cm diameter, 122cm long DWHR system used in Chapter 6.

Table A-19 Experimental results for the 5.1cm diameter, 92cm long DWHR system by Manufacturer A tested in Chapter 6.

Tcold-in (°C)	Thot-in (°C)	Cold Flowrate (LPM)	Hot Flowrate (LPM)	ε (%)	q-cold (kW)
9.7	37.7	5.50	5.44	49.55%	5.26
9.9	37.9	7.00	6.96	44.28%	6.01
9.5	37.9	9.01	8.94	39.39%	6.96
9.8	38.1	10.01	9.95	37.68%	7.38
9.8	38.1	12.02	11.98	35.01%	8.27
9.5	38.0	14.02	13.93	32.94%	9.11
14.6	44.9	12.98	10.53	39.91%	8.87
14.7	44.6	7.96	6.03	51.51%	6.47
4.8	35.1	7.99	13.50	47.48%	8.01
4.8	34.9	6.02	10.97	54.47%	6.88

The experimental results for the 7.6 cm diameter, 102cm long DWHR system used in Chapter 6.

Table A-20 Experimental results for the 7.6cm diameter, 102cm long DWHR system by Manufacturer B tested in Chapter 6.

Tcold-in (°C)	Thot-in (°C)	Cold Flowrate (LPM)	Hot Flowrate (LPM)	ε (%)	q-cold (kW)
10.0	37.8	5.49	5.45	51.55%	5.43
9.9	37.8	7.00	6.95	47.20%	6.38
9.8	37.9	9.01	8.95	42.41%	7.43
9.8	38.0	10.01	9.97	40.66%	7.96
9.7	38.0	12.02	11.96	37.93%	8.94
9.8	38.0	14.02	13.96	35.40%	9.73
10.5	38.1	25.28	24.83	27.83%	13.30
10.5	37.9	16.04	15.92	33.51%	10.21
9.6	38.1	22.06	21.78	29.42%	12.70
9.6	37.9	19.32	19.05	31.23%	11.74
9.7	38.0	19.18	7.07	57.67%	8.04
9.7	37.9	15.95	9.00	48.24%	8.54
9.8	38.0	12.09	16.05	40.86%	9.72
9.7	38.0	10.01	19.02	48.47%	9.56
14.6	44.9	14.02	13.93	36.35%	10.71
14.7	44.7	9.00	8.96	43.44%	8.16
14.8	44.4	5.47	5.42	52.66%	5.89
14.9	45.0	14.01	10.05	45.23%	9.52
14.9	44.8	11.97	9.03	46.62%	8.76
4.8	35.1	14.06	13.97	34.90%	10.29
4.8	35.0	9.00	8.92	41.85%	7.85
5.1	34.8	5.49	5.44	51.16%	5.77
4.8	35.1	9.03	13.99	47.34%	9.02
4.8	35.0	7.03	9.99	51.03%	7.55

The experimental results for the 10.2 cm diameter, 122cm long DWHR system used in Chapter 6.

Table A-21 Experimental results for the 10.2cm diameter, 122cm long DWHR system by Manufacturer B tested in Chapter 6.

Tcold-in (°C)	Thot-in (°C)	Cold Flowrate (LPM)	Hot Flowrate (LPM)	ε (%)	q-cold (kW)
10.1	38.0	5.50	5.46	56.15%	5.97
9.9	37.8	6.99	6.97	52.83%	7.15
9.8	37.9	9.01	8.97	50.25%	8.83
9.8	37.9	10.01	9.97	48.33%	9.46
9.8	38.0	12.02	11.97	44.88%	10.57
9.8	38.1	14.06	13.96	42.29%	11.65
9.6	38.1	18.03	13.01	47.72%	12.33
9.5	37.9	17.00	8.05	62.98%	10.03
9.7	38.1	9.02	18.97	60.40%	10.76
9.7	38.0	10.95	16.01	51.81%	11.18
12.2	37.1	12.99	9.50	54.03%	8.90
12.2	36.9	9.98	8.07	55.65%	7.73
7.1	34.8	10.53	13.49	49.95%	10.14
7.0	34.2	8.51	12.46	56.15%	9.05

Experimental Data for Appendix A

The results used to generate the plots in Appendix A for flow rates of 5.5, 9.5 and 14 LPM are shown in Table A-22, Table A-23 and Table A-24, respectively.

Table A-22 - The effectiveness of DWHR tested as part of Appendix-A, for a flow rate of 5.5 LPM.

Tilt Angle (°)	ε (%)					
	Pipe #1	Pipe #2	Pipe #3	Pipe #4	Pipe #5	Pipe #6
0	49.1	46.3	55.0	60.8	60.2	65.0
2	48.7	44.9	55.0	60.8	60.1	64.2
5	44.2	41.8	55.1	59.0	59.6	62.6
10	36.1	35.4	49.5	44.1	52.2	52.1
15	35.7	32.1	43.0	41.5	44.0	43.8

Table A-23 - The effectiveness of DWHR tested as part of Appendix-A, for a flow rate of 9.5 LPM.

Tilt Angle (°)	ε (%)					
	Pipe #1	Pipe #2	Pipe #3	Pipe #4	Pipe #5	Pipe #6
0	37.5	38.5	46.3	52.1	50.8	56.5
2	37.2	38.0	44.7	50.4	50.7	55.6
5	34.5	36.0	42.4	46.1	49.8	53.4
10	29.1	31.8	37.7	37.4	46.5	48.4
15	27.8	28.0	31.5	33.7	41.9	43.9

Table A-24 - The effectiveness of DWHR tested as part of Appendix-A, for a flow rate of 14 LPM.

Tilt Angle (°)	ε (%)					
	Pipe #1	Pipe #2	Pipe #3	Pipe #4	Pipe #5	Pipe #6
0	31.8	32.9	40.0	45.9	45.6	51.4
2	30.8	32.2	38.7	43.8	45.5	50.6
5	27.8	30.3	35.9	38.8	44.1	47.7
10	24.3	26.7	30.0	31.7	40.0	41.8
15	22.6	22.7	26.2	28.3	35.4	37.0